Characterisation of Optical Metamaterials
-
Effective Parameters and Beyond

Dissertation
zur Erlangung des akademischen Grades

doctor rerum naturalium (Dr. rer. nat.)

vorgelegt dem Rat der Physikalisch-Astronomischen Fakultät
der Friedrich-Schiller-Universität Jena

von Diplom-Physiker Christoph Menzel
geboren am 03.10.1981 **in** Halle (Saale)

1. Gutachter: Prof. Dr. rer. nat. habil. Falk Lederer, Univ. Jena, Germany
2. Gutachter: Prof. Dr. rer. nat. Thomas Zentgraf, Univ. Paderborn, Germany
3. Gutachter: Prof. Dr. rer. nat. Costas Soukoulis, Iowa State Univ., USA

Tag der Disputation: 01.11.2011

Contents

1 Introduction

The development of metamaterials was driven by the desire to achieve artificial materials with optical properties inaccessible by natural available media. Natural isotropic homogeneous materials are characterized by a frequency dependent permittivity $\varepsilon(\omega)$ and permeability $\mu(\omega)$. Both describe the response of the material to an electromagnetic field, where $\varepsilon(\omega)$ accounts for the electric polarization induced by an electric field and $\mu(\omega)$ accounts for the magnetic polarization induced by a magnetic field. In the optical domain, where the magnetic susceptibility $\chi_m(\omega) = \mu(\omega) - 1$ is vanishing, the permeability is a constant $\mu(\omega) = 1$. Metamaterials (MMs) are understood to break this limit by offering a frequency dependent permeability $\mu(\omega)$. Moreover, the reals parts of ε and μ may become even arbitrarily large or extremely small and also negative. Hence, the complete space of optical properties formed by both (see Fig. 1.1) can be accessed [1]. One of the first publications speculating in particular about media with both, the permittivity and the permeability being negative, has been presented by Victor Veselago in 1968 [2]. For a long time, this work was almost forgotten until John Pendry came up in 2000 with the idea to use a slab of a medium with $\varepsilon = -1$ and $\mu = -1$ as a perfect lens [3]. This was motivated by research on effective magnetism arising from inherently non-magnetic structures [4, 5]. With more than 3000 citations (end of 2010) his proposal of the perfect lens can be understood as the birth and the main driving force of MM's research.

In his seminal work [2] Veselago concluded, that a medium would have dramatically different propagation characteristics stemming from the change in sign of the phase velocity. This renders the appearance of many physical effects to be opposite to what we know about them from our daily life experience. It includes a reversal of both the Doppler shift and Cherenkov radiation, anomalous refraction, and even the reversal of radiation pressure to radiation tension [5]. The possibilities offered by MMs seem to be unlimited.

Beside the proposal of fancy devices like the hyperlens [6, 7], the trapped rainbow [8], the perfect absorber [9] or the cloaking device [10–14], also general concepts were established like transformation optics [15, 16] and MMs with extreme parameters [1, 17]. Surprising phenomena were revealed like metamaterials with simultaneous negative group and phase velocity [18], giant optical activity [19–21] or asymmetric transmission [22–26]. A lot of efforts were made to investigate the properties of chiral metamaterials [27–31] after Pendry's

proposal of negative refraction due to chirality [32]. Metamaterials were even shown to allow for an enhancement of nonlinear effects [33–38].

This list can be extended almost arbitrarily, since even most simple systems like plane layers of negative index MMs show astonishing effects like guides modes with zero group velocity [8,39,40] or bounded surface states irrespective of the polarization [39,41]. MMs simply seem to be the holy grail for the design of optical devices with unprecedented functionalities.

But how to realize such materials? To be described by effective optical properties the entities, often called metaatoms, comprising the MMs have to be small compared to the wavelength. Hence, the aim is to create metaatoms that provide, either already as single elements or upon interaction with each other, the desired optical property or functionality.

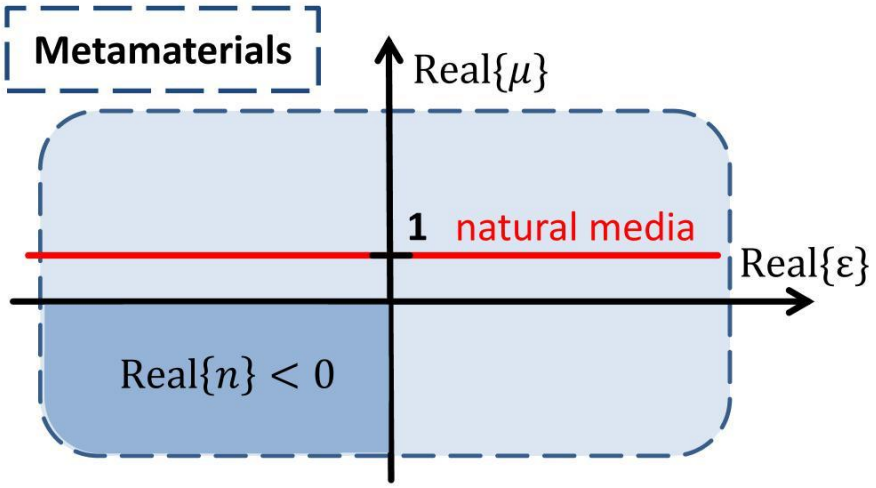

Figure 1.1: Optical parameter space spanned by the real parts of the permittivity ε and the permeability μ. MMs are understood to access the overall parameter space, whereas natural materials are restricted to the red line at optical frequencies. The real part of the refractive index becomes negative where both the real part of ε and μ are simultaneously negative for lossless MMs. For lossy materials, the condition for a negative refractive index becomes more complicated ($\Re(n) < 0$ if $\Re(\varepsilon) \cdot \Im(\mu) + \Re(\mu) \cdot \Im(\varepsilon) < 0$) [42–45]. MMs with large permittivity/permeability are called 'materials with extreme parameters'.

Thinking of MMs as periodically arranged metaatoms, these are supposed to act similar to natural crystals but to offer optical properties beyond their natural analogues.

At the beginning of their investigation the focus was on artificial magnetism. Probably the first metaatom proposed to show a resonance enhanced artificial magnetism in the microwave domain was the Split Ring Resonator (SRR) [4, 46, 47]. There, the SRR is made of a conducting material, and the slits in the ring allow for a resonantly enhanced current driven by the external field. Whereas for millimeter waves an experimental realization of the structure is rather easily accomplished by well developed fabrication techniques, transferring these concepts towards the optical domain remained a cumbersome issue for several reasons.

At first and by assuming non-dispersive constituent materials, the ratio of the unit cell size to the wavelength must remain small and constant to obtain a certain resonance frequency. Hence, the structure sizes have to scale inversely with the desired resonance frequency, eventually becoming challengingly small for optical frequencies. And at second with an increasing operational frequency the intrinsic material dispersion tends to be increasingly important, and limits the scaling behavior of the resonances fundamentally [48]. Whereas by adjusting the geometrical size of the SRR it is possible to increase the resonance frequency towards to infrared regime (IR) [49, 50], tremendous further efforts were made to realize MMs showing an artificial magnetism also in the optical domain [51]. Some kind of breakthrough and today one of the most extensively used designs showing artificial magnetism in the optical domain is the fishnet MM [52], which is investigated in detail in chapter 4. Although all the aforementioned structures are composed of conducting materials, which are characterized by resonantly driven current distributions, it is worth to mention that alternative concepts for achieving artificial magnetism using high permittivity materials exist [53–56]. They can be treated analogously with the methods proposed later on but are not discussed in detail here.

All of the structures have in common, that the metaatoms they are made of are small compared to the wavelength, where topological resonances are exploited to achieve a wide range of effective optical properties. Hence, a lower limit for the smallness of the metaatoms compared to the wavelength exists if topological resonances are to be exited reasonably. This will have a tremendous influence on the applicability of effective media approaches, as is shown in this work.

Although these considerations suggest a certain understanding of MMs, a straightforward definition of what exactly should be considered as a MM remains a subtle issue [57]. It is important to distinguish it from terms and topics like photonic crystals, plasmonics and nanooptics. In the most general sense of understanding MMs as structures, which are designed to control the light propagation, these fields of research are indistinguishable from MMs. On the other hand, defining man-made materials to be MMs, only if an effective homogeneous medium description of these systems is valid, is too restrictive, as is shown in chapter 4. So MMs can be defined as systems that are composed of functional elements (metaatoms/metamolecules), which are small compared to the wavelength and characterized by topological resonances, with the averaged distance between the metaatoms being also small compared to the wavelength and which are intended to affect the characteristics of light propagation effectively.

In the context of MMs research, it is also necessary to discuss the role of spatial dispersion (SD). Whereas a frequency dependence of optical parameters, known as frequency dispersion, is well understood and accepted, for MMs it might be necessary to take into account a dependency of the optical parameters on the wavevector $\mathbf{k}$, too. This dependency is called

spatial dispersion [58]. It is understood to take into account the effects of the finite length scales in a MM, i.e. the metaatoms and their average distance are not infinitesimal small compared to the wavelength, in general. The issue of SD entered the understanding of MMs by a legendary footnote of Landau and Lifshitz in their famous course on theoretical physics (see [59], §103). They state, that '[...] die Permeabilität μ im optischen Frequenzbereich ihren Sinn verliert. In diesem Bereich sind im Allgemeinen die Effekte, die mit einer Abweichung der magnetischen Permeabilität von 1 verbunden sind, nicht von den Effekten der räumlichen Dispersion in der dielektrischen Funktion zu unterscheiden.' That essentially happens due to the impossibility to distinguish the physical origin of the magnetization currents $\nabla \times \mathbf{M}$ and the polarization current $\partial_t \mathbf{P}$ at large frequencies, where it becomes more meaningful to simply include all field matter interactions into a complex, spatially dispersive permittivity $\varepsilon(\mathbf{k}, \omega)$ with $\mu = 1$ (see [59], §79). Vice versa, a complex, spatially dispersive response might be linked to an artificial magnetism. The framework of SD sets the basement for the theoretical description of MMs nowadays. This theoretical framework is used to determine the most general form of local constitutive relations for a certain class of systems and the role and understanding of SD is discussed comprehensively in chapter 2.

For the present thesis the question of characterizing MMs is of utmost importance. In particular, the characterisation in terms of an effective description by means of material parameters, which describe the response of the medium to an electromagnetic field, or wave parameters, which describe the properties of the waves propagating in the medium, is in the focus. Here, several approaches exist. At first, the classical effective medium approaches (a broad overview is provided by the book of Ari Sihvola [60] and the contributions of R. Ruppin [61, 62]). These approaches are in particular applicable to systems composed of metaatoms, which are very small compared to the effective wavelength and are hence operating in the so called quasi-static regime. Although these approaches are well developed and rigorous, they generally suffer from the necessity of having analytical solutions for the response (basically the polarizabilities) of the metaatoms at hand. However they can be used to determine the effective optical properties of more complex metaatoms, too, once the polarizability is calculated e.g. numerically [63]. In the same manner so called multipole approaches might be applied to determine the effective optical properties [64, 65] (see also chapter 2). A lot of efforts were made to analyze the multipolar response of metaatoms recently [63, 66–69]. Also extensions of these methods beyond the quasi-static regime in particular by assuming given dipole polarizabilities were put forward [70–73]. The second class contains methods based on the direct averaging of the numerically calculated electromagnetic fields [74–79]. However, these approaches are rarely employed due to obvious difficulties in determining the overall electromagnetic fields sufficiently precise and inherent drawbacks [4]. The third approach, which is commonly applied nowadays, relies on the inversion of the scattering coefficients

obtained at finite systems of MMs (see the detailed discussion in chapter 3). Although originally proposed by Nicholson, Ross and Weir already in 1970's [80, 81] this approach attracted great attention only after the proposition by D.R. Smith et al. in 2002 [82], to whom the S-parameter retrieval is mainly attributed. This approach was later on extended by several authors and is as much discussed controversial as it is used for the characterisation of MMs (see chapter 3 for further details). In particular, the range of applicability of the method and the physical meaning of the retrieved parameters was at the focus of many scientific publications [71, 83–90]. In this thesis the original proposal is extended to oblique incidence and also to chiral MMs. In particular the retrieval for oblique incidence provides a tool to test for the reasonability of the effective material parameters. This algorithm is also discussed in the language of periodic media, providing ultimate limitations of its applicability.

Contrary to the aforementioned approaches aiming at a determination of the effective optical parameters, more general approaches were recently put forward, that focus on the characterisation in terms of symmetry and characteristic scattering . A comprehensive introduction and detailed review can be found in the PhD theses of Eric Plum [91] and Christian Helgert [92]. Instead of retrieving effective optical parameters, MMs are studied and classified here in terms of their symmetry related characteristic scattering properties. Solely based on symmetry considerations it is possible to determine the general form of the reflection and the transmission matrix and hence all effects e.g. on the polarization state of scattered light are known in general. Chapter 5 introduces to that approach and presents a scheme to classify all periodic MMs. The presented method is, in particular, advantageous for complex shaped metaatoms, which manipulate the state of polarization in a complex manner and for which a description in terms of effective optical parameters is too complicated. Besides, it circumvents any subtleties regarding the physical meaning and focusses application oriented on the response to be tailored.

The present thesis is organized in 4 main chapters, where each can be read and understood on its own consistently. In chapter 2 basic consideration on the understanding of the macroscopic Maxwell equations as applied to MMs are made. In particular the necessary local constitutive relations are derived and discussed. Chapter 3 focusses on the determination of effective optical properties within the framework of the S-parameter retrieval making explicit use of the constitutive relations derived before. The S-parameter retrieval is discussed in the language of photonic crystals, providing a clear picture of its applicability to MMs. In chapter 4 the S-parameter retrieval is applied to discuss the optical properties of prominent negative index MMs, where emphasize is put on the physical meaning of the retrieved parameters. Eventually in chapter 5 an efficient alternative approach being suitable in particular for complex shaped, polarization manipulating structures is proposed and discussed in detail.

2 Setting the stage - deriving the constitutive relations

In this chapter the equations governing light propagation in homogeneous media are derived. In the framework of this thesis particularly the transition from microscopic to the macroscopic Maxwell equations for systems composed of localized particles is explained and discussed. Thereby we basically follow the statements given in [93–95]. The main focus is set here on the derivation of local constitutive relations to shed light on the origin of artificial magnetism, which is potentially the main driving force for metamaterial research.

Starting point is the set of microscopic Maxwell equations in the presence of localized currents and charges

$$\nabla \cdot \mathbf{e}(\mathbf{r},t) = \frac{\eta(\mathbf{r},t)}{\varepsilon_0}, \quad \nabla \times \mathbf{b}(\mathbf{r},t) - \frac{1}{c^2}\frac{\partial \mathbf{e}(\mathbf{r},t)}{\partial t} = \mu_0 \mathbf{j}(\mathbf{r},t) \tag{2.1}$$

$$\nabla \cdot \mathbf{b}(\mathbf{r},t) = 0, \quad \nabla \times \mathbf{e}(\mathbf{r},t) + \frac{\partial \mathbf{b}(\mathbf{r},t)}{\partial t} = 0. \tag{2.2}$$

The quantities given by small letters are microscopic quantities, namely the electric and the magnetic field $\mathbf{e}(\mathbf{r},t)$ and $\mathbf{b}(\mathbf{r},t)$ and the charge and current density $\eta(\mathbf{r},t)$ and $\mathbf{j}(\mathbf{r},t)$. μ_0 and ε_0 are the vacuum permeability and the vacuum permittivity. The first set of equations (2.1) are the inhomogeneous equations and the second set (2.2) are the homogeneous ones. The fields as well as the currents and charges are coupled and have to be solved self-consistently in general. However, solving this set is an impossible venture due to the generally large number of microscopic entities. Fortunately, the problem can often be simplified while considering the fields as well as the matter by means of smeared out quantities leading to macroscopic equations for the averaged fields and matter distributions. The requirement on the fields as well as on the matter to allow for this homogenization is a small variation of the averaged quantities in space with respect to each other. In a sufficiently small volume that still contains a large numbers of particles, the averaged fields have to be approximately constant. Different ways to derive these macroscopic equations might be considered, namely either a so called multipole approach or a phenomenological approach. Both will be discussed below. However, the final aim are equations describing the matter as a homogeneous medium, where the applicability of the homogenization will be judged by verifying the predictive power from

case to case. Without specifying the averaging scheme here (see e.g. [93,96]), we will simply give the system of macroscopic equations

$$\nabla \cdot \mathbf{E}(\mathbf{r},t) = \frac{\rho(\mathbf{r},t)}{\varepsilon_0}, \quad \nabla \times \mathbf{B}(\mathbf{r},t) - \frac{1}{c^2}\frac{\partial \mathbf{E}(\mathbf{r},t)}{\partial t} = \mu_0 \mathbf{J}(\mathbf{r},t) \tag{2.3}$$

$$\nabla \cdot \mathbf{B}(\mathbf{r},t) = 0, \quad \nabla \times \mathbf{E}(\mathbf{r},t) + \frac{\partial \mathbf{B}(\mathbf{r},t)}{\partial t} = 0, \tag{2.4}$$

where $\mathbf{E} = \langle \mathbf{e} \rangle$, $\mathbf{B} = \langle \mathbf{b} \rangle$, $\rho = \langle \eta \rangle$ and $\mathbf{J} = \langle \mathbf{j} \rangle$ are spatially but not temporally averaged quantities. These equations as well as their derivation will be the subject of the following sections, where emphasis is put to establish the relation to the field of metamaterials as it is important to the present thesis.

We proceed as follows. At first, the derivation is made by means of the multipole approach, which is most intuitive and less abstract. The multipole approach is in particular advantageous for media composed of localized structures. This excludes the description of plasma, which have to be treated separately by a different approach (hydrodynamic equations for the induced current [97–99]). At second we choose a phenomenological approach, which is rather abstract but completely general. Also, this approach accentuates possible ambiguities with respect to the definitions of the material fields $(\mathbf{D}, \mathbf{H})$ and stresses offered possibilities. Since we do not want to deal explicitly with the modeling of the multipolar response, the latter approach will be discussed in greater detail and the relation between both approaches will be evinced. The phenomenological approach will be of major importance, since its more general results serve as a prerequisite for the description of light propagation in the following. Eventually, it provides a derivation and justification of an adequate description for media, that show an artificial magnetic response - the main driving force for bulk metamaterials [100–104] at all.

2.1 The multipole approach

The transition from microscopic to macroscopic Maxwell equations, the averaging and homogenization of natural microscopic systems, is investigated by many authors in numerous publications. Probably most renowned is the work of Russakoff [96] and Mazur and Nijboer [105]. Comparing different approaches it remains hard to bring them down to a common denominator, although leading basically to the same results, i.e. the well known set of macroscopic Maxwell equations. In the following we will therefore recapitulate the essential points and clear up possible misconceptions.

The most intuitive but mathematically most challenging way consists in the time-dependent multipole expansion of the electromagnetic potentials of the localized charge and current distributions, leading to an expansion series of the averaged densities [95]. The essence is

summarized and interpreted as follows:
Take discrete volumes v_i, especially the volume containing a single localized object i, and expand the charge and current density in v_i into a multipole series. The situation is schematically shown in Fig. 2.1, where the blue squares represent the complex charge and current densities. Every localized object is now described and conceptually replaced by its multipole moments (red circles in Fig. 2.1), where the expansion is made at a reasonably chosen origin relative to the localized object. Now the averaging is performed over a larger vol-

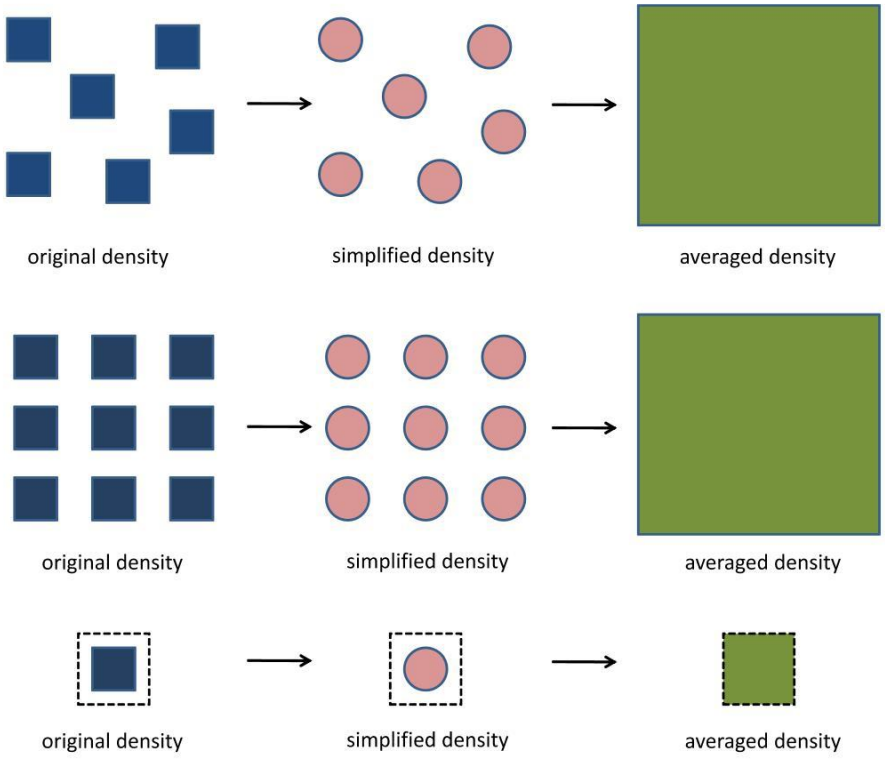

Figure 2.1: Schematic drawing of the averaging procedure. The small, blue squares represent the microscopic, complex charge and current densities. They are localized in the volume v_i. The multipole expansion of these distributions up to a certain order results in the multipole densities in v_i, which are shown as small red circles. Smearing out these densities in the supervolume V leads to a homogeneous density, shown as a green square. Upper row: Choice of the different volumes for an amorphous structure. Center row: Choice of the volumes for periodic systems. Lower row: For periodic systems we can obviously choose $V = v$ leading to a homogeneous density.

ume $V = \bigcup v_i$ containing a larger number of small volumes v_i. The average of every single moment gives the moment density in that area, where V is still small compared to the wavelength (green squares with volume V in Fig. 2.1). Here the smallness is essential, because it is obviously meaningless to average over (in extreme) a whole period where all averaged quantities except the monopole contribution will vanish (see also Fig. 2.2). That means, in particular, that the densities and the fields in each volume V have to be approximately constant. The fields and densities are then de facto discretized.

In fact, only for amorphous systems it is necessary to perform the average on a superset V to smear out and hence to remove possible inhomogeneities. For periodic media we can simply choose for the unit cell volume $V_{cell} = V$ and determine the multipole moment there. The multipole moment densities are given by normalization to the volume of the unit cell. Hence, the requirements on the homogenization of a periodic structure are weaker in general compared to amorphous systems composed of identical molecules or metaatoms. Here, the averaged fields are discretized on the lattice. The lattice period, however, must be small compared to the effective wavelength of the medium to avoid an under-sampling of the fields. Therefore, the unit cell must be at least several times smaller than the wavelength (rigorously speaking at least half of the wavelength; see Fig. 2.2).

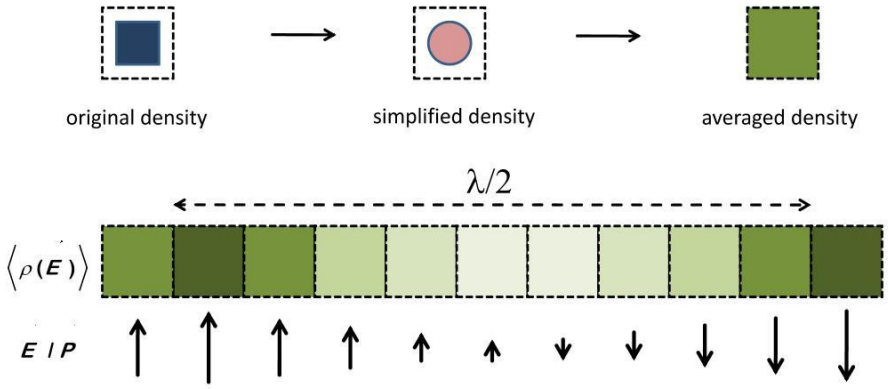

Figure 2.2: Upper row: averaging procedure for periodic structures as shown in Fig. 2.1. The squares and circles form the unit cells. Lower row: Schematic drawing of the density and field-variation across the periodic structure. The densities depend per definition linear on the field. Both quantities can be understood as being discretized. Therefore, a field variation below $\lambda/2$ cannot be resolved anymore, setting the upper bounds for a meaningful homogenization.

Note that the moment densities of the induced charges and currents are of course inhomogeneous across the entire structure since the generating field may be inhomogeneous. Contrarily, the corresponding multipole polarizability densities are homogeneous.

To consider the space formally as being discretized may seem paradox, if only continuous quantities are used finally. However, this has two important conceptual advantages with respect to the understanding and interpretation of the equations. On one hand, it is clear that a minimal wavelength exists for which the description of the medium as a homogeneous one is just valid. On the other hand, the underlying physical space is necessarily inhomogeneous. This is in particular advantageous for the understanding of spatial dispersion, i.e. the non-local dependency of the medium response to external electromagnetic fields. If the physical space would be perfectly homogeneous, only dipole moments could be induced and hence the response would be purely local. The introduction of spatial dispersion allows to describe an essentially inhomogeneous medium as a homogeneous one. Therefore, the concept of spatial

dispersion might be understood as a kind of perturbation ansatz, where only weak spatial dispersion is meaningful for crystals [58].

The issue of determining the effective properties is now shifted to the determination of the multipole densities depending on the self-consistent field. Any modeling of the densities is beyond the scope of this text and we refer to the work of J. Petschulat et al. [64,65,106,107].

Alternatively, and given here only for the sake of completeness, the fields of the mesoscopic system (rigorous treatment of the fields in periodic sub-wavelength structures) might be calculated directly. After performing an appropriate averaging the effective properties might be extracted from the averaged fields [74–79]. These approaches are usually termed dynamic homogenization in particular in contrast to the static or quasi-static treatment [60].

We content ourselves with an formal solution to the expansion and simply present it here as used later on. Apart from that, the reader is referred to the book of Raab and de Lange [95].

With the charge density being expanded into a multipole series, the inhomogeneous divergence equation reads as

$$\rho_{\text{ext}}(\mathbf{r},t) = \partial_i \left(\varepsilon_0 E_i + P_i - \frac{1}{2}\partial_j Q_{ij} + \frac{1}{6}\partial_k \partial_j Q_{ijk} + ... \right) = \partial_i D_i(\mathbf{r},t). \tag{2.5}$$

The overall charge density $\rho(\mathbf{r},t)$ is separated into the external $\rho_{\text{ext}}(\mathbf{r},t)$ and the induced charge density $\rho_{\text{ind}}(\mathbf{r},t)$, where the induced part is rewritten as the divergence of the multipole densities. Here $\mathbf{P}(\mathbf{r},t)$ is the electric dipole density, $Q_{ij}(\mathbf{r},t)$ is the electric quadrupole density and $Q_{ijk}(\mathbf{r},t)$ the electric octupole density. Note that the densities beyond the dipole order are contributing to the overall induced charge density by means of their spatial derivatives. This equation implicitly defines the dielectric displacement $\mathbf{D}(\mathbf{r},t)$, which contains besides the electric field $\mathbf{E}(\mathbf{r},t)$ also all induced multipole contributions of the charge density.

With the current density being expanded analogously and with the help of the continuity equation, we get for the inhomogeneous curl equation:

$$\begin{aligned} (\nabla \times \mathbf{H})_i &= \varepsilon_{ijk}\partial_j \left(\mu_0^{-1} B_k - M_k + \frac{1}{2}\partial_l M_{kl} + ... \right) = ... \\ ... &= J_{\text{ext},i} + \frac{\partial}{\partial t}\left(\varepsilon_0 E_i + P_i - \frac{1}{2}\partial_j Q_{ij} + \frac{1}{6}\partial_k \partial_j Q_{ijk} + ... \right) = \left(\mathbf{J}_{\text{ext},i} + \frac{\partial \mathbf{D}}{\partial t} \right)_i . \end{aligned} \tag{2.6}$$

Again, the external part of the current was separated and an expansion of the induced part was performed. Besides the temporal derivatives of the electric multipole densities, some terms are obtained, which are a priori divergence free. In the truncated form of the series given here these are the magnetic dipole density $\mathbf{M}$ and the magnetic quadrupole density M_{kl}, which enter the equations again by their spatial derivatives. The magnetic field $\mathbf{H}$ as defined here contains next to the magnetic induction $\mathbf{B}$ all magnetic multipole densities.

The truncation orders of the charge and current densities are coupled. I.e., if magnetic quadrupole terms are retained one consistently has to take into account electric octupolar contributions, too. Both are on the same order of the multipole expansion [95].

As already given on page 25f in [95] the definition of $\mathbf{D}$ and $\mathbf{H}$ is not unique. Assuming time-harmonic fields or performing the transition to frequency space (Fourier transformation), respectively, one can also define:

$$D_i'(\mathbf{r},\omega) = \varepsilon_0 E_i(\mathbf{r},\omega) + P_i(\mathbf{r},\omega) - \frac{1}{2}\partial_j Q_{ij} + \frac{1}{6}\partial_k\partial_j Q_{ijk} + \frac{i}{\omega}\varepsilon_{ijk}\partial_j\left(M_k - \frac{1}{2}\partial_l M_{kl}\right) + ... \quad (2.7)$$

and

$$B_i'(\mathbf{r},\omega) = \mu_0 H_i(\mathbf{r},\omega). \quad (2.8)$$

However, these new definitions $(\mathbf{D}', \mathbf{B}')$ contain no new physics. In fact, for the bulk medium the definitions of $\mathbf{D}$ and $\mathbf{H}$ are even arbitrary and must not be introduced at all. In chapter 7 of [95] it is already discussed how to use this ambiguity to obtain the most simple equations, that lead in particular to physically meaningful results. This issue is beyond the scope of this paragraph and will be discussed from a more abstract point of view in the following section.

2.2 The phenomenological approach

In the following we will at first use the averaged equations (2.3) and (2.4) as initial assumption and introduce the corresponding constitutive relations analogously to the basic electrodynamics courses. This serves as an easy introduction for the reader to the more abstract considerations later on. It will turn out, that several problems for complex materials and ambiguities in the definitions of the response fields occur. The considerations serve as a prelude to deduce the most general response for reciprocal media. Then the important limit of weak spatial dispersion will be elaborated. In particular, the origin of a possible artificial magnetic response and the most general local constitutive relations will be identified. At first, the averaged charge density is separated into an induced part and a free or external part [93], respectively, i.e.

$$\rho(\mathbf{r},t) = \rho_{\mathrm{ind}}(\mathbf{r},t) + \rho_{\mathrm{ext}}(\mathbf{r},t). \quad (2.9)$$

Since an integration of the averaged charge density over the entire volume yields the overall charge

$$Q = \int_V (\rho_{\mathrm{ind}} + \rho_{\mathrm{ext}}) dV = Q_{\mathrm{ext}}, \quad (2.10)$$

the induced part can be written as the divergence of a vector field $\mathbf{P}(\mathbf{r},t)$

$$\rho_{\mathrm{ind}}(\mathbf{r},t) = -\nabla\cdot\mathbf{P}(\mathbf{r},t), \quad (2.11)$$

where $\mathbf{P}(\mathbf{r},t)$ is not necessarily the dipole density but it describes a general polarization density. The averaged current is separated into one part, which takes into account the induced polarization charges, and another part, which replaces closed circulating currents, that are per definition divergence free. The latter one describes e.g. any response of magnetic moments. For the current we have

$$\mathbf{J}(\mathbf{r},t) = \mathbf{J}_{\mathrm{ind}}(\mathbf{r},t) + \mathbf{J}_{\mathrm{magn}}(\mathbf{r},t) + \mathbf{J}_{\mathrm{ext}}(\mathbf{r},t). \tag{2.12}$$

By using the continuity equation

$$\nabla \cdot \mathbf{J}(\mathbf{r},t) + \frac{\partial \rho(\mathbf{r},t)}{\partial t} = 0 \tag{2.13}$$

we have for the different parts of the averaged current:

$$\nabla \cdot \left(\mathbf{J}_{\mathrm{ind}} - \frac{\partial}{\partial t}\mathbf{P} \right) = 0, \quad \nabla \cdot \mathbf{J}_{\mathrm{ext}} + \frac{\partial \rho_{\mathrm{ext}}}{\partial t} = 0, \quad \nabla \cdot \mathbf{J}_{\mathrm{magn}} = 0. \tag{2.14}$$

The last equation is fulfilled trivially by an arbitrary, differentiable vector field $\mathbf{M}$ and we can define

$$\mathbf{J}_{\mathrm{magn}}(\mathbf{r},t) = \nabla \times \mathbf{M}(\mathbf{r},t). \tag{2.15}$$

Again, $\mathbf{M}(\mathbf{r},t)$ is not necessarily a magnetic dipole density. Since the divergence of the magnetic part of the current is vanishing, this part may be identified with the closed circulating currents of all kind and in particular, if only magnetic dipoles are existing, with the magnetic dipole density [59, 93, 97]. $\mathbf{J}_{\mathrm{ind}} = \partial_t \mathbf{P}$ is often called polarization current.

The separation of the current is commonly performed in the context of the transition from microscopic to macroscopic electrodynamics [59, 93]. In fact, it is only meaningful, if justified by the appearance of magnetizable media, i.e., if the magnetization $\mathbf{M}(\mathbf{r},t)$ is a function of the magnetic field only. In the optical domain such a magnetic response is unlikely, since the entities carrying the magnetic moments cannot follow the fast oscillations of the electromagnetic field (see [59], §79).

Very generally the quantities $\mathbf{P}(\mathbf{r},t)$ and $\mathbf{M}(\mathbf{r},t)$ which are introduced formally above, can be identified and physically interpreted with the electric and magnetic dipole densities only retrospectively by comparison with the multipole approach. Assuming that all higher induced moments are vanishing is equivalent to the quasi-static limit, which means, that the response of all entities is driven completely by the local field. In the limit of $\mathbf{k} \to 0$ only materials that are intrinsically magnetic might show a non-vanishing magnetic dipole density. Later on, we will identify the physical origin of artificial magnetism in the optical domain.

Starting with the above definitions of the fields $\mathbf{P}$ and $\mathbf{M}$, the induction fields $\mathbf{D}$ and $\mathbf{H}$ can be defined as:

$$\mathbf{D}(\mathbf{r},t) = \varepsilon_0 \mathbf{E}(\mathbf{r},t) + \mathbf{P}(\mathbf{r},t) \text{ and } \mathbf{H}(\mathbf{r},t) = \mu_0^{-1}\mathbf{B}(\mathbf{r},t) - \mathbf{M}(\mathbf{r},t) \tag{2.16}$$

where the material response is described entirely by means of $\mathbf{P} = \mathbf{P}(\mathbf{E}, \mathbf{B})$ and $\mathbf{M} = \mathbf{M}(\mathbf{E}, \mathbf{B})$. The equations for $\mathbf{D}$ and $\mathbf{H}$ are termed constitutive relations. This leads to inhomogeneous Maxwell equations of the form

$$\nabla \times \mathbf{H}(\mathbf{r}, t) = \frac{\partial \mathbf{D}(\mathbf{r}, t)}{\partial t} + \mathbf{J}_{\text{ext}}(\mathbf{r}, t) \tag{2.17}$$

and

$$\nabla \cdot \mathbf{D}(\mathbf{r}, t) = \rho_{\text{ext}}(\mathbf{r}, t). \tag{2.18}$$

Together with the homogeneous equations (2.4) and the constitutive relations (2.16) they build the complete set of field equations.

As already mentioned in the context of the multipole approach the definitions for $\mathbf{D}$ and $\mathbf{H}$ (2.16) are not unique. In fact, the field equations are invariant under the transformation:

$$\mathbf{D}'(\mathbf{r}, t) = \mathbf{D}(\mathbf{r}, t) + \nabla \times \mathbf{Q}(\mathbf{r}, t), \text{ and } \mathbf{H}'(\mathbf{r}, t) = \mathbf{H}(\mathbf{r}, t) + \frac{\partial \mathbf{Q}(\mathbf{r}, t)}{\partial t} \tag{2.19}$$

with an arbitrary but differentiable vector field $\mathbf{Q}(\mathbf{r}, t)$. Hence, the fields $\mathbf{P}$ and $\mathbf{M}$ are not unique, too. On one hand, the separation of the induced current becomes arbitrary and on the other it is only meaningful, if physically motivated. The only relevant modification of such a transformation concerns the boundary conditions, which have to be used. In fact, that is the important advantage of such transformations. Exactly this type of transformation will be used below to obtain simple boundary conditions.

For optical frequencies or more generally speaking for all non-magnetic materials, it is neither possible nor necessary to perform a separation of the induced current into the polarization and the magnetization current. I.e., the overall response can be put in a single induced current. We therefore rewrite the equations in frequency space as:

$$\nabla \times \mathbf{E}(\mathbf{r}, \omega) = i\omega \mathbf{B}(\mathbf{r}, \omega), \quad \frac{1}{\mu_0} \nabla \times \mathbf{B}(\mathbf{r}, \omega) = -i\omega \mathbf{E}(\mathbf{r}, \omega) + \mathbf{J}_{\text{ind}}(\mathbf{r}, \omega) + \mathbf{J}_{\text{ext}}(\mathbf{r}, \omega) \tag{2.20}$$

$$\varepsilon_0 \nabla \cdot \mathbf{E}(\mathbf{r}, \omega) = \rho_{\text{ind}}(\mathbf{r}, \omega) + \rho_{\text{ext}}(\mathbf{r}, \omega), \quad \nabla \cdot \mathbf{B}(\mathbf{r}, \omega) = 0, \tag{2.21}$$

where the transition to frequency space is performed via Fourier transformation being defined as:

$$\mathbf{E}(\mathbf{r}, \omega) = \int_{-\infty}^{\infty} \mathbf{E}(\mathbf{r}, t) e^{-i\omega t} dt. \tag{2.22}$$

One formally defines

$$\mathbf{D}(\mathbf{r}, \omega) = \varepsilon_0 \mathbf{E}(\mathbf{r}, \omega) - \frac{\mathbf{J}_{\text{ind}}(\mathbf{r}, \omega)}{i\omega}, \quad \mathbf{H}(\mathbf{r}, \omega) = \frac{\mathbf{B}(\mathbf{r}, \omega)}{\mu_0}. \tag{2.23}$$

The overall response is driven by the electric field [108, 109] and we can write formally:

$$\mathbf{J}(\mathbf{r}, \omega) = \int_V \overline{\overline{R}}(\mathbf{r}, \mathbf{r}', \omega) \mathbf{E}(\mathbf{r}', \omega) dV' \tag{2.24}$$

with the overall volume V of the medium. The response tensor $\overline{\overline{R}}(\mathbf{r}, \mathbf{r}', \omega)$ describes in a very abstract and general form the averaged response of the medium upon the electric field $\mathbf{E}$. In this form even possible boundaries of the medium and even inhomogeneous media are described correctly. However, this form is as impracticable as general. In fact, such a representation is only evident in the context of microscopic fields, since it appears paradox to speak about an averaged, homogeneous response if the response tensor is still explicitly depending on $\mathbf{r}$ and $\mathbf{r}'$. Under the assumption of a homogeneous and ideally infinitely extended medium it simplifies to

$$\mathbf{J}(\mathbf{r}, \omega) = \int_V \overline{\overline{R}}(\mathbf{r} - \mathbf{r}', \omega)\mathbf{E}(\mathbf{r}', \omega)dV'. \tag{2.25}$$

The response in now depending only on the difference $\mathbf{r} - \mathbf{r}'$, i.e. the response (induced current) is given by a convolution of the response tensor with the exciting electric field. Again it is advantageous to consider the physical space as being discretized on the microscopic or mesoscopic level, since the assumption above is obviously justified if only discrete lattice points $\mathbf{r}$ are allowed for periodic media.

Assuming, that the response of the medium at a certain point depends only on the actual value of the electric field at that position, the response is said to be local. Different unit cells within the structure are then identical to those at the boundary. If, however, the response depends also on the environment, i.e. neighboring unit cells, no hard boundaries of the homogeneous medium exist. In the simplest case there exists a transition region, which is modeled, even if the structure is isotropic, as an anisotropic layer called Drude transition layer [71, 110, 111]. Such transition layers are important not only on a mesoscopic but also on a microscopic scale and were taken into account already in the early beginning of effective medium theories [112], although their influence for natural media is quite negligible. Some schemes aiming at the determination of effective parameters take these layers phenomenological into account [113]. Note, that within the discretized media picture the macroscopic fields are discretized on the lattice of the periodic structure, too.

Considering the response of a single complex entity it seems to be contradictory to assume, that the response does not depend on neighboring unit cells and not on the local field $\mathbf{E}(\mathbf{r})$ alone. This conflict is resolved by dropping the concept that a non-local response suggests a dependency of the response on the environment. It is better understood as the dependency of the response not only on the field at the position $\mathbf{r}$ but also on arbitrary derivatives of the field at that point. This perception, however, does not exclude the dependency on the environment, since the continuously differentiable fields and its derivatives are determined by the environment. With this modified understanding, which is justified more detailed later on, a consistent understanding seems to be in reach.

Some remarks concerning the concepts above are necessary. Two important limiting cases

exist, which require the introduction of a non-local response. At first, and even if there is no interaction between neighboring unit cells, if the response depends on spatial derivatives of the field and, physically speaking, higher order multipole moments may become important. And at second, if the response is depending on the environment, whereas the single molecules or metaatoms might have only electric and magnetic dipole moments, as it is e.g. for periodic structure with lattice periods that are not negligibly small compared to the wavelength [71]. In any case the non-locality is necessarily related to the ratio of wavelength to unit cell size and averaging volume, respectively.

Returning to the general form of the response in Eq. (2.25) we perform a Fourier transformation with respect to space and end up with:

$$\mathbf{J}(\mathbf{k},\omega) = \tilde{R}(\mathbf{k},\omega)\mathbf{E}(\mathbf{k},\omega) \tag{2.26}$$

where the tensor $\tilde{R}(\mathbf{k},\omega)$ is the spatial Fourier transform of $\overline{\overline{R}}(\mathbf{r},\omega)$. In fact, we arrived here at the most general response of a homogeneous medium with

$$\mathbf{D}(\mathbf{k},\omega) = \varepsilon_0\mathbf{E}(\mathbf{k},\omega) - \frac{1}{i\omega}\tilde{R}(\mathbf{k},\omega)\mathbf{E}(\mathbf{k},\omega) = \varepsilon_0\tilde{\varepsilon}(\mathbf{k},\omega)\mathbf{E}(\mathbf{k},\omega), \tag{2.27}$$

where the tilde indicates the tensorial nature of the permittivity $\tilde{\varepsilon}(\mathbf{k},\omega)$. The Maxwell equations in Fourier space $(\mathbf{k},\omega)$ are then given by:

$$\mathbf{k}\times\mathbf{E}(\mathbf{k},\omega) = \omega\mathbf{B}(\mathbf{k},\omega), \quad \mathbf{k}\cdot\mathbf{D}(\mathbf{k},\omega) = 0, \tag{2.28}$$

$$\mathbf{k}\times\mathbf{H}(\mathbf{k},\omega) = -\omega\mathbf{D}(\mathbf{k},\omega), \quad \mathbf{k}\cdot\mathbf{B}(\mathbf{k},\omega) = 0. \tag{2.29}$$

Hence, we can write for the wave equation for $\mathbf{E}$:

$$\mathbf{k}\times\mathbf{k}\times\mathbf{E}(\mathbf{k},\omega) - \frac{\omega^2}{c^2}\tilde{\varepsilon}(\mathbf{k},\omega)\mathbf{E}(\mathbf{k},\omega) = 0. \tag{2.30}$$

The solution to this eigenvalue equation results in a relation $\omega(\mathbf{k})$ - the dispersion relation of plane waves.

This form is as appealing as impracticable, since only light propagation in a homogeneous, infinitely extended medium can be described, whereas nothing can be said about the boundaries. To handle the interface problem, it is necessary to return to real space via Fourier transformation and to derive adequate transition conditions for the fields at the interfaces. To perform the transition to real space without the convolution integral, the response $\tilde{R}(\mathbf{k},\omega)$ is expanded into a three-dimensional Taylor series at $\mathbf{k} = 0$. While retaining expansion terms of the second order it reads as

$$\tilde{R}(\mathbf{k},\omega) \approx \tilde{R}_{ij}(\mathbf{k}=0,\omega) + \left.\frac{\partial\tilde{R}_{ij}(\mathbf{k},\omega)}{\partial k_k}\right|_{\mathbf{k}=0} k_k + \frac{1}{2}\left.\frac{\partial\tilde{R}_{ij}(\mathbf{k},\omega)}{\partial k_k\partial k_l}\right|_{\mathbf{k}=0} k_k k_l \tag{2.31}$$

$$= -i\omega[a_{ij}(\omega) + a_{ijk}(\omega)k_k + a_{ijkl}(\omega)k_k k_l], \tag{2.32}$$

where the factor $-i\omega$ was separated for convenience and summation over repeating indices is assumed.

Here, some remarks are necessary. At first, for arbitrary small particles the response is local and depends on the field at the position $\mathbf{r}$ only. Its response is entirely expressed by the first term of the expansion. As soon as the variation of the field across the averaging volume is no longer negligible, the response depends in a slightly refined approximation on the wavevector $\mathbf{k}$, too. This is represented by the second term of the sum in Eq. 2.32. For particles that are even larger compared to the wavelength higher terms of the series may contribute in general as well. But generally the particles are small compared to the wavelength, since the averaging volume has to be small to allow for the homogenization. Therefore, the expansion is meaningful at $\mathbf{k} = 0$ only. Indeed the truncation of the series corresponds to a spatial filtering analogous to the truncation of the multipole expansion as we will see later on when comparing both approaches.

At second, certain relations are obtained for the coefficients. Due to the interchangeability of the spatial derivatives for continuously differentiable functions, the indices $k, l, ...$ indicating spatial derivatives can be interchanged arbitrarily. Also, from the Casimir-Onsager-relations for reciprocal media we have $a_{ij} = a_{ji}$, $a_{ijk} = -a_{jik}$ and $a_{ijkl} = a_{jikl}$ and analogously for higher order terms [94].

The approximate expression for $\tilde{R}(\mathbf{k}, \omega)$ can now be reinserted into the current (2.26):

$$J_i(\mathbf{k}, \omega) \approx -i\omega \left[a_{ij}(\omega)E_j(\mathbf{k}, \omega) + a_{ijk}(\omega)k_k E_j(\mathbf{k}, \omega) + a_{ijkl}(\omega)k_j k_k E_j(\mathbf{k}, \omega)\right]. \tag{2.33}$$

Via inverse Fourier-transformation into real space we have:

$$J_i(\mathbf{r}, \omega) \approx -i\omega \left[a_{ij}(\omega)E_j(\mathbf{r}, \omega) + a_{ijk}(\omega)\partial_k E_j(\mathbf{r}, \omega) + a_{ijkl}(\omega)\partial_l\partial_k E_j(\mathbf{r}, \omega)\right]. \tag{2.34}$$

Therefore, we get for $\mathbf{D}$:

$$D_i(\mathbf{r}, \omega) = [\varepsilon_0\delta_{ij} + a_{ij}(\omega)]E_j(\mathbf{r}, \omega) + a_{ijk}(\omega)\partial_k E_j(\mathbf{r}, \omega) + a_{ijkl}(\omega)\partial_l\partial_k E_j(\mathbf{r}, \omega). \tag{2.35}$$

Together with

$$\mathbf{H}(\mathbf{r}, \omega) = \mu_0^{-1}\mathbf{B}(\mathbf{r}, \omega) \tag{2.36}$$

these equations represent the constitutive relations for spatially dispersive media up to the second order spatial dispersion.

Note that the dielectric displacement $\mathbf{D}$ depends not only on the electric field $\mathbf{E}$, but also on its derivatives. This drastically changes the boundary conditions for the fields at interfaces. If $\mathbf{D}$ is not related locally to $\mathbf{E}$ anymore, we cannot conclude via

$$\nabla \times \mathbf{H}(\mathbf{r}, \omega) = -i\omega\mathbf{D}(\mathbf{r}, \omega) \tag{2.37}$$

on the continuity of the tangential components of **H**. Hence, depending on the truncation order of the series, i.e. the number of derivatives of the electric field, additional boundary conditions (ABC) are required [94]. Their introduction is discussed controversially in the literature [114–118] and favorably avoided, whenever possible. Circumventing ABC's is achieved by exploiting the freedom of choice for the definition **D** and **H** as already expressed in Eq. 2.19.

At first we focus on the first derivatives in Eq. (2.35). We choose for **Q**:

$$Q_i = \frac{1}{4}\varepsilon_{jlm}(a_{ilm} - a_{iml} + a_{mli})E_j \tag{2.38}$$

so that we get for **D** and **H**:

$$D_i = \varepsilon_0\varepsilon_{ij}E_j + i\xi_{ij}B_j + a_{ijkl}\partial_l\partial_k E_j, \quad H_i = \mu_0^{-1}B_i + \xi_{ji}E_j \tag{2.39}$$

where $\varepsilon_0\varepsilon_{ij} = \varepsilon_0\delta_{ij} + a_{ij}$ and $\xi_{ij} = \frac{\omega}{4}\varepsilon_{jlm}(a_{ilm} - a_{iml} + a_{mli})$ with ε_{jlm} being the Levi-Civita symbol. Note, that $\tilde{\xi}(\omega)$ as well as $a_{ijkl}(\omega)$ are not dimensionless.

Assuming that the second order derivatives can be neglected, we are at the following bianisotropic constitutive relations

$$\mathbf{D}(\mathbf{r},\omega) = \varepsilon_0\tilde{\varepsilon}(\omega)\mathbf{E}(\mathbf{r},\omega) + i\tilde{\xi}(\omega)\mathbf{B}(\mathbf{r},\omega), \quad \mathbf{H}(\mathbf{r},\omega) = \mu_0^{-1}\mathbf{B}(\mathbf{r},\omega) + i\tilde{\xi}^T(\omega)\mathbf{E}(\mathbf{r},\omega). \tag{2.40}$$

Importantly, by this transformation (2.38) not only the constitutive relations are changed but also the corresponding boundary conditions. The solution of the electromagnetic problem, however, remains the same, independent of the particular choice of constitutive relations. For media with spatial dispersion up to this first order, whose constitutive relations do not contain spatial derivatives explicitly, the boundary conditions are the standard ones, i.e. the continuity of the tangential **E** and **H** components and of the normal **D** and **B** components. In fact, achieving these simple boundary conditions is the reason for performing this transformation.

Media that are characterized by a non-vanishing parameter $\tilde{\xi} \neq 0$ (chirality parameter) are termed chiral media due to a certain geometrical property. For the sake of simplicity let us assume an isotropic medium where $\tilde{\xi} = \xi\mathbb{I}$. If the medium is mirror-symmetric, its optical properties remain the same under reflection, i.e. the material parameters including ξ are even upon space inversion. Since **D** and **B** behave different upon inversion (one is even, the other is odd), we must have $\xi = 0$ [94]. Hence, for mirror-symmetric (achiral) media $\xi = 0$. Mirror-asymmetric media are called chiral. In fact, the definition of chirality is more restrictive. A medium is called chiral, if its mirror image is not super-imposable with the original structure by a proper rotation. I.e., in the general anisotropic case the first derivatives do not vanish for directions where the structure is not mirror-symmetric, although the overall structure might be achiral. That is for example the case for media, that

have at most two orthogonal mirror planes like such as the SRR [46, 119]. Only in isotropic media the lack of a mirror symmetry in a certain direction means that there is no mirror symmetry at all, rendering the structure essentially chiral.

Since the relations given above are purely algebraic, it is always possible to determine two of them, if the other two are given. More commonly one defines accordingly:

$$\mathbf{D}(\mathbf{r},\omega) = \varepsilon_0\tilde{\varepsilon}(\omega)\mathbf{E}(\mathbf{r},\omega) + i\frac{1}{c}\tilde{\kappa}(\omega)\mathbf{H}(\mathbf{r},\omega) \tag{2.41}$$

$$\mathbf{B}(\mathbf{r},\omega) = \mu_0\tilde{\mu}(\omega)\mathbf{H}(\mathbf{r},\omega) - i\frac{1}{c}\tilde{\kappa}^T(\omega)\mathbf{E}(\mathbf{r},\omega), \tag{2.42}$$

where the tensor of magnetoelectric coupling $\kappa(\omega)$ is dimensionless as well as $\varepsilon(\omega)$ and $\mu(\omega)$.

The terms containing the second order derivatives are much more difficult to handle and an unique decomposition is possible only in case of an isotropic medium [58, 94, 120]. One can show, that the only isotropic differential operators are given by $(\nabla\nabla\cdot)$ and $(\nabla\times\nabla\times)$. Therefore, we have for isotropic media the constitutive relations:

$$\mathbf{D} = \varepsilon_0\varepsilon\mathbf{E} + i\xi\mathbf{B} + \beta\nabla\nabla\cdot\mathbf{E} + \gamma\nabla\times\nabla\times\mathbf{E} \tag{2.43}$$

$$\mathbf{H} = \mu_0^{-1}\mathbf{B} + i\xi\mathbf{E}. \tag{2.44}$$

Since $\nabla\times\mathbf{E} = i\omega\mathbf{B}$ we can try to find another transformation $\mathbf{Q}$, which allows to transfer the second order derivatives into $\mathbf{H}$. This is accomplished by choosing

$$\mathbf{Q} = -\gamma\nabla\times\mathbf{E} = -i\omega\gamma\mathbf{B}. \tag{2.45}$$

Together with

$$\mu(\omega) = \frac{1}{1-\omega^2\mu_0\gamma(\omega)} \tag{2.46}$$

we have:

$$\mathbf{D} = \varepsilon_0\varepsilon\mathbf{E} + i\xi\mathbf{B} + \beta\nabla\nabla\cdot\mathbf{E}, \quad \mathbf{H} = \mu_0^{-1}\mu^{-1}\mathbf{B} + i\xi\mathbf{E}. \tag{2.47}$$

We can conclude that magnetic properties of reciprocal media are manifestations of second-order spatial dispersion. That is the important message for research on metamaterials.

Let us assume that the parameter β is negligible. This is the case, if the structures are designed such, that the induced currents resemble clearly defined circular paths. In this case the electric quadrupole moment is negligible compared to the magnetic dipole moment. Compare e.g. the multipole moments of the cut-wire-plates and split ring resonators [63, 69]. If $\beta = 0$, we arrive at the most general constitutive relations for isotropic, local media.

Since in most cases the structures do not posses cubic symmetry (generally speaking symmetries leading to isotropic properties in the quasi-static limit), it is necessary to elaborate the case of anisotropic media. Here, the second order derivatives cannot be decomposed

as simply as in the isotropic case. Only requirements on the expansion coefficients can be derived, such that the response can be described by local constitutive relations. To obtain local constitutive relations with an anisotropic artificial magnetic response, we require only that the following identity holds:

$$a_{ijkl}\partial_k\partial_l E_j = \sum_{j=1}^{3}\sum_{k=1}^{3}\sum_{l=1}^{k}\tilde{a}_{ijkl}\partial_k\partial_l E_j \stackrel{!}{=} (\nabla\times[\tilde{\gamma}\nabla\times\mathbf{E}])_i \tag{2.48}$$

$$= \begin{pmatrix} \gamma_{yy}\partial_x\partial_z E_z - \gamma_{yy}\partial_z\partial_z E_x + \gamma_{zz}\partial_x\partial_y E_y - \gamma_{zz}\partial_y\partial_y E_x \\ \gamma_{xx}\partial_y\partial_z E_y - \gamma_{xx}\partial_z\partial_z E_y + \gamma_{zz}\partial_x\partial_y E_x - \gamma_{zz}\partial_x\partial_x E_y \\ \gamma_{xx}\partial_y\partial_z E_y - \gamma_{xx}\partial_y\partial_y E_z + \gamma_{yy}\partial_x\partial_z E_x - \gamma_{yy}\partial_x\partial_x E_z \end{pmatrix} \tag{2.49}$$

where we have assumed, that the tensor $\tilde{\gamma}$ can be diagonalized. The sum on the left is truncated, since we have $a_{ijkl}(\omega) = a_{ijlk}(\omega)$. Comparing the coefficients results in:

$$\begin{pmatrix} \underline{\tilde{a}_{xzxz}=\gamma_{yy}}\,, & \tilde{a}_{xxzz}=-\gamma_{yy}\,, & \underline{\underline{\tilde{a}_{xyxy}=\gamma_{zz}}}\,, & \tilde{a}_{xxyy}=-\gamma_{zz} \\ \underline{\underline{\tilde{a}_{yzyz}=\gamma_{xx}}}\,, & \tilde{a}_{yyzz}=-\gamma_{xx}\,, & \underline{\underline{\tilde{a}_{yxyx}=\gamma_{zz}}}\,, & \tilde{a}_{yyxx}=-\gamma_{zz} \\ \underline{\underline{\tilde{a}_{zyzy}=\gamma_{xx}}}\,, & \tilde{a}_{zzyy}=-\gamma_{xx}\,, & \underline{\tilde{a}_{zxzx}=\gamma_{yy}}\,, & \tilde{a}_{zzxx}=-\gamma_{yy} \end{pmatrix}$$

where the underline means, that these coefficients are necessarily identical to fulfill relation (2.48). Note that the coefficients fulfill the following important relations:

$$a_{ijkl}(\omega) = a_{jikl}(\omega) \quad \text{and} \quad a_{ijkl}(\omega) = a_{ijlk}(\omega).$$

For media without magneto-electric coupling we have:

$$D_i = (\varepsilon_0\delta_{ij} + a_{ij})E_j + a_{ijkl}\partial_k\partial_l E_j = \varepsilon_0\varepsilon_{ij}E_j + (\nabla\times[\tilde{\gamma}\nabla\times\mathbf{E}])_i\,. \tag{2.50}$$

We then choose

$$Q = \tilde{\gamma}\nabla\times\mathbf{E}. \tag{2.51}$$

to get

$$D_i(\mathbf{r},\omega) = \varepsilon_0\varepsilon_{ij}(\omega)E_j(\mathbf{r},\omega) \quad \text{und} \quad H_i(\mathbf{r},\omega) = \mu_0^{-1}B_i + \gamma_{ij}(\omega)B_j = \mu_0^{-1}\mu_{ij}^{-1}(\omega)B_j(\mathbf{r},\omega). \tag{2.52}$$

We can conclude that a medium, which is homogenizable and which can be characterized by weak spatial dispersion, might be described by local constitutive relations under some restrictions ($\beta = 0$). On the other hand, it is always possible to transform local bi-anisotropic constitutive relations (at optical frequencies, excluding intrinsic magnetism) into constitutive relations with only a single but generally complicated spatially dispersive permittivity $[\varepsilon_{ij}(\mathbf{k},\omega)]$ [75, 118].

Eventually, a comparison between the expansion within the multipole approach and the phenomenological approach is performed. At first, is seems that there is a discrepancy

between the equations in both approaches. We have shown above in the context of the phenomenological approach, that an artificial magnetic response, can exist, which manifests itself in second order spatial dispersion. I.e., the response is related to the second order derivatives of the electric field. Such an magnetic response is often accompanied by an electric quadrupolar response. On the contrary, if the equations of the multipole expansion are considered, the electric quadrupole density as well as the magnetic dipole density are related to first order derivatives. Also, the manifestations of chirality are related to first order derivatives in the phenomenological picture, whereas in [95] the authors note, that chirality appears within 'magnetic-dipole' - 'electric-quadrupole' order. Obviously, e.g. quadrupoles may contribute in terms of first order as well as in second order but generally also within higher order spatial dispersion. The reason for the apparent conflict arises from the modeling of the microscopic dynamic of the multipole densities. This is explained at the example of an electric quadrupole. The primitive quadrupole moment q_{ij} is defined as [95]:

$$q_{ij} = \int_V \rho(\mathbf{r}) x_i x_j \, dV, \tag{2.53}$$

where $\rho(\mathbf{r})$ is the microscopic charge density. This density might depend on the actual value of the field at the position $\mathbf{r}$, but also on arbitrary derivatives of the field, i.e.

$$\rho(\mathbf{r}) = \rho(\mathbf{r}(\mathbf{E}, \nabla\mathbf{E}, ...)). \tag{2.54}$$

Hence, the quadrupole moment will depend on the field as well as on its derivatives, too. The quadrupole moment appears in the expansion within the phenomenological picture in all terms with at least a single spatial derivative. A simple example can be found in [64]. There, the density depends on the gradient of the field and therefore the effective permittivity depends on the second derivatives.

As a more general conclusion, we can state, that the difference between both approaches finally lies in the ordering of the terms entering the constitutive relations. Whereas in the multipole approach the terms are sorted according to their physical appearance, i.e. the multipole moments, in the phenomenological approach they are sorted according to their impact in terms of derivatives. Hence, a direct comparison is only possible for a particular structure.

2.3 Chapter summary and concluding remarks

In the preceding chapter the derivation of the macroscopic Maxwell equations for homogeneous media was recapitulated. Emphasis was put on the non-uniqueness of the definition of the material fields $\mathbf{D}$ and $\mathbf{H}$. This non-uniqueness can be used to obtain a customized

form of the Maxwell equations, i.e. of the constitutive relations, leading to a simple form of the boundary conditions. Furthermore it was shown, that a complex, spatially dispersive material response can lead to an artificial magnetic response - the main driving force of metamaterials today.

To conclude on the applicability of the averaging and the expansion it is necessary to compare their predictions to the actual response. Hence, one has to consider each metamaterial of interest individually, whether the response can be described by homogeneous equations and effective material parameters or not. The discussion was expediently restricted to local effective material parameters. If the considered media cannot be described by these local effective parameters, it is better to refuse from using an effective homogeneous description. It is more appropriate to use the general framework of periodic media, i.e. to drop the assumption of a homogeneous medium and to work within an inhomogeneous description with all its subtleties. Describing the medium's response with constitutive relations beyond the local ones leads to a cumbersome increase of effective tensorial parameters and the issue of additional boundary conditions remains, rendering such a description inefficient.

The constitutive relations for local effective materials derived above will be compared in the following chapters with the actual response of the certain systems and it is shown under which circumstances such an effective description can be applied.

3 The S-parameter retrieval

In the previous chapter the description of MMs in terms of local material parameters was motivated and possible constitutive relations were derived. The question remains, how to determine these material parameters for a particular MM. There exists a variety of methods dedicated to their calculation ranging from quasi-static [60] and integral methods [74–79] to those we will focus on here, namely the so called S-parameter retrieval (S-PR). By S-PR we want to understand the determination of effective material parameters form the complex reflection and transmission coefficients R and T of a slab with finite thickness. The basic idea is quite simple. Analytical expressions for the complex reflection and transmission coefficients are calculated for a slab of a medium obeying certain constitutive relations. Then these expressions are inverted to determine the material parameters. Depending on the assumed constitutive relations several pairs of R and T are in general necessary to obtain the complete set of material parameters. For example, for local isotropic media and also for local bi-isotropic media only a single pair of R and T is necessary, as will be shown in section 3.1 and 3.2. In its initial proposal by Nicholson, Ross and Weir [80,81] and later on by D.R. Smith et al. [82] the retrieval was established for normal incidence and scalar values of the effective permittivity and permeability. The extension to oblique incidence [88] and chiral structures was first reported by us [121] and D. H. Kwon [122], respectively. Furthermore, extensions to bianisotropic systems were proposed by Chen [123] and Kriegler [124], which are in particular suitable for the effective description of systems containing split ring resonators. Also versions taking into account surface layers [113], different terminations of the system [90], procedures applicable to half-spaces [125] and so called wave propagation methods [126, 127] were put forward. Here, however, the focus is on the retrieval from R and T at finite systems. The meaning of the reduction of R and T to a few parameters describing the physics of the basic light matter interaction is quite obvious highly appreciated, since R and T are depending even for a fixed frequency still on the polarization and the propagation direction, the shape of the structure and its size.

In the following sections expressions for the retrieval of the material parameters for anisotropic media with diagonal permittivity and permeability tensors for normal as well as oblique incident plane waves are derived for specific illumination directions. An analogous procedure to obtain the material parameters of an bi-isotropic slab system is elaborated

afterwards. Both systems are governed by local constitutive relations, i.e. the retrieval of effective material parameters will be restricted to those of a local medium. Furthermore, the retrieval of effective parameters at oblique incidence will provide a powerful tool to probe for the locality of the system under consideration. Namely, if the wave parameters k and ξ, which are properties of the wave propagating inside the structure, cannot be reduced uniquely to the simpler set of material parameters, the slab system cannot be considered as a local medium.

After having elucidated the retrieval procedure of effective material parameters, the retrieval procedure is discussed from a periodic medium perspective in section 3.3. The reflection and transmission coefficients for periodically arranged unit cells, each consisting of an arbitrary number of stratified layers, are derived. It will be shown that the effective wave parameters k and ξ as retrieved from R and T are well defined for arbitrary symmetric systems. Hence, the retrieval of wave parameters at stratified media is proven to be essentially meaningful, whereas effective material parameters need not to be assigned in general. That scheme is then extended to the more important case of three-dimensional structures. It is equally shown that the wave parameters are usually well defined and the range of applicability of the retrieval to three-dimensional systems is discussed. The retrieved parameters are proven to be generally convergent for lossy systems with an increasing thickness of the structure. Their analogues with respect to the periodic medium perspective are identified. In particular the issue of the convergence of the effective parameters as a function of the thickness of the considered layer plays an important role for their physical interpretation. This necessarily asks for a discussion of the meaning of effective parameters depending on the thickness of the considered slab. In this summarizing section we also formulate some take home messages. They may serve as more basic guidelines to discuss the physics of effective properties in such systems.

3.1 The S-parameter retrieval for anisotropic metamaterials

In this subsection the complex reflection and transmission coefficients R and T for a slab of an biaxial anisotropic material are briefly derived and it is shown how to obtain the wave and eventually the material parameters by inversion of the analytic expressions for R and T. In particular the choice of the correct signs for the wave parameters and issues related to the interpretation of the effective parameters are discussed in detail.

Starting by the assumption of a medium, that possesses three orthogonal mirror planes, each of them coinciding with two principal coordinate axes, we are dealing with the most

general local constitutive relations

$$D_i(\mathbf{r},\omega) = \varepsilon_0 \varepsilon_{ij}(\omega) E_j(\mathbf{r},\omega)\,, \;\; B_i(\mathbf{r},\omega) = \mu_0 \mu_{ij}(\omega) H_j(\mathbf{r},\omega) \tag{3.1}$$

with the electric field $\mathbf{E}$, the magnetic field $\mathbf{H}$, the electric displacement $\mathbf{D}$ and the magnetic induction $\mathbf{B}$. For this geometry the permittivity tensor $\varepsilon_{ij}(\omega) = \varepsilon_i(\omega)\delta_{ij}$ and the permeability tensor $\mu_{ij}(\omega) = \mu_i(\omega)\delta_{ij}$ are diagonal, due to the alignment of the crystal axis with the principal coordinate system. In the following the frequency dependency as well as the spatial dependency of the fields and material parameters is suppressed but kept in mind. Such an anisotropic medium is in general biaxial without a so called ordinary polarized wave. The eigenmodes are linearly polarized orthogonal plane waves with different propagation vector $\mathbf{k}$ (see e.g. [97, 128]). For the general case of light propagation in an arbitrary direction the reflection and transmission problem is solved by the so called 4x4 formalism (see e.g. [128, 129]).

However, here the focus is on calculating R and T at a finite slab of such medium for the case of light propagation with $\mathbf{k}$ being parallel to one of the mirror planes. This dramatically simplifies the calculation and even more important the inversion. The geometry is shown in Fig. 3.1. Without lost of generality the slab is assumed to be infinitely extended in the

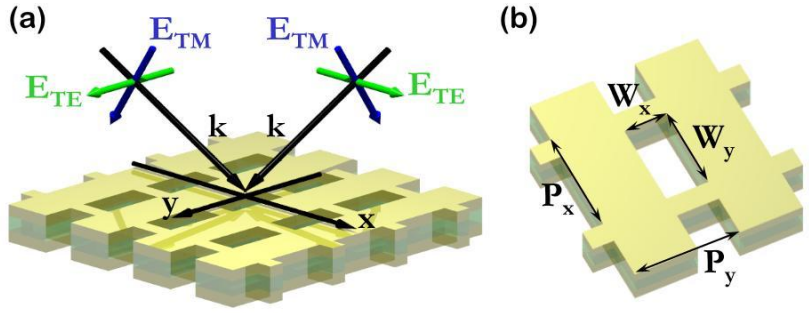

Figure 3.1: (a) Schematic view of the geometry with the four principal directions for the retrieval at the example of the single fishnet layer. The halfspace above the MMs slab ($z < 0$) is called substrate. The halfspace below ($z > d$) is called cladding. (b) Unit cell of the fishnet with $P_x = P_y = 600\,\text{nm}$, $W_x = 284\,\text{nm}$, $W_y = 500\,\text{nm}$ embedded in air as used for the calculations in chapter 4. The thickness of the silver layer is $d_{\text{Ag}} = 45\,\text{nm}$ and the thickness of the intermediate MgF_2 ($n = 1.38$) layer is $d = 30\,\text{nm}$

x-y-direction with a finite thickness d in the z-direction. Furthermore it is assumed to be embedded between two isotropic half-space named substrate (index s) and cladding (index c). Then the wavevector $\mathbf{k}$ can be separated into a tangential part $k_\text{t} \in \{k_x, k_y\}$ and the propagation constant k_z, where $k_\text{t} = \text{const.}$ in all domains. The eigenmodes of the overall system can be separated into those, which are perpendicularly polarized to the plane of incidence (TE) and those which are parallel polarized (TM) with their electric field. In that case light that is TE(TM)-polarized maintains its polarization state in transmission as well

as in reflection. Hence, the calculation of R and T at the anisotropic slab is almost identical to the calculation of R and T at its isotropic counterpart. This allows to use the simpler 2x2 formalism. Such a simplification seems to be unjustified, but it is completely sufficient for our purposes, namely retrieving the effective material tensors. Already from four pairs of R and T the complete set of tensors elements of ε_{ij} and μ_{ij} can be determined as we will see later on. Finally the treatment of isotropic and anisotropic slabs is completely analogous since the R-T-problem is entirely determined by the propagation constant k_z inside the film/slab (index f) and the ratio of the continuous tangential field components given by the tangential impedance $Z_\mathrm{t} = E_\mathrm{t}/H_\mathrm{t}$. These two quantities are the basic wave parameters of the system. That finding has important consequences, when the R-T-problem is discussed for symmetric unit cells of stratified media as shown in 3.3.

By introducing polarization dependent abbreviations it is possible to treat both, TE and TM polarization, simultaneously. The reflection and transmission coefficients for propagation in z-direction are given by

$$T = \frac{2\xi_\mathrm{s}\xi_\mathrm{f}A}{\xi_\mathrm{f}(\xi_\mathrm{s}+\xi_\mathrm{c})\cos(kd) - i(\xi_\mathrm{f}^2+\xi_\mathrm{s}\xi_c)\sin(kd)} \tag{3.2}$$

$$R = \frac{\xi_\mathrm{f}(\xi_\mathrm{s}-\xi_\mathrm{c})\cos(kd) + i(\xi_\mathrm{f}^2-\xi_\mathrm{s}\xi_\mathrm{c})\sin(kd)}{\xi_\mathrm{f}(\xi_\mathrm{s}+\xi_\mathrm{c})\cos(kd) - i(\xi_\mathrm{f}^2+\xi_\mathrm{s}\xi_\mathrm{c})\sin(kd)} \tag{3.3}$$

where $k = k_z$ is the normal component of the propagation constant inside the film and ξ_i is, depending on the polarization, proportional to the tangential impedance or its inverse, respectively. Note that these expressions for R and T are generally valid not only for both polarizations but for normal as well as oblique incidence. The introduced polarization dependent abbreviations are given by

$$A_\mathrm{TE} = 1,\ A_\mathrm{TM} = \sqrt{\frac{\varepsilon^\mathrm{s}\mu^\mathrm{c}}{\varepsilon^\mathrm{c}\mu^\mathrm{s}}},\ \xi_\mathrm{i} = \alpha^\mathrm{i}k_z^\mathrm{i},\ k = k_z^\mathrm{f},\ k_z^\mathrm{i} = \sqrt{\frac{\omega^2}{c^2}\beta^\mathrm{i} - \gamma^\mathrm{i}k_\mathrm{t}^2} \tag{3.4}$$

and are connected to the material parameters by the following substitution table. The

	TE		**TM**	
	$k_x = 0$	$k_y = 0$	$k_x = 0$	$k_y = 0$
α	$1/\mu_y$	$1/\mu_x$	$1/\varepsilon_y$	$1/\varepsilon_x$
β	$\varepsilon_x\mu_y$	$\varepsilon_y\mu_x$	$\varepsilon_y\mu_x$	$\varepsilon_x\mu_y$
γ	μ_y/μ_z	μ_x/μ_z	$\varepsilon_y/\varepsilon_z$	$\varepsilon_x/\varepsilon_z$

Table 3.1: Substitution table for the relevant coefficients depending on the polarization and the incidence plane.

isotropic cladding and the substrate are characterized in their properties by $\varepsilon_{ij}^{\mathrm{s,c}} = \varepsilon^{s,c}\delta_{ii}$ and

$\mu_{ij}^{\mathrm{s,c}} = \mu^{\mathrm{s,c}}\delta_{ii}$ and hence $\gamma^{\mathrm{s,c}} = 1$. The equations for R and T are given in this compact form because it conveniently allows to invert of R and T to obtain k and $\xi = \xi_{\mathrm{f}}$. Then we have

$$kd = \pm \arccos\left(\frac{\xi_{\mathrm{s}}(1-R^2) + \xi_{\mathrm{c}}(T/A)^2}{(T/A)[\xi_{\mathrm{s}}(1-R) + \xi_{\mathrm{c}}(1+R)]}\right) + 2m\pi \tag{3.5}$$

with $m \in \mathbb{Z}$ and

$$\xi = \pm\sqrt{\frac{\xi_{\mathrm{s}}^2(R-1)^2 - \xi_{\mathrm{c}}^2(T/A)^2}{(R+1)^2 - (T/A)^2}}. \tag{3.6}$$

The two complex quantities R and T are now replaced by k and ξ. Upon inversion some degrees of freedom emerge due to the periodic functions while inverting the trigonometric functions and choosing the proper sign for the square root. However, there exists only a single physical solution. At first the sign of k can be fixed by imposing the constraint of passivity, i.e. we do not allow for exponentially growing waves if the materials the unit cell is made of are all intrinsic passive [82]. Hence, the imaginary part of k has to be positive for the chosen coordinate system. In fact, this ultimately fixes also the sign of ξ, since only by simultaneously changing the signs of k and ξ, R and T remain unaltered (see Eqs. 3.2 and 3.3). However, as will be shown later, also the sign of ξ can be fixed by physical constraints independent of k, if ξ is well defined. At second, due to the periodicity of the trigonometric functions, the value of m needs to be fixed. That is indeed more subtle and difficult to disclose experimentally. As kd is the phase advance upon single transmission inside the slab, it has to vanish for $d \to 0$ or $k \to 0$. Since the phase advance can be larger than π, it is generally not possible to conclude on the value of m by only taking a single functional layer. The best method, which is unfortunately not applicable in experiments, is to scale down the unit cell size in propagation direction, i.e. maintaining the transversal geometry while decreasing the thickness of all individual layers in propagation direction continuously. For an infinitesimal thin slab the phase advance has to be zero and hence $m = 0$. The value of m for the thickness of interest can then be adjusted by increasing the structure to the original size while enforcing a continuous phase advance. Any discontinuity that would occur in this scaling process can be compensated by adjusting the branch number m. The more practicable method is to increase the wavelength towards infinity, hence reaching $k_0 \to 0$ and therefore $kd \to 0$. Again by assuming for the largest wavelength $m = 0$, the real part of k can be chosen continuously. But that limit is often hard to reach for example for metallic structures having a strong dispersion for larger wavelength, too. Of course for non-dispersive systems scaling down the size is equivalent to an increase of the wavelength.

As already said before, the sign of ξ is fixed by the sign of k in general. However, lets have a closer look at that quantity. Lets assume a fixed propagation direction with $k_y = 0$. Depending on the polarization we have with $\xi_{\mathrm{i}} = \alpha^{\mathrm{i}} k_z^{\mathrm{i}}$

$$\text{TE: } \xi_{\mathrm{i}} = \frac{k_z^{\mathrm{i}}}{\mu_y^{\mathrm{i}}} = \frac{\omega}{c}\frac{1}{Z_{\mathrm{i,t}}^{xy}}\ , \quad \text{TM: } \xi_{\mathrm{i}} = \frac{k_z^{\mathrm{i}}}{\varepsilon_y^{\mathrm{i}}} = \frac{\omega}{c} Z_{\mathrm{i,t}}^{yx} \tag{3.7}$$

where $Z^{kl}_{\mathrm{i,t}} = \frac{E_k}{H_l}$ is the tangential impedance in medium $i \in \{\mathrm{s,c,f}\}$ determined by the tangential components E_k and H_l. Let us briefly prove that. Consider a plane wave in TE-polarization ($\mathbf{E} = E_y\mathbf{e_y}$). The tangential magnetic field H_x of that plane wave is then determined by the curl equation

$$\nabla \times \mathbf{E} = i\mathbf{k} \times \mathbf{E} = i\omega\mu_0 \begin{pmatrix} \mu_x H_x \\ 0 \\ \mu_z H_z \end{pmatrix}, \tag{3.8}$$

so the ratio of the tangential field components (H_x is pointing into the negative x-direction) is given by

$$\frac{E_y}{-H_x} = \frac{\omega\mu_0\mu_x}{k_z} = \frac{k_0\mu_x}{k_z}\sqrt{\frac{\mu_0}{\varepsilon_0}} = k_0 Z_0 \frac{1}{\xi} = Z^{xy}_{\mathrm{t}} Z_0. \tag{3.9}$$

Hence, for TE-polarization ξ gives the inverse of the relative tangential impedance Z_{t} times the vacuum wavenumber k_0. For TM-polarization the calculation is done analogously. This relation holds for normal as well as for oblique incidence. In particular at normal incidence we have

$$\text{TE: } \xi_{\mathrm{i}} = \frac{\omega}{c}\frac{\sqrt{\varepsilon^{\mathrm{i}}_x \mu^i_y}}{\mu^i_y} = \frac{\omega}{c}\frac{1}{Z^{xy}_{\mathrm{t}}}\ , \quad \text{TM: } \xi_{\mathrm{i}} = \frac{\omega}{c}\frac{\sqrt{\varepsilon^{\mathrm{i}}_y \mu^{\mathrm{i}}_x}}{\varepsilon^{\mathrm{i}}_y} = \frac{\omega}{c} Z^{yx}_{\mathrm{t}}. \tag{3.10}$$

The superscripts (k,l), that indicate the polarization, will be suppressed in the following. Here a second constraint can be applied. For passive media the Poynting vector being proportional to the real part of the impedance has to be positive [82]. Hence, the sign of ξ can be chosen such, that the real part is positive. However, as said before the sign of ξ is fixed anyway and for truly local media the real part is then positive already by the constraint of passivity on the imaginary part of k. One practical note might be in order. Though the sign of ξ is fixed by the sign of k, it is unknown. Therefore, this second constraint is of practical importance. The best way to fix the sign of ξ is to adjust it so that the values of R and T calculated by the retrieved values of k and ξ coincide with the original ones.

At this stage the parameters k and ξ are completely determined. Those two parameters are an equivalent representation of the reflection and the transmission coefficients of a certain slab. As both are describing the properties of the wave propagating inside the structure, they are named wave parameters. Both can, however, depend on the direction of light propagation, i.e. they are functions of the frequency and the angle of incidence. If the assumption of a local medium is valid, the number of coefficients can be reduced to the six angle independent tensor elements $\varepsilon_{ij}(\omega)$ and $\mu_{ij}(\omega)$. This can be done quite easily. At first, the parameter α is given by the ratio $\alpha = \xi/k$. Depending on the polarization α is the inverse of a local parameter. Therefore, α is supposed to be independent on the angle of incidence. This finding provides a very powerful tool, since the investigation of the angular dependency provides the possibility to probe for the locality of the system. Only if α is independent on

the angle of incidence, local material parameters might be assigned. Otherwise, either more complex, nonlocal constitutive relations should be used, which properly take into account the non-locality of the system (that results in different analytical expressions for R and T). Or the retrieval should be restricted to the wave parameters, that might be well defined anyway. (The greater generality of the wave parameters retrieved from the expressions of R and T above, will be shown in section 3.3.) At second, assuming that α is a function of the frequency only, the value of β can be determined from k at normal incidence and then from oblique incidence the value of γ. By using table 3.1 the elements of the material tensors are determined. Of course all of them have to be functions of the frequency only to support the assumption of locality. Eventually, if the retrieved parameters depend on the angle of incidence, the assumption of locality has to be dropped. Then, the system is better described as an essentially inhomogeneous system, maybe in terms of angle dependent wave parameters. Note that the reduction to angle dependent wave parameters is still useful when their values do not depend on the number of functional layers (see section 3.3). The issue of thickness dependent parameters will be discussed below.

A few comments on the retrieval algorithm are necessary. At normal incidence, only four of the tensor elements can be probed, namely the x and y components of the effective parameters. At normal incidence any arbitrarily polarized light can be decomposed in two orthogonal polarizations that are parallel to the x- or y-axis. Hence, only two measurements are linearly independent and every tensor component can be probed only once. From such a measurement one cannot conclude on locality at all. From a single measurement it is not possible to conclude on the applicability of the retrieval. That's the reason why the assignment of effective material parameters by the S-PR was done for such a long time without being questioned. Effective material parameters were assigned at normal incidence only before we proposed a method to investigate the angular dependency. The locality of the material parameters is essential for the applicability of the retrieval of effective material parameters. Presumed that the parameters are local, an additional measurement of the complex R and T coefficients at oblique incidence is necessary to probe for the normal components of the material tensors. Only at oblique incidence γ can be resolved, whereas α and β are identical to normal incidence. To resolve all six tensor elements four pairs of complex R and T are necessary, namely for TE and TM and both at two different angles of incidence.

Finally, the applicability of the retrieval from a more abstract point of view is discussed. The retrieval of the parameters k and ξ is applicable to any system that is maintaining the polarization of the incidence light. This is true for light propagating parallel to a mirror plane of any structure. All information about the scattered far field is captured in R and T as soon as only a zeroth propagating order exists, i.e. the system has to be subwavelength in

lateral direction. In that case k and ξ, entering the equations of R and T independently, are a well defined representation of the complex scattering coefficients. Since k and ξ are generally independent functions with respect to the angle of incidence, there is no contradiction in expressing R and T by the wave parameters k and ξ. But these values cannot be identified with physical quantities in general. They are simply another representation of R and T for a specific illumination scenario at a specific slab system. However, contradictions may arise when material parameters are assigned, which are required to be constant with the angle of incidence. The assignment of effective material parameters is generally much more demanding. So the set of media, where effective wave parameters are applicable contains the set of local media. Even if wave parameters can be assigned uniquely, local material parameters are not generally assignable.

3.2 The S-parameter retrieval for chiral metamaterials

In this subsection the complex reflection and transmission coefficients for a slab of an isotropic chiral medium are derived [121]. Then the inversion to determine, in particular, the chirality parameter $\kappa(\omega)$, which accounts for the optical activity of a chiral medium, is performed. Such an isotropic chiral medium is termed Pasteur-medium [130] and obeys constitutive relations of the form

$$\mathbf{D}(\mathbf{r},\omega) = \varepsilon_0\varepsilon(\omega)\mathbf{E}(\mathbf{r},\omega) - i\frac{\kappa(\omega)}{c}\mathbf{H}(\mathbf{r},\omega)\,, \quad \mathbf{B}(\mathbf{r},\omega) = \mu_0\mu(\omega)\mathbf{H}(\mathbf{r},\omega) + i\frac{\kappa(\omega)}{c}\mathbf{E}(\mathbf{r},\omega) \quad (3.11)$$

with the permittivity $\varepsilon(\omega)$, the permeability $\mu(\omega)$ and the chirality parameter $\kappa(\omega)$. The frequency dependency will be suppressed in the following. As the medium is isotropic one can choose $\mathbf{k} = k\mathbf{e_z}$ without lost of generality. The eigenpolarisations of such are medium are left and right circularly polarized plane waves with the following propagation constants

$$\mathbf{E}_+ = (1, +i, 0) \;:\; k_+^{\pm} = \frac{\omega}{c}(\pm\sqrt{\varepsilon\mu} - \kappa) \quad (3.12)$$

$$\mathbf{E}_- = (1, -i, 0) \;:\; k_-^{\pm} = \frac{\omega}{c}(\pm\sqrt{\varepsilon\mu} + \kappa) \quad (3.13)$$

where the lower index sign designates the eigenstate and the upper $\pm$ sign accounts for forward and backward propagation. As a very important property of such a medium, a particular eigenwave (index + or -) propagating in opposing directions has a different propagation constant and a different rotation direction. I.e., upon reflection right circularly polarized light (rcp) changes to left circularly polarized light (lcp) and vice versa, where the outer medium is assumed to be bi-isotropic in general. This becomes more obvious, when the boundary conditions are considered. As all fields $(\mathbf{E}, \mathbf{D}, \mathbf{B}, \mathbf{H})$ are finite, we can conclude from Maxwell's curl equations that the ordinary boundary conditions can be applied, i.e. the continuity of the tangential $\mathbf{E_t}$ and $\mathbf{H_t}$ fields. As we are only considering normal incidence,

the entire **E** and **H** fields are continuous. Due to the isotropy, any component of e.g. the electric field is affected indistinguishable upon reflection. Hence, the polarization state is maintained and no cross-coupling occurs between the eigenstates at the boundary between two generally bi-isotropic media. As an example consider $\mathbf{E}_+$-polarized light impinging on an interface. The reflected field is then given by

$$\mathbf{E}^R(z,t) = R\mathbf{E}_+ e^{ik_+^- z} e^{-i\omega t} \tag{3.14}$$

with the complex scalar reflection coefficient R. Lets now rotate the coordinate system by 180 degrees with respect to the x-axis yielding a forward propagating wave ($y \to -y$, $z \to -z$). Then the reflected field is given by

$$\mathbf{E}^R(-z,t) = R\mathbf{E}_- e^{ik_-^+ z} e^{-i\omega t} \tag{3.15}$$

with $k_+^- = -k_-^+$. I.e., the reflected $\mathbf{E}_+$ -wave as seen from the backside is a forward propagating $\mathbf{E}_-$ -wave. From these considerations we can already conclude that the additional phase resulting from κ accumulated in transmission, is compensated upon reflection. Therefore, an isotropic chiral medium changes the polarization state of linearly polarized light only in transmission but not in reflection. This will be shown in the next paragraph by direct calculation.

As already said before, the calculation of R and T can be done for both eigenstates independently since they do not couple. Hence, both polarizations can be treated simultaneously. To calculate R and T we need the continuity of both the electric and the magnetic field. The magnetic field is determined at first. From the curl equation we get

$$\nabla \times \mathbf{E} = \begin{pmatrix} -\partial_z E_y \\ \partial_z E_x \\ 0 \end{pmatrix} = i\omega \left[\mu_0\mu \begin{pmatrix} H_x \\ H_y \\ 0 \end{pmatrix} + i\frac{\kappa}{c} \begin{pmatrix} E_x \\ E_y \\ 0 \end{pmatrix} \right] \tag{3.16}$$

Rearranging the terms and expressing the **E**-fields and the **H**-fields in terms of the eigenstates $\mathbf{E} = (1, \pm i, 0)^T E_\pm = E_\pm \mathbf{e}_\pm$, $\mathbf{H} = (\pm i, 1, 0)^T H_\pm = H_\pm \mathbf{h}_\pm$ we get

$$\begin{pmatrix} \mp i\partial_z + \omega\frac{\kappa}{c} \\ \partial_z \pm i\omega\frac{\kappa}{c} \\ 0 \end{pmatrix} E_\pm = i\omega\mu_0\mu \begin{pmatrix} H_x \\ H_y \\ 0 \end{pmatrix} = i\omega\mu_0\mu \begin{pmatrix} \pm i \\ 1 \\ 0 \end{pmatrix} H_\pm \tag{3.17}$$

Of course, both equations are the same due to the isotropy. So we get for $H_\pm$

$$H_\pm = \frac{1}{i\omega} \left(\partial_z \pm i\omega\frac{\kappa}{c} \right) \frac{E_\pm}{\mu_0\mu}. \tag{3.18}$$

Inserting an ansatz for the electric field of such a forward propagating plane wave we obtain with the help of the Eq. (3.13) for the $H_\pm$ field

$$E_\pm = E_0 e^{ik_\pm^+ z} \ , \quad H_\pm = \frac{1}{\omega} \left(k_\pm^+ \pm \frac{\omega}{c}\kappa \right) \frac{E_0}{\mu_0\mu} e^{ik_\pm^+ z} = \frac{E_\pm}{Z_0 Z} \tag{3.19}$$

with the vacuum impedance $Z_0 = \sqrt{\mu_0/\varepsilon_0}$ and the impedance $Z = \sqrt{\mu/\varepsilon}$. Interestingly, the ratio of the electric and magnetic field is generally independent of κ and given by the common impedance definition. For backward propagating fields one obtains in complete analogy $H_\pm = -E_\pm/(Z_0 Z)$. The equations for the R-T-problem are now easily written down.

The bi-isotropic slab of thickness D, which is called film (index f), is assumed to be embedded in bi-isotropic half spaces named substrate (index s) and cladding (index c). We then choose the following ansatz for the electric field in the substrate

$$\mathbf{E}_\mathrm{s} = E_\pm^I e^{ik_\pm^{\mathrm{s},+} z}\mathbf{e}_\pm + E_\pm^R e^{ik_\pm^{\mathrm{s},-} z}\mathbf{e}_\pm, \tag{3.20}$$

in the film

$$\mathbf{E}_\mathrm{f} = E_\pm^A e^{ik_\pm^{\mathrm{f},+} z}\mathbf{e}_\pm + E_\pm^B e^{ik_\pm^{\mathrm{f},-} z}\mathbf{e}_\pm \tag{3.21}$$

and in the cladding

$$\mathbf{E}_\mathrm{c} = E_\pm^T e^{ik_\pm^{\mathrm{c},+}(z-D)}\mathbf{e}_\pm. \tag{3.22}$$

The continuity of the tangential electric and magnetic fields give the following system of equation

$$\begin{aligned}
E_\pm^I + E_\pm^R &= E_\pm^A + E_\pm^B && (3.23)\\
\frac{1}{Z_\mathrm{s}}\left(E_\pm^I - E_\pm^R\right) &= \frac{1}{Z_\mathrm{f}}\left(E_\pm^A - E_\pm^B\right) && (3.24)\\
E_\pm^A e^{ik_\pm^{\mathrm{f},+} D} + E_\pm^B e^{ik_\pm^{\mathrm{f},-} D} &= E_\pm^T && (3.25)\\
\frac{1}{Z_\mathrm{f}}\left(E_\pm^A e^{ik_\pm^{\mathrm{f},+} D} - E_\pm^B e^{ik_\pm^{\mathrm{f},-} D}\right) &= \frac{E_\pm^T}{Z_\mathrm{c}}. && (3.26)
\end{aligned}$$

Now, that only the propagation constants of the film are involved, these quantities are replaced by

$$k_\pm^{\mathrm{f},+} = k \mp k_0\kappa\ , \quad k_\pm^{\mathrm{f},-} = -k \mp k_0\kappa \tag{3.27}$$

with $k = k_0\sqrt{\varepsilon\mu}$ and the free space wavenumber $k_0 = \omega/c$. That yields for the last two equations

$$\begin{aligned}
\left(E_\pm^A e^{ikD} + E_\pm^B e^{-ikD}\right) &= E_\pm^T e^{\pm ik_0\kappa D} && (3.28)\\
\frac{1}{Z_\mathrm{f}}\left(E_\pm^A e^{ikD} - E_\pm^B e^{-ikD}\right) &= \frac{E_\pm^T}{Z_\mathrm{c}} e^{\pm ik_0\kappa D}. && (3.29)
\end{aligned}$$

Obviously, the substitution $T = T_\pm e^{\pm ik_0\kappa D} = E_\pm^T/E_\pm^I e^{\pm ik_0\kappa D}$ and $R = R_\pm = E_\pm^R/E_\pm^I$ results in equations for R and T completely free of the chirality parameter κ. I.e., the equations and hence their solution is identical to the equations for an ordinary isotropic slab with permittivity ε and permeability μ [see Eqs. (3.2),(3.3)]. As stated before, the chirality

affects the polarization state only in transmission, whereas in reflection the polarization state is preserved. The retrieval of the effective permeability and the effective permittivity can be accomplished by the procedure given section 3.1, as soon as R and T are known. Note that the measurable quantities are $R_\pm$ and $T_\pm$. The knowledge of the chirality parameter is a prerequisite for the retrieval of ε and μ. Therefore, the retrieval of $\kappa(\omega)$ is derived in the following.

Consider the transmission for linearly polarized, the common polarization used in experiments and simulations. Due to the isotropy and without lost of generality, it can be assumed that the incident electric field $\mathbf{E}^I$ is x-polarized and decomposed into the eigenstates

$$\mathbf{E}^I = \frac{1}{2}\left[(1,i,0)^T + (1,-i,0)^T\right] = (1,0,0)^T. \tag{3.30}$$

The transmitted field $\mathbf{E}^T$ is then given by

$$\mathbf{E}^T = \frac{T_+}{2}\mathbf{e}_+ + \frac{T_-}{2}\mathbf{e}_- = \frac{T}{2}\left[\begin{pmatrix}1\\ i\\ 0\end{pmatrix} e^{-ik_0\kappa D} + \begin{pmatrix}1\\ -i\\ 0\end{pmatrix} e^{ik_0\kappa D}\right] = T\begin{pmatrix}\cos(k_0\kappa D)\\ -\sin(k_0\kappa D)\\ 0\end{pmatrix} = \begin{pmatrix}T_x\\ T_y\\ 0\end{pmatrix}. \tag{3.31}$$

For real valued κ the transmitted field is simply rotated by the angle $-k_0\kappa D$ with respect to the x-axis. As soon as T_x and T_y are determined for the x-polarized incident light, κ is determined as

$$\kappa = -\frac{1}{k_0 D}\arctan\left(\frac{T_y}{T_x}\right). \tag{3.32}$$

For lossy materials the chirality parameter is complex valued in general $\kappa = \kappa' + i\kappa''$ and the transmitted light is elliptically polarized. In the system of the principal axis the equation for the polarization ellipse is $\xi^2/\alpha^2 + \eta^2/\beta^2 = 1$. The real part κ' describes the rotation angle ϕ of the ellipse which can be easily shown by algebraic manipulation. The imaginary part κ'' determines the ratio between the small and the large axis of the ellipse $\alpha/\beta = \tanh[k_0\kappa'' D]$; i.e. the imaginary part κ'' determines the ellipticity of the polarization state. It is therefore responsible for the effect of circular dichroism. Obviously, κ' and κ'' are connected by a Kramers-Kronig relation since $\kappa(\omega)$ has to be a meromorphic function [131]. Therefore, dispersive circular dichroism can not occur without a polarization rotation resulting from a non-vanishing real part κ'. For large absolute values of κ'' the tanh-function tends to be ± 1, i.e. either lcp-waves or rcp-waves are transmitted. For vanishing κ'' the polarization remains linear. There are no constraints on the value of κ except that $\Im(k^\pm)$ has to remain positive for the reason of passivity

$$\Im(k^\pm) = \Im\left(\sqrt{\varepsilon\mu} \pm \kappa\right) > 0. \tag{3.33}$$

Once κ is determined, T can be calculated as

$$T = \frac{T_x}{\cos(k_0\kappa D)} = -\frac{T_y}{\sin(k_0\kappa D)} \tag{3.34}$$

and by $R = R_{\pm}$ and T the values k and ξ. As the retrieval procedure is only proposed for normal incidence, one cannot conclude on the validity of effective material parameters ε and μ here if determined from k and ξ. However, the strength of the proposed retrieval lies in the determination of $\kappa(\omega)$, which provides a measure for the capability of the medium to rotate the polarization of light in transmission, and of the propagation constant k, which is again meaningful anyway.

Finally the applicability of the retrieval for chiral media is discussed from a more abstract point of view. All reciprocal sub-wavelength systems that have an fourfold rotational symmetry with respect to the propagation direction are polarization independent. A rotation of the polarization state occurs only in transmission and not in reflection as it is the case for Pasteur media. Hence, the value of κ can be retrieved from the transmission only. As the transmission in different directions is identical for reciprocal systems the value of κ can be retrieved uniquely without any contradiction, providing us with a direct measure for the polarization rotation. For the retrieval of k and ξ we have to enforce additionally that the system is symmetric with respect to propagation in opposing directions. Under these assumptions the optical response contained in R and T can be properly translated into the set (k, ξ, κ) or $(\varepsilon, \mu, \kappa)$,respectively. Note, that these parameters are wave parameters in general and are only valid for a particular system and illumination scheme.

3.3 The S-parameter retrieval from a periodic medium perspective

Although MMs are conceptionally composed of small metaatoms that are in general arranged in an arbitrary fashion, they are mostly fabricated and even more important theoretically modeled as periodic systems. Hence, they can be understood as metallo-dielectric photonic crystals [132]. Although the concepts of photonic crystals are most important for structures with typical unit cell sizes in the order of the wavelength, they are generally valid on an arbitrary scale. As soon as a MM is operated in the quasi-static limit, the optical response can certainly be modeled by effective medium theories; rendering the description in terms of photonic crystals to be exaggerated. However, the quasi-static limit is most often not applicable to MMs and hence a general description in terms of a periodic medium is necessary to determine the optical properties exactly. It is therefore necessary to familiarize with the concept of Bloch modes (BMs) and to elucidate the transition from the photonic crystal to the effective medium regime. In this subsection the S-PR is recapitulated from a photonic crystal's point of view , i.e. the equations for the transmission and reflection at a finite photonic crystal slab are derived. This will provide a better understanding of the retrieved

wave parameters, elucidates the issue of the convergence of the parameters with increasing thickness of the system and finally determines the limits of the applicability of the S-PR [83].

The considerations are divided into two parts. In the first part, one-dimensional photonic crystal slabs made of stratified layers are discussed [128]. This will be proven to be the realm of the S-PR providing a clear picture for the interpretation of the retrieved effective parameters. In the second part, three-dimensional systems and their peculiarities are discussed. It will be shown, that the retrieval can be applied as soon as the three-dimensional system becomes equivalent to an one-dimensional one.

The periodic arrangement tremendously simplifies the numerical computation of the optical response of the system since for periodic systems the Bloch theorem can be applied. For periodic systems $\varepsilon(\mathbf{r}+\mathbf{R}) = \varepsilon(\mathbf{r})$ with $\mathbf{R} \in \mathbb{G}$ holds, where $\mathbb{G}$ is the set of lattice vectors. According to the Bloch-theorem the electromagnetic field in such a system can be expressed as

$$\mathbf{E}(\mathbf{r}) = \mathbf{e}_{\mathbf{K}}(\mathbf{r})e^{i\mathbf{K}\cdot\mathbf{r}}, \quad \text{with} \quad \mathbf{e}_{\mathbf{K}}(\mathbf{r}+\mathbf{R}) = \mathbf{e}_{\mathbf{K}}(\mathbf{r}), \tag{3.35}$$

$$\mathbf{H}(\mathbf{r}) = \mathbf{h}_{\mathbf{K}}(\mathbf{r})e^{i\mathbf{K}\cdot\mathbf{r}}, \quad \text{with} \quad \mathbf{h}_{\mathbf{K}}(\mathbf{r}+\mathbf{R}) = \mathbf{h}_{\mathbf{K}}(\mathbf{r}), \tag{3.36}$$

where $\mathbf{K}$ is the generally complex Bloch-wavevector and $\mathbf{e}_{\mathbf{K}}(\mathbf{r}), \mathbf{h}_{\mathbf{K}}(\mathbf{r})$ are the Bloch-amplitudes. Therefore, the calculation of the electromagnetic field in a periodic structure can be reduced to the determination of the Bloch-wavevector $\mathbf{K}$ and the calculation of the Bloch-amplitudes in a single unit cell.

3.3.1 One-dimensional periodic systems

At first it will be proven, that an arbitrary but symmetric sequence of layers can be replaced by a single equivalent homogeneous layer. Here the mirror symmetry with respect to the center of the unit cell, the elements comprising the sequence, is of major importance. The calculations are restricted to the case of TE-polarized fields without lost of generality. The case of TM-polarization can be treated analogously. The eigenmodes of such a periodic medium are BMs of the form:

$$\mathbf{E}(\mathbf{r},\omega) = E_y^{\pm}(z,\omega)e^{i(k_x x-\omega t)}\mathbf{e}_y = e_{\pm}(z,\omega)e^{\pm iKz}e^{i(k_x x-\omega t)}\mathbf{e}_y \tag{3.37}$$

where $K = k_z$ is the normal component and k_x the tangential component of the wavevector. The $\pm$ sign indicates forward and backward propagating modes, respectively, and $e_{\pm}(z + n\Lambda) = e_{\pm}(z)$ with the period Λ and $n \in \mathbb{Z}$. The frequency dependence is again suppressed in the following. In the case of a symmetric unit cell, forward propagating modes in positive z-direction are identical to backward propagating modes in negative z-direction, i.e.

$$E_y^{+}(z) = E_y^{-}(-z) \quad \text{and hence} \quad e_{+}(z) = e_{-}(-z). \tag{3.38}$$

Therefore, we have

$$\partial_z E_y^{\pm}(z) = \pm\partial_z E_y^{+}(z) \quad \text{and} \quad e_+(0) = e_+(d) = e_-(0) = e_-(d). \tag{3.39}$$

The tangential component $H_x(\mathbf{r},\omega) = H_x^{\pm}(z)e^{i(k_x x-\omega t)}$ of the corresponding magnetic field is then given by

$$H_x^{\pm}(z) = -\frac{i}{\omega\mu_0}\partial_z E_y^{\pm}(z) = h_{\pm}(z)e^{\pm iKz} = \mp\frac{i}{\omega\mu_0}\partial_z E_y^{+}(z) \quad \text{with} \quad h_{\pm}(0) = h_{\pm}(d). \tag{3.40}$$

These relations are very important, because it follows that the ratios $E_y^{+}(n\Lambda)/H_x^{+}(n\Lambda) = Z_\mathrm{t}$ and $E_y^{-}(n\Lambda)/H_x^{-}(n\Lambda) = -Z_\mathrm{t}$, i.e. the ratios of magnetic and electric field of both Blochmodes, are identical at the boundary of the unit cells with respect to their modulus. The quantity Z_t is introduced here as the tangential impedance connecting the continuous tangential components of the fields. The subscript t will be suppressed for convenience. As soon as an inversion symmetry exists, it becomes obvious that forward and backward

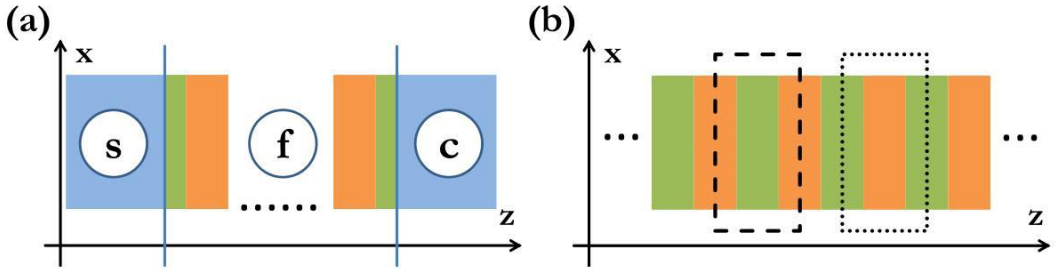

Figure 3.2: (a) Schematic drawing of the photonic crystal slab (film f), embedded between substrate (s) and cladding (c) halfspace. The film consists of an arbitrary number of unit cells with period Λ in propagation direction. Each unit cell may consist either of stratified media or layers, which are again periodic in tangential directions. Such a tangential period is assumed to be subwavelength compared to the embedding medium. (b) Sequence of symmetric unit cells, with the two symmetric realizations of the unit cell. The infinite medium composed of either unit cell is indistinguishable. For finite realizations of such a medium, the chosen unit cell is, however, of great importance since the surface termination determines the impedance and hence the coupling properties.

propagating modes are indistinguishable. Exactly this property is fulfilled also by a homogeneous layer. Any symmetric unit cell, like any homogeneous layer is characterized by a single impedance. However, the ratio of the fields is only identical at the boundaries of the symmetric unit cell. Any periodic sequence of symmetric unit cells can be defined by a second sequence resulting in the same periodic system [see Fig. 3.2 (b)].

In general, this unit cell is characterized by a different impedance. Both impedances converge towards each other, if the amplitude of the BMs reach constant, z-independent values. This happens exactly in the quasi-static limit, where the definition of the unit cell

becomes arbitrary. The tangential components of the BMs converge then to simple plane waves.

In general, the number of impedances necessary to solve the reflection/transmission problem at a finite system is of no importance since they are assumed to be known. For one-dimensional systems the number of impedances is limited to two. However, for the inversion of the problem we have to restrict to a single impedance if only a single set (R, T) is known.

If one has two different impedances for forward and backward propagating modes, respectively, both can be determined by solving the reflection problem at a semi-infinite half-space for both directions, i.e. surface terminations, as we will see below. In each case an incident plane wave can couple only to the corresponding forward or backward propagating mode.

3.3.1.1 The symmetric 1D slab

Now, the equations for the reflection/transmission problem at a finite sequence of symmetric unit cells are derived. For the sake of simplicity the system is assumed to be embedded into vacuum. Then three distinct regions exist, namely substrate (index s), film (index f) and cladding (index c) [see Fig. 3.2 (a)]. The field in the substrate is given by

$$E_{\mathrm{s},y}(x,z) = e^{ik_x x}\left(e^{ik_z z} + Re^{-ik_z z}\right),\ H_{\mathrm{s},x}(x,z) = \frac{k_z}{\omega\mu_0}e^{ik_x x}\left(e^{ik_z z} - Re^{-ik_z z}\right) \tag{3.41}$$

with $k_x^2 + k_z^2 = \omega^2/c^2$. The field in the cladding is given by

$$E_{\mathrm{c},y}(x,z) = Te^{ik_x x}e^{ik_z(z-D)},\ H_{\mathrm{c},x}(x,z) = \frac{k_z}{\omega\mu_0}Te^{ik_x x}e^{ik_z(z-D)}. \tag{3.42}$$

The field in the film (n-fold sequence of layers with period Λ) is given by

$$E_{\mathrm{f},y}(x,z) = e^{ik_x x}\left(AE^+(z) + BE^-(z)\right),\ H_{\mathrm{f},x}(x,z) = e^{ik_x x}\left(AH^+(z) + BH^-(z)\right) \tag{3.43}$$

where the subscripts f, x and y at the scalar quantities $E^\pm$ and $H^\pm$ are suppressed for convenience. The continuity of the tangential fields requires:

$$\begin{aligned}
AE^+(0) + BE^-(0) &= 1 + R && (3.44)\\
AE^+(D) + BE^-(D) &= AE^+(0)e^{iKn\Lambda} + BE^-(0)e^{-iKn\Lambda} = T && (3.45)\\
AH^+(0) + BH^-(0) &= AZ_{\mathrm{f}}^{-1}E^+(0) - BZ_{\mathrm{f}}^{-1}E^-(0) = Z_{\mathrm{s}}^{-1}(1-R) && (3.46)\\
AH^+(D) + BH^-(D) &= AH^+(0)e^{iKn\Lambda} + BH^-(0)e^{-iKn\Lambda} && (3.47)\\
&= AZ_{\mathrm{f}}^{-1}E^+(0)e^{iKn\Lambda} - BZ_{\mathrm{f}}^{-1}E^-(0)e^{-iKn\Lambda} = Z_{\mathrm{c}}^{-1}T, && (3.48)
\end{aligned}$$

where the properties of the BMs for symmetric unit cells are used. Without lost of generality, the BMs are assumed to be normalized according to $E^\pm(0) = 1$. With $n\Lambda = D$ following

system of equations is obtained:

$$\begin{aligned} A + B &= 1 + R && (3.49)\\ Ae^{iKD} + Be^{-iKD} &= T && (3.50)\\ Z_{\mathrm{f}}^{-1}(A - B) &= Z_{\mathrm{s}}^{-1}(1 - R) && (3.51)\\ Z_{\mathrm{f}}^{-1}(Ae^{iKD} - Be^{-iKD}) &= Z_{\mathrm{c}}^{-1}T. && (3.52) \end{aligned}$$

Solving for the reflection R and the transmission T leads to

$$T = \frac{2Z_{\mathrm{c}}Z_{\mathrm{f}}}{Z_{\mathrm{f}}(Z_{\mathrm{c}} + Z_{\mathrm{s}})\cos(KD) - i(Z_{\mathrm{s}}Z_{\mathrm{c}} + Z_{\mathrm{f}}^2)\sin(KD)} \tag{3.53}$$

$$R = \frac{Z_{\mathrm{f}}(Z_{\mathrm{c}} - Z_{\mathrm{s}})\cos(KD) + i(Z_{\mathrm{s}}Z_{\mathrm{c}} - Z_{\mathrm{f}}^2)\sin(KD)}{Z_{\mathrm{f}}(Z_{\mathrm{c}} + Z_{\mathrm{s}})\cos(KD) - i(Z_{\mathrm{s}}Z_{\mathrm{c}} + Z_{\mathrm{f}}^2)\sin(KD)} \tag{3.54}$$

These equations are exactly identical to the equations (3.2) and (3.3) of the R-T-problem of a homogeneous layer with the thickness D, the tangential impedance Z_{f} and the propagation constant K at an arbitrary angle of incidence for TE-polarization. Hence, we found in particular the relation between the quantities determined within the S-PR and the corresponding quantities in the photonic crystals picture. The value of k as retrieved by inversion of R and T is identical to the value of K and depending on the polarization ξ/k_0 is identical to Z_{f} or its inverse, respectively. That implies that the S-PR is indeed meaningful to determine the propagation constant and the tangential impedance at symmetric slab systems at any angle of incidence. Therefore, any symmetric one-dimensional system can be replaced by a single equivalent homogeneous layer.

Problems will arise only, if effective material parameters are assigned additionally, since further restrictions have to be imposed on the form of the dispersion relation as well as on the impedance as discussed in section 3.1. Let us therefore elucidate the case when the impedance is identified with its homogeneous analogue. For the case of TE-polarization considered here and assuming non-magnetic media, the impedance is supposed to obey

$$Z_{\mathrm{f}} = \frac{\omega\mu_0}{K} \tag{3.55}$$

This is in general not valid as will be shown in the following. The magnetic field of the forward propagating mode is given by

$$\begin{aligned} H_x^+(x,z) &= -\frac{i}{\omega\mu_0}\partial_z E^+(x,z) = -\frac{i}{\omega\mu_0}\left[iKe_+(z) + \partial_z e_+(z)\right]e^{ik_x x}e^{iKz}\\ &= \frac{K}{\omega\mu_0}e_+(z)\left(1 - i\frac{\partial_z e_+(z)}{Ke_+(z)}\right)e^{ik_x x}e^{iKz} && (3.56) \end{aligned}$$

The tangential impedance at the boundary is

$$Z_{\mathrm{f}} = \frac{E_y^+(0)}{H_x^+(0)} = \frac{\omega\mu_0}{K}\left(1 - i\frac{\partial_z e_+(0)}{Ke_+(0)}\right)^{-1}. \tag{3.57}$$

The tangential impedance is obviously equal to its homogeneous analogue, if the variation of the amplitude is negligible compared to the variation of the Bloch phase. Both impedances are exactly identical as soon as the amplitude is constant $e_{\pm}(z) = 1$, i.e. in the limit of a plane wave. In that case the ratio between the magnetic and the electric field is independent of the spatial coordinate z. That is, in fact, the limit of an homogeneous slab. The deviation, however, can be compensated by assuming a potential magnetic response of the system. Then the tangential impedance is given by

$$Z_{\mathrm{f}} = \frac{\omega\mu_0\mu_x}{K} \tag{3.58}$$

and we have

$$\mu_x = \left(1 - i\frac{\partial_z e_+(0)}{K e_+(0)}\right)^{-1}. \tag{3.59}$$

I.e., the non-homogeneity of the slab system is translated into an artificial magnetic response, which is now occurring although only non-magnetic materials are considered for the slab system. If the unit cell is chosen in its second symmetric configuration (see Fig. 3.2), the impedance is changing due to a change of the ratio of the electric and magnetic part of BM and hence a different value for the permeability

$$\mu_x = \left(1 - i\frac{\partial_z e_+(\Lambda/2)}{K e_+(\Lambda/2)}\right)^{-1}. \tag{3.60}$$

is obtained. If the impedance is not independent on the termination (chosen unit cell), i.e. if $\partial_z e_+(z)$ is not vanishing, an assignment of unique effective material parameters is not possible.

3.3.1.2 The asymmetric 1D slab

The problem becomes more obvious, if non-symmetric unit cells (slab systems) are considered. The impedances of forward and backward propagating modes defined at the boundary of the unit cells or the slab, respectively, are different in general. If these impedances are known, the R/T problem is solvable of course. An inversion of the equations from a single set (R, T) is not possible, since three complex quantities, namely the two impedances and the propagation constant have to be retrieved. Consider the equations for the boundary conditions at a system of asymmetric unit cells and define

$$E_x^{\pm}(n\Lambda)/H_x^{\pm}(n\Lambda) = \pm Z^{\pm} \tag{3.61}$$

in accordance with the definitions above. With $E^{\pm}(0) = 1$

$$A + B = 1 + R \tag{3.62}$$

$$Ae^{iKn\Lambda} + Be^{-iKn\Lambda} = T \tag{3.63}$$

$$A(Z_{\mathrm{f}}^{+})^{-1} - B(Z_{\mathrm{f}}^{-})^{-1} = Z_{\mathrm{s}}^{-1}(1 - R) \tag{3.64}$$

$$A(Z_{\mathrm{f}}^{+})^{-1}e^{iKn\Lambda} - B(Z_{\mathrm{f}}^{-})^{-1}e^{-iKn\Lambda} = Z_{\mathrm{c}}^{-1}T \tag{3.65}$$

is obtained. Reflection and transmission at an asymmetric slab system are then determined by the three quantities $K, Z_\mathrm{f}^+, Z_\mathrm{f}^-$. These four linearly independent equations contain seven unknowns $A, B, R, T, K, Z_\mathrm{f}^+, Z_\mathrm{f}^-$. The coefficients A and B are generally unknown. Contrarily the quantities $K, Z_\mathrm{f}^+, Z_\mathrm{f}^-$ are generally predictable by calculation and R and T are predictable by calculation or measurement. It is not possible to solve the system only by knowledge of R and T.

It is possible, however, to determine the 3 quantities in different ways. On the one hand the system can be operated from the backside. We then have for the system of equations

$$\begin{aligned} A' + B' &= T' && (3.66)\\ A'e^{iKn\Lambda} + B'e^{-iKn\Lambda} &= 1 + R' && (3.67)\\ A'(Z_\mathrm{f}^+)^{-1} - B'(Z_\mathrm{f}^-)^{-1} &= -Z_\mathrm{s}^{-1}T' && (3.68)\\ A'(Z_\mathrm{f}^+)^{-1}e^{iKn\Lambda} - B'(Z_\mathrm{f}^-)^{-1}e^{-iKn\Lambda} &= -Z_\mathrm{c}^{-1}(1 - R'). && (3.69) \end{aligned}$$

With $Z_\mathrm{c} = Z_\mathrm{s} = Z$ and $Z_\mathrm{f}^\pm = Z^\pm$ we get the following solutions for the ratios

$$\frac{T}{T'} = 1\,,\ \frac{R}{R'} = \frac{Z^+ - Z}{Z^+ + Z}\frac{Z^- + Z}{Z^- - Z}. \tag{3.70}$$

The transmission from both sides is obviously equal as required for reciprocal systems. Contrarily the reflection is different for different sides. Hence, an additional determination of R' allows for solving Z^+, Z^- and K.
On the other hand, the reflection at an semi-infinite half-space can be determined for both surface terminations. With $B, A', n\Lambda = 0$ we have

$$R = \frac{Z^+ - Z}{Z^+ + Z}\,,\ R' = \frac{Z^- - Z}{Z^- + Z}. \tag{3.71}$$

Together with the propagation constant K the three quantities describing the system are determined. Obviously, for symmetric unit cells $R = R'$ and hence $Z^+ = Z^-$.

These equations for the reflection are of major practical relevance. Consider, e.g., a strongly absorptive slab system where multiple reflection between the entrance and output facette can be neglected. In that case the reflection at the finite system is equal to that of the semi-infinite one. Then the impedance is completely defined by reflection and vice versa.

3.3.1.3 The case of strong absorption

Since the case of strong absorption occurs frequently, it is elaborated here for a slab system of generally asymmetric unit cells in greater detail. The issues discussed here will appear in three dimension again, even for symmetric systems. We will in particular discuss the results of the PR for symmetric systems if applied for asymmetric ones. The neglect of multiple

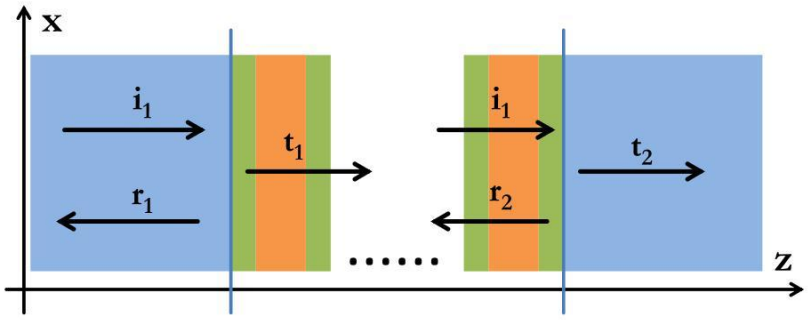

Figure 3.3: Schematic drawing of the scattering at a strongly absorptive photonic crystal slab. Due to the strong absorption, multiple reflection between the front and rear interface can be neglected and hence the transmission can be decomposed into three independent processes - scattering at both interfaces and the propagation in between. The coefficients $i_{1,2}$, $r_{1,2}$ and $t_{1,2}$ are the respective incident, reflected and transmitted amplitudes similar to the common Fabry-Perot formulas [128].

reflection implies, that the transmission T is given as the product of propagation e^{iKD} and transmission at the first and second surface t_1 and t_2 (see Fig. 3.3). The reflection at these surfaces are given by r_1 and r_2 and by assuming $r_2 e^{iKD} \approx 0$ we have $R = r_1$ for the overall reflection. Analogously to the calculations above we have:

$$t_1 = \frac{2Z^+}{Z^+ + Z}\,,\; t_2 = \frac{Z(Z^+ + Z^-)}{Z^+(Z + Z^-)}\,,\; T = t_1 t_2 e^{iKD} = (1 - R^2)e^{iKD} \tag{3.72}$$

and

$$R = r_1 = \frac{Z^+ - Z}{Z^+ + Z}\,,\; r_2 = \frac{Z^-(Z - Z^+)}{Z^+(Z + Z^-)}. \tag{3.73}$$

If the retrieval for symmetric slab systems is now unthoughtful used for asymmetric ones, the obtained effective impedance will converge towards those of the forward propagating BM Z^+, as soon as multiple reflection can be neglected. Both equations will become equal. The calculation of the effective wave parameters for strongly absorptive systems results in

$$k_{\text{eff}} = \frac{1}{iD}\ln\left(\frac{T}{1 - R^2}\right) = K + \frac{1}{iD}\ln\left(\frac{t_2}{\tilde{t}_2}\right)\,,\quad Z_{\text{eff}} = Z^+ \tag{3.74}$$

with the $\tilde{t}_2$ being the transmission through the second interface in the case of $Z^- = Z^+$. I.e., the effective k is also converging towards the propagation constant K of the BM for an increasing thickness D. Hence, the application of the retrieval leads to quantities converging towards the expected ones. However, that limiting case is in a certain sense only of academic interest, as at first strong absorption is necessary and at second the parameters, if converged, only allow to describe even thicker systems correctly. Note that a different choice of the unit cell leads to the same propagation constant but a different impedance in general.

If the system is free of absorption, the application of the retrieval for symmetric systems to asymmetric slab systems does not converge at all, but leads to a solution periodic in

D, completely free of any physical meaning. This can be easily proven by reinserting the equations for R and T for the asymmetric system into the equations for Z_{eff} and k_{eff} of a symmetric system.

3.3.2 Three-dimensional periodic systems

In the case of three-dimensional periodic structures, the analysis gets much more complicated as the field inside the structure is generally determined by a larger set of BMs instead of a single one [133]. In general, an incoming plane wave can couple to several BMs that have to be considered to describe the propagation of light through the periodic structure correctly. For convenience and without lost of generality we focus here on the case of normal incidence, where the MM is embedded in air. The field inside the periodic structure is then given as a superposition of BMs

$$\mathbf{E}(x,y,z) = \sum_l \alpha_{+l}\mathbf{e}_{+l}(x,y,z)e^{iK_{+l}z} + \alpha_{-l}\mathbf{e}_{-l}(x,y,z)e^{iK_{-l}z} \tag{3.75}$$

with the Bloch amplitudes $\mathbf{e}_{\pm l}(x,y,z)$, the coefficients $\alpha_{\pm l}$ and the Bloch propagation constants $K_{\pm l}$. The corresponding magnetic field reads as

$$\mathbf{H}(x,y,z) = \sum_l \alpha_{+l}\mathbf{h}_{+l}(x,y,z)e^{iK_{+l}z} + \alpha_{-l}\mathbf{h}_{-l}(x,y,z)e^{iK_{-l}z} \tag{3.76}$$

The forward as well as the backward propagating BMs are assumed to be ordered in terms of the imaginary part of their propagation constant, i.e. $\Im(K_{\pm 0}) \leq \Im(K_{\pm 1}) \leq ....$

At first the problem of coupling light from a homogeneous half space to a three-dimensional periodic structure, which is extended infinitely in the second half space, is considered. The incident plane wave is y-polarized, with the y-z-plane being a plane of mirror symmetry for the overall structure. In that case the reflected light is also y-polarized. The equations of continuity of the tangential fields at $z = 0$ are given by

$$E_y^I + \sum_{nm} E_{y,mn}^R e^{i(K_{x,m}x+K_{y,m}y)} = \left(\sum_l \tau_{+l}\mathbf{e}_{+l}(x,y)\right)\cdot\mathbf{e}_y = E_y^T(x,y) \tag{3.77}$$

$$H_x^I + \sum_{nm} H_{x,mn}^R e^{i(K_{x,m}x+K_{y,m}y)} = \left(\sum_l \tau_{+l}\mathbf{h}_{+l}(x,y)\right)\cdot\mathbf{e}_x = H_x^T(x,y) \tag{3.78}$$

$$\sum_{nm} E_{x,mn}^R e^{i(K_{x,m}x+K_{y,m}y)} = \left(\sum_l \tau_{+l}\mathbf{e}_{+l}(x,y)\right)\cdot\mathbf{e}_x = E_x^T(x,y) \tag{3.79}$$

$$\sum_{nm} H_{y,mn}^R e^{i(K_{x,m}x+K_{y,m}y)} = \left(\sum_l \tau_{+l}\mathbf{h}_{+l}(x,y)\right)\cdot\mathbf{e}_y = H_y^T(x,y), \tag{3.80}$$

where the superscripts denote the incident (I), the reflected (R) and the transmitted (T) field components. Since we are interested in the far-field response only, i.e. the zeroth diffraction

order, it is sufficient to consider the cell averaged quantities

$$E_y^I + E_{y,00}^R = \langle E_y^T(x,y)\rangle \tag{3.81}$$
$$H_x^I + H_{x,00}^R = \langle H_x^T(x,y)\rangle \tag{3.82}$$
$$0 = \langle E_x^T(x,y)\rangle \tag{3.83}$$
$$0 = \langle H_y^T(x,y)\rangle, \tag{3.84}$$

where $\langle f\rangle = \Lambda_x^{-1}\Lambda_y^{-1}\int\int f(x,y)\,dx\,dy$ with the periods Λ_x, Λ_y in x- and y-direction, respectively. The averaged reflected E_x and H_y components are vanishing in the sub-wavelength domain due to the assumed mirror symmetry. Again, the tangential impedance Z_t can be introduced as

$$Z_\mathrm{t} = \frac{\langle E_y^T(x,y)\rangle}{\langle H_x^T(x,y)\rangle}. \tag{3.85}$$

The subscript t will be suppressed for convenience. By additional use of the relations

$$T = \frac{\langle E_y^T(x,y)\rangle}{E_y^I},\ R = \frac{E_{y,00}^R}{E_y^I},\ Z_0 = \frac{E_y^I}{H_x^I} \ \text{ and } \ Z_0 = -\frac{E_{y,00}^R}{H_{x,00}^R} \tag{3.86}$$

we obtain

$$1 + R = T \tag{3.87}$$
$$Z(1-R) = Z_0 T. \tag{3.88}$$

Hence, the zeroth order reflection at the half space is determined by the tangential impedance Z only

$$R = \frac{Z - Z_0}{Z + Z_0}. \tag{3.89}$$

That impedance is, however, defined by a sum of BMs weighted with an individual excitation amplitude rather than a single one

$$Z = \frac{\langle \sum_l \tau_l \mathbf{e}_l(x,y)\rangle}{\langle \sum_l \tau_l \mathbf{h}_l(x,y)\rangle}. \tag{3.90}$$

Only in case of the single BM approximation, i.e. $\sum_l \tau_l \mathbf{e}_l \approx \tau_{+0}\mathbf{e}_{+0}$, we have

$$Z = \frac{\langle \mathbf{e}_{+0}(x,y)\rangle}{\langle \mathbf{h}_{+0}(x,y)\rangle}. \tag{3.91}$$

Once the complex reflection coefficient at a half space is known, the tangential impedance can be determined. Nevertheless, from such a measurement it is not possible to conclude on the validity of the single BM approximation and hence it has to be assumed that R is given by the sum of several BMs in general.

In a next step, the reflection and transmission problem at a finite slab of the periodic structure is determined. Let us at first assume, that the single BM approximation is valid. In that

case the finite system behaves exactly like an effective homogeneous slab with the impedance Z and the propagation constant K_0 (K_{+0}) in perfect analogy to the one-dimensional case. The equations for the reflection and transmission coefficient are identical to the ones for the 1D case and are not repeated here. If the retrieval leads to results for k and ξ which are independent of the thickness of the system, we have to conclude that the single BM approximation is valid and the three-dimensional structure can be replaced by an one-dimensional one properly with $k = K_0$ and $\xi/k_0 = Z$ (or $\xi/k_0 = Z^{-1}$,respectively). However, the single BM approximation is very demanding and for realistic structures seldom justified. But as soon as multiple BMs are contributing to the overall reflection and transmission, it is cumbersome to provide analytical expressions. It is, however, possible to prove that the results of the PR are converging under the assumption of rather strong absorption. If the thickness D of the system under consideration is increasing, multiple reflections become negligible. Then the determination of the overall reflection and the transmission can be decomposed into three distinct processes, namely transmission t_1 and reflection r_1 at the front interface at $z = 0$, propagation of the field through the structure over the distance D and transmission t_2 and reflection r_2 at the rear interface at $z = D$ (see Fig. 3.3). Let us consider these processes separately.

1. **The front interface**
   The front interface is governed by Eqs. (3.77)-(3.91) with $Z_1 = Z$.

2. **The propagation through the structure**
   We have to assume that multiple BMs are excited at the front facet and hence the field inside the structure is given by a superposition of forward propagating BMs
   $$\mathbf{E}^T(x,y,z) = \sum_l \tau_{+l}\mathbf{e}_{+l}(x,y,z)e^{iK_{+l}z},\ \mathbf{H}(x,y,z) = \sum_l \tau_{+l}\mathbf{h}_{+l}(x,y,z)e^{iK_{+l}z}. \quad (3.92)$$
   The assumption of an optically thick structure also implies that at the rear facette only the BM with the smallest imaginary part of the propagation constant is contributing to the total field, i.e.
   $$\sum_l \tau_{+l}\mathbf{e}_{+l}(x,y,D)e^{iK_{+l}D} \approx \tau_{+0}\mathbf{e}_{+0}(x,y,D)e^{iK_{+0}D}. \quad (3.93)$$

3. **The rear interface**
   Although at the rear interface we have only the zeroth order BM contributing to the 'incident field', we have to assume that the reflected field again consists of a superposition of all BMs in general. We therefore have
   $$\mathbf{e}_{+0}(x,y) + \sum_l \rho_{-l}\mathbf{e}_{-l}(x,y) = \sum_{nm} E^T_{y,mn}e^{i(K_{x,m}x+K_{y,m}y)} \quad (3.94)$$
   $$\mathbf{h}_{+0}(x,y) + \sum_l \rho_{-l}\mathbf{h}_{-l}(x,y) = \sum_{nm} H^T_{x,mn}e^{i(K_{x,m}x+K_{y,m}y)}. \quad (3.95)$$

Performing again an averaging over the interface we have

$$\langle \mathbf{e}_{+0}(x,y)\rangle + \langle \sum_l \rho_{-l}\mathbf{e}_{-l}(x,y)\rangle = E^T_{y,00} \tag{3.96}$$

$$\langle \mathbf{h}_{+0}(x,y)\rangle + \langle \sum_l \rho_{-l}\mathbf{h}_{-l}(x,y)\rangle = H^T_{x,00}. \tag{3.97}$$

By introducing the following abbreviations

$$Z_{+0} = \frac{\langle \mathbf{e}_{+0}(x,y)\rangle}{\langle \mathbf{h}_{+0}(x,y)\rangle},\ Z_2 = -\frac{\langle \sum_l \rho_{-l}\mathbf{e}_{-l}(x,y)\rangle}{\langle \sum_l \rho_{-l}\mathbf{h}_{-l}(x,y)\rangle},\ Z_0 = \frac{E^T_{y,00}}{H^T_{x,00}}$$

$$r_2 = \frac{\langle \sum_l \rho_{-l}\mathbf{e}_{-l}(x,y)\rangle}{\langle \mathbf{e}_{+0}(x,y)\rangle} \quad \text{and} \quad t_2 = \frac{E^T_{y,00}}{\langle \mathbf{e}_{+0}(x,y)\rangle} \tag{3.98}$$

where Z_{+0} is the tangential impedance of the zeroth order BM, Z_2 is the tangential impedance of the field reflected at the second (rear) interface and Z_0 is the vacuum impedance, we eventually obtain

$$1 + r_2 = t_2 \tag{3.99}$$

$$Z^{-1}_{+0} - r_2 Z^{-1}_2 = Z^{-1}_0 t_2. \tag{3.100}$$

The solution is trivial and the only interesting quantity t_2 amounts to

$$t_2 = \frac{Z_0(Z_{+0}+Z_2)}{Z_{+0}(Z_0+Z_2)}. \tag{3.101}$$

If light is only reflected from the zeroth order mode in the same backward propagating one, we have $Z^{-1}_{+0} = Z^{-1}_2$ and hence $t_2 = \frac{2Z_0}{Z_0+Z_2}$ as expected for a single mode medium.

The overall reflection R and transmission T amount to

$$R = r_1 = \frac{Z_1 - Z_0}{Z_1 + Z_0} \quad \text{and} \quad T = \tau_{+0}\frac{Z_0(Z_{+0}+Z_2)}{Z_{+0}(Z_0+Z_2)}e^{iK_{+0}D} = const.e^{iK_{+0}D}. \tag{3.102}$$

These are very similar compared to the equations (3.72) and (3.73) for an asymmetric system of layers. Hence, we can conclude that the retrieval firstly converges and secondly ξ/k_0 converges to the impedance (or its inverse ,respectively) of the first interface and k converges to the propagation constant K_l with the smallest imaginary part. Note that the impedance of the first interface is in general rather determined by a certain number of BMs than by the zeroth order mode only. However from the knowledge of the general convergence of the retrieval for absorptive systems and the instantaneous convergence for the single BM approximation we can conclude that the faster the retrieval is converging the better is the single BM approximation. The converged values are usually called the bulk parameters of the structure. Note that for three-dimensional system any substrate can induce an undesired bianisotropy [134] changing the effective properties of the metamaterial [135], in general. In general and if the single BM approximation is not perfectly valid, the system has then to be treated as an asymmetric one even if the MMs structure itself is symmetric.

3.4 Chapter summary and concluding remarks

In the previous subsections we have at first shown how to determine effective wave parameters, i.e. parameters the light propagation in and interaction with the bulk MM. They have been retrieved by inversion of the complex reflection and transmission coefficients. Subsequently, we have shown how to obtain effective material parameters from the wave parameters and discussed in particular the constraints on the wave parameters to allow for their reduction to the smaller set of material parameters. For local anisotropic media the reduction basically requires a linear dependency of the wave parameters. If they are linearly independent, material parameters cannot be assigned, since contradictive results would be retrieved for different illumination scenarios. This makes the inaccuracy of a description in terms of material parameters obvious. So the retrieval of wave parameters is a prerequisite for obtaining material parameters.

The retrieval is then discussed in the context of BMs, which are the normal modes of a periodic medium. By considering layers of stratified media, i.e. one-dimensional photonic crystals, the S-PR was shown to be perfectly suited for obtaining the wave parameters of symmetric systems. The principal property of the system allowing for the application of the PR procedure is the occurrence of only a single BM that dominates light propagation inside the bulk material. Independent on the thickness of the symmetric system, the S-PR determines correctly the propagation constant of the BM. The second parameter, the impedance, is defined by the tangential components of the Bloch amplitudes at the boundary. Both parameters are not subject to any convergence issues but can always be unambiguously determined. That basically proves that any symmetric slab system can properly be replaced by a homogeneous layer with the same propagation constant and the same impedance both at normal as well as at oblique incidence. These wave parameters need not to be reduced to material parameters in general as there were no restrictions made on the size of the systems at all. An arbitrary symmetric system obviously cannot be described by local constitutive relations. However, as soon as the unit cells become very small compared to the wavelength, i.e. in the quasi-static limit, the tangential components of the Bloch amplitudes reach constant values across the unit cell in longitudinal direction. The tangential impedance becomes independent on the termination of the system and it eventually becomes proportional to the propagation constant. In that limit the slab system can be described by local material parameters.

In the last subsection we then shed some light on the more important case of three-dimensional systems. The more interesting the investigation of such systems is, the more difficult it is, too. In general, a larger number of BMs determines the response of the system rather than a single one. As soon as only a single BM determines the optical response, the

system is obviously equivalent to an one-dimensional one, with the same conclusion to be drawn as above. If multiple BMs are excited, the convergence of the S-PR cannot be guaranteed at all. However, for the important case of lossy systems, we have shown that the S-PR indeed converges. Namely, the propagation constant converges towards the Bloch propagation constant of the lowest damped BM and the impedance to the tangential impedance of the first interface. In general, lossy systems are somewhere in between these limiting cases of the occurrence of only a single BM and the convergence due to losses, i.e. a decreasing influence of higher order BMs. The faster the convergence with an increasing thickness, the better the single BM approximation. Strictly speaking, only in case of instantaneous convergence it is worth to discuss about the reduction of the wave parameters to local material parameters at all.

Here, some remarks from a more physical point of view are necessary. It seems to be reasonable to assume that a single layer of metaatoms behaves differently than the bulk material. The metaatoms which are surrounded by other metaatoms experience a different environment leading to a different response. Then the parameters obtained for different thicknesses are supposed to converge to their bulk values as soon as the influence of the surface becomes negligible compared to the overall size of the structure. The bulk response may then be properly described by the zeroth order BM and the higher order BMs take into account all surface effects. In that context one might expect, that the response of the system is properly described by effective material parameters, which simply depend on the thickness of the system.

However, the S-PR for anisotropic materials, as introduced here, is capable of retrieving such parameters and, more importantly, allows to conclude on the validity of local effective parameters by investigating their angular dependency, since local effective parameters cannot depend on the angle of incidence at all. If, by any means, local effective material parameters can be introduced, they can be determined by the proposed S-PR.

Interestingly, to conclude on the locality of the system it is sufficient to consider the dispersion relation of the dominating BM. The bulk response of any material is certainly determined by the lowest damped, i.e. by the zeroth order BM. The propagation constant of that mode can be determined either by the S-PR for increasing thickness of the system or by other suitable methods (typically by solving the eigenvalue problem). The assumption of local constitutive relations necessarily restricts the form of the dispersion relation to ellipsoids (at least for media with 3 orthogonal mirror planes). If the dispersion relation of that zeroth order BM cannot be described by ellipse equations, the assumption of locality has to be dropped. That will be used later in section 4.4.

4 Investigation of left-handed metamaterial structures

In the present chapter the theoretical concepts introduced in chapter [2] and [3] are applied to different metamaterial (MM) structures. In particular, the developed S-parameter retrieval is used to characterize the optical response of left handed (also called negative index) metamaterials [136]. A medium is called left-handed, if the Poynting vector $\mathbf{S} = \Re[\mathbf{E}] \times \Re[\mathbf{H}]$ is antiparallel to the wavevector $\mathbf{k}$. Roughly speaking, this is equivalent to the requirement of $\Re[\mathbf{k}] < 0$ and hence $n < 0$. After elucidating the working principles of MMs showing the left-handed behavior or a negative refractive index, respectively, structures with increasing symmetry are investigated. Eventually a specific isotropic design of a negative index MM is discussed. Applying the theoretical concepts to specific examples will considerably enhance the understanding of the applied methods and in particular their restrictions.

For the numerical characterisation of all systems investigated here we used a non-commercial implementation of the Fourier Modal Method [137–143] and tabulated data for the permittivity of the metals [144], if not stated differently.

4.1 The working principles of left-handed metamaterial

The main driving force for the investigation of MMs is an artificial magnetic response of manmade structures in frequency domains where natural available materials do not posses an intrinsic magnetic response. Once such an artificial magnetic response of considerable strength is achieved, materials may be constructed that posses a negative refractive index in a certain frequency range by combining the magnetic constituents with elements that have an negative, typically metal-like, effective permittivity. Let us therefore have a closer look at elements (metaatoms) that show a magnetic dipolar response which is induced solely by the electric field. Since magnetic dipoles are associated with current loops we have to look for structures, where oscillating currents can be induced. Quite obviously a metallic ring-like structure may support such current distributions (see Fig. 4.1). However, if the ring is closed the current cannot be resonant and hence the induced magnetic dipole moment will be too small. It is therefore necessary to introduce a split into the ring at a certain

position to get it resonant at a certain frequency. The resulting element is called split ring resonator [46, 145–147] (SRR) and one of the most widely investigated metaatoms at all. It was at first discussed in the microwave regime [46] where an explanation in terms of an LC-resonator is usually applied to describe its electromagnetic response. In the optical domain its response is commonly described in terms of antenna resonances [119], although the LC explanation equally has predictive power [49]. The current eigenmodes of the SRR

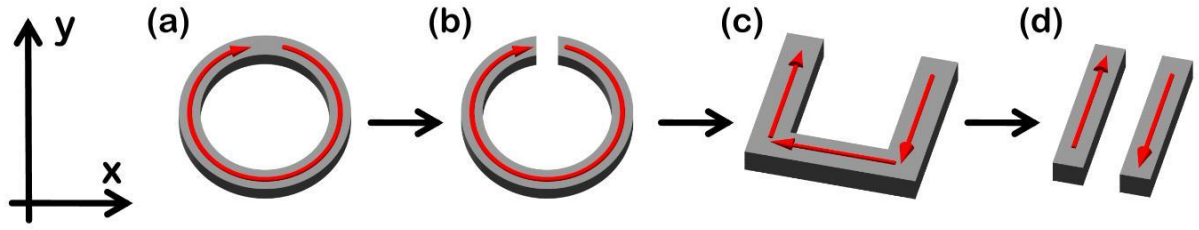

Figure 4.1: Developing a small particle with strong artificial magnetic resonances. The electric field exciting the current is polarized parallel to y with its gradient along x-direction. (a) Closed ring with non-resonant current. (b) Split ring with current being resonant due to the gap. (c) SRR similar to (b). (d) Cut wire pair with resonant antisymmetric current after removal of the SRR base in (c).

and their excitation are studied extensively and are well understood [119, 148, 149]. Maybe the most enlightening description of the eigenmodes of the SRR and their excitation as well as of other artificial magnetic metaatoms is given in terms of an coupled oscillator model as published in [64, 65]. Here only the necessary statements are recapitulated briefly. Basically two illumination schemes can be distinguished for which a current distribution is excited, that gives rise to a magnetic dipole moment parallel to the z-axis and parallel to the magnetic field of the exciting plane wave. For the first one the external electric field is along the x-direction. With the magnetic field parallel to the z-axis the propagation is along the y-axis. This scenario is undesirable since the SRR is not mirror-symmetric with respect to the propagation direction and effects of bi-anisotropy have to be taken into account to describe its response correctly [123, 150, 151]. The second scheme with the electric field parallel to the y-axis, preserving the mirror symmetry in propagation direction, is more desirable. In that case the desired current distribution is only excitable, if the electric field is varying with x, i.e. retardation becomes important. Hence, the SRR cannot be arbitrarily small. On the other hand, to achieve a resonant magnetic dipolar response in the optical domain the SRR must be small compared to the wavelength. To further increase the resonance frequency and to achieve structures that are optically small the geometry has to be modified. The simplest and best way is to remove the base of the SRR. The resulting structure, called cut wire pair, is composed of two near field coupled metallic/plasmonic wires only [see Fig. 4.1 (d)]. Each of these wires acts as a resonant dipole. For low frequencies the coupled system basically supports two modes, a symmetric one at higher frequencies and an antisymmetric one at

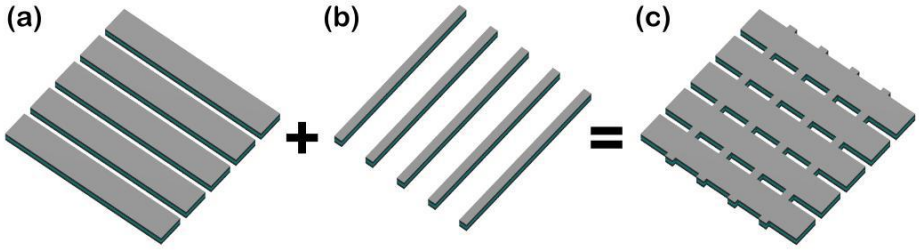

Figure 4.2: Schematic construction of the Fishnet MM. (a) Metallic double-wires separated by a dielectric spacer serve as a double cut-wires supporting the desired antisymmetric plasmonic eigenmode. (b) Metallic wires providing the diluted metal-like behavior. These wires are also separated by an dielectric spacer, which only serves to keep the structure technologically feasible without any functional meaning. The desired response is obtained for an exciting incident field, that is polarized parallel to the thin wires only. (c) Combining both elements leads to the fishnet structure. Only a single functional layer is shown, which can be realized experimentally by a three layer fabrication scheme.

lower frequencies. These eigenmodes and their frequency splitting can be understood in terms of a hybridization model [152]. The antisymmetric mode clearly resembles the desired current distribution, that leads to the magnetic dipolar response. The symmetric one results in a strong electric dipole-like response [69].

The second ingredient for a negative index MM, namely a structure with a negative effective permittivity, is found easily. Simple wires, as used for any wire grid polarizer, basically behave like a diluted metal with a plasma frequency determined by the metal itself and the filling fraction of the metal. Of course, the metal-like behavior is achieved, only if the electric field is oriented parallel to the wires.

The magnetic metaatoms are combined with the metallic wires to achieve a negative refractive index MM. The first negative index MM was composed of metallic wires with SRRs in the microwave domain [5]. For the optical domain cut wire pairs together with wires are used to achieve the same [153–155]. In Fig. 4.2 the construction of the fishnet MM [52] is shown schematically. The fishnet MM is often preferred in the optical domain due to its superior performance in terms of a figure of merit defined as $\mathrm{FOM} = -\Re(n)/\Im(n)$ [156]. The larger the FOM the more negative the refractive index and the less absorptive the material is. Note, that absorption is often the limiting factor but intrinsic to the used metals. Due to its geometry the fishnet is biaxial anisotropic and even for normal incidence sensitive to the polarization. This polarization sensitivity is undesirable and hence a large of amount of variations of the fishnet were proposed [156–158] to achieve a polarization independent or even an isotropic negative index MM. The first step towards the desired isotropy is to create a structure that has a fourfold rotational symmetry with respect to the z-axis [159–161]. In Fig. 4.3 the construction of the Swiss cross (SC) [162] MM, which is investigated later on in

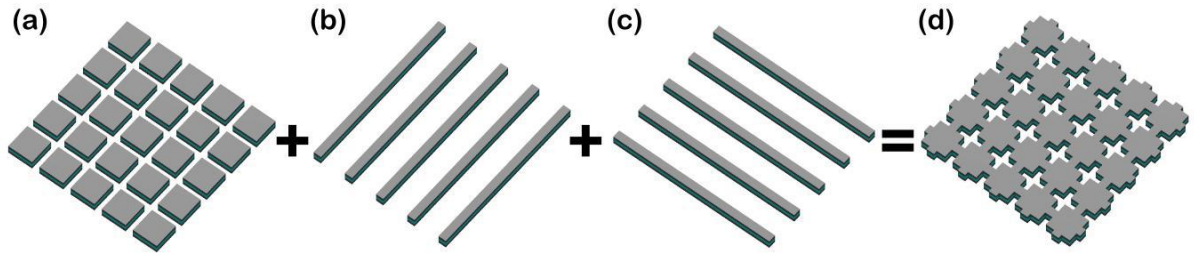

Figure 4.3: Schematic construction of the C_4-symmetric Swiss cross MM. (a) The double plates serve to support the desired antisymmetric plasmonic resonance. Combining the plates with an orthogonal mesh of thin wires as shown in (b) and (c) finally provides (d) the C_4-symmetric Swiss cross negative index MM. Again the structure can be easily fabricated due to the three layer scheme.

detail, is shown schematically. The response of the SC in the quasi-static limit is uniaxial anisotropic with the optical axis being parallel to the z-axis. The actual performance of the MMs proposed above is investigated comprehensively in the following subsections.

4.2 The fishnet - a left-handed metamaterials at optical frequencies

In this subsection the characterisation of the fishnet MM in the optical frequency range is discussed in detail. At first the response at normal incidence is investigated with respect to the convergence of the effective properties towards their bulk values. At second the investigation is extended to oblique incidence. It is shown, that the principal response of the fishnet is only weakly depending on the actual number of functional layers used to build up the system and the main characteristics are determined by the zeroth order Bloch mode (BM) - the lowest damped one. This proves, that the fishnet might be properly described by effective wave parameters. Contrarily, it will be shown in the last part of the present section, that the fishnet might not be described by local effective material parameters in general. The results presented here are published in [88, 89, 163].

The fishnet is probably the most prominent negative index MM investigated so far. Its superior performance in terms of the FOM is employed in all frequency domains ranging from microwave frequencies to visible light. We are interested here only in its characterisation in the optical domain, whereas most of the general results and conclusions do also apply to other frequency domains. The general difference between the different frequency domains stems, of course, only from the underlying material dispersion of the used materials.

We choose here, for several reasons that will be explained below, a particular set of geometrical parameters for the fishnet and discuss the principal results. The principal geometry under investigation is shown in Fig. 4.4. Its unit cell consist of two perforated metallic layers

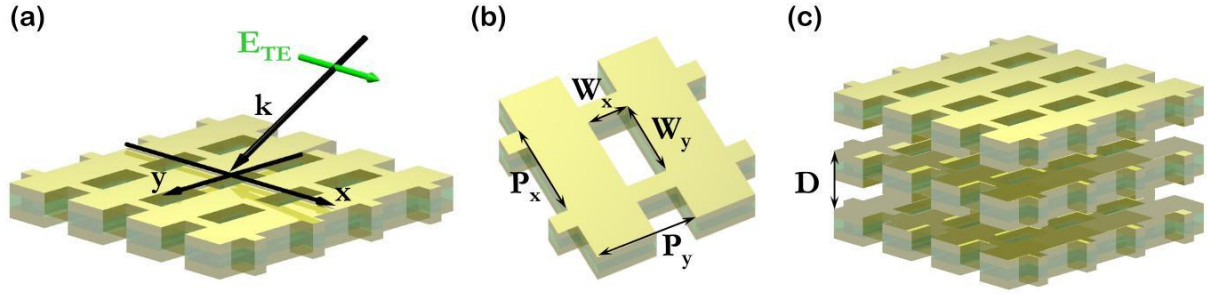

Figure 4.4: Schematic drawing of the fishnet MM. (a) Single functional layer consisting of two metallic (silver) layers (thickness $d_{\mathrm{Ag}} = 45\,\mathrm{nm}$) separated by a dielectric spacer (MgF_2 - $\varepsilon_{\mathrm{MgF_2}} = 1.38^2$, thickness $d_{\mathrm{MgF_2}} = 30\,\mathrm{nm}$), principal coordinate system and principal operating scheme with $\mathbf{k} \perp \mathbf{x}$ and $\mathbf{E} \parallel \mathbf{x}$. (b) Top view of the unit cell with $P_x = P_y = 600\,\mathrm{nm}$, $W_x = 284\,\mathrm{nm}$ and $W_y = 500\,\mathrm{nm}$. (c) Stack of three functional layers defining the thickness of a single functional layer ultimately to $D = 200\,\mathrm{nm}$. The geometry shown here is kept fixed in all calculations, except the investigation of the scaling behavior, where all formerly mentioned parameters were multiplied by a scaling factor f.

separated by a dielectric spacer. This three layer system is usually called a single functional layer. Subsequent functional layers are separated in propagation direction for convenience by an air gap, where the size of the air gap is determined by the period in z-direction. Such an air gap is defined meaningfully only for systems composed of several functional layers. For a single functional layer the definition of the thickness of the unit cell is rather arbitrary and the air gap is then introduced only for conceptional reasons that will become more obvious below. Of course, restricting to a particular geometry limits the generality of the results, but is important since already for a single set of geometrical parameters the characterisation of the entire optical response becomes demanding. Changing the geometrical parameters of a functional layer will have a strong influence, in particular, on the frequency of the resonances. This effect is naturally exploited while upscaling the spectral domain of operation. It was recently shown, that the dependency of the resonance position on the geometrical parameters can be used to tailor the optical response of multiple-functional-layer fishnets [164]. The geometrical parameters of the functional layers are chosen such that the strength of the negative refractive index resonance is reasonably large at relatively large frequencies, where the influence of the lateral and vertical size is discussed in the preceding section. Another important parameter is the distance between subsequent functional layers, i.e. the size of the air gap. The smaller the air gap is the larger the coupling between subsequent functional layers. In first approximation, where a coupling between subsequent functional layers can be neglected, the decrease of the distance simply leads to an increase of the density (the filling fraction) of the resonant elements and hence to an increase of the resonance strength of the equivalent homogeneous medium. On the next level of approximation subsequent functional layers are weakly coupled. The convergence of the effective parameters depending on the number of

functional layers towards the bulk properties will become worse, since a single functional layer will behave significantly different compared to a sequence of functional layers or even an infinite structure. In the context of BMs that simply means, that the parasitic influence of higher order BMs increases [165–167]. A further decrease of the distance eventually leads to major modifications in the optical response [104, 168] and in general a larger number of BMs contributes to the light propagation inside the medium. Hence, very desirable is a balance between a high filling fraction, leading to strong resonances, and a weak coupling of subsequent functional layers, preserving the response of the individual layer. This regime is reasonably achieved by choosing an unit cells size in propagation direction of $a_z = 200\,\mathrm{nm}$.

A final important issue concerns the termination of the structure. Whereas a homogeneous medium is independent on its termination, mesoscopic systems like MMs do not fulfill this requirement a priori. A dependency e.g. of the reflection coefficient on the choosen termination logically results from different impedances of the equivalent homogeneous medium, while the propagation constant remains the same. Consistently, effective parameters like the permittivity and the permeability are different for different terminations. In an extreme case this may lead to a medium, that is double negative, i.e. ε and μ have simultaneously negative real parts, at one termination, whereas it is single negative for a different termination. However, we will not discuss this dependency here and focus on a fixed termination as shown in Fig. 4.4.

The anisotropic fishnet as shown is Fig. 4.4 is designed to be operated with x-polarized light. I.e., only light with an electric field being polarized along the x-axis is supposed to show the negative index behavior. Therefore, the investigations are restricted to that case in the following. At first the response at normal incidence is investigated and the results for different finite as well as for the infinite system are discussed. Then the optical response is investigated for oblique incidence [50, 169] and finally the requirements on the size of the fishnet are elaborated, which are necessary to adequately describe it by effective material parameters.

The results for the effective parameters n and ξ as well for the derived effective parameters ε and μ at normal incidence are shown in Fig. 4.5. The solid, colored lines correspond to the values as determined by the S-parameter retrieval for an increasing number of functional layers (1, 2, 4 and 8). The black dotted lines correspond to the values as obtained from the dispersion relation of the infinite system. All subfigures have in common that the results for the finite system are converging very well with an increasing number of functional layers towards their bulk counterpart; at least for frequencies up to 250 THz. The deviations for larger frequencies will be explained later on. Let us focus for the moment on the values for the effective refractive index as shown in Fig. 4.5 (a) and (b). Here the refractive index is shown instead of the propagation constant, since the refractive index is usually the quantity of

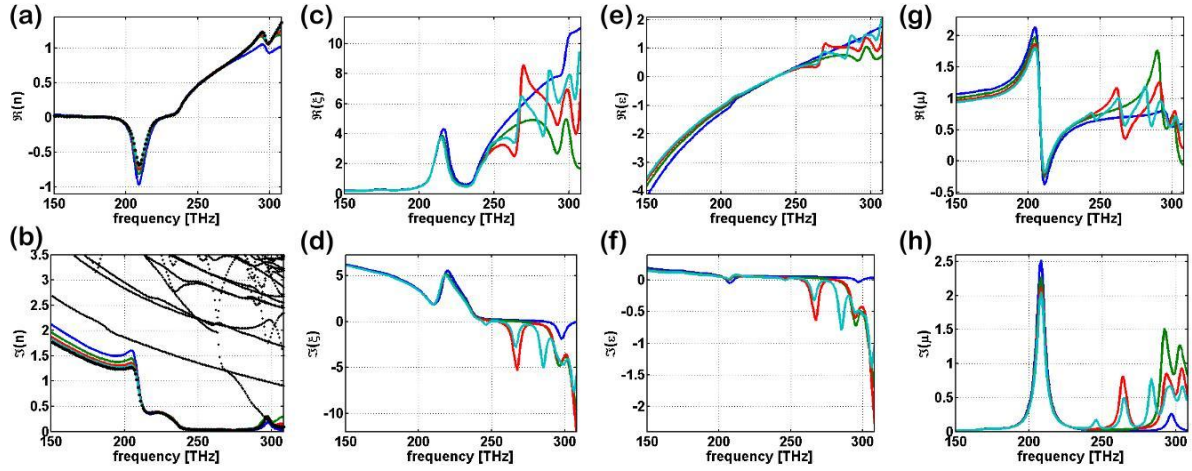

Figure 4.5: Upper row: Real part of the effective parameters n, ξ, ε and μ over the frequency. Lower row: Corresponding imaginary parts of the effective parameters. The solid lines correspond to values as obtained by the S-parameter retrieval method at normal incidence, applied to fishnets consisting of different numbers functional layers (1-blue, 2-green, 4-red and 8-cyan). The black dotted line in (a) is the real part of the effective index of the lowest damped BM. In (b) the imaginary parts of all BMs are shown. Note the convergence of the effective parameter with increasing number of functional layers and the convergence of the effective index with an increasing number of functional layers to the n of the BM.

interest. However, at normal incidence the refractive index is simply given as the normalized propagation constant $n = k_z/k_0$. In (a) the real part of n is given for the finite system (solid) and the real part of n for the lowest damped BM [see also Fig. 4.5 (b)]. Clearly, in the entire range, also for frequencies larger than 250 THz, the values for the finite system are converging exactly towards the n of the lowest damped BM. The effective refractive index is negative for frequencies around 210 THz. Figure 4.5 (b) shows the imaginary part of n for the finite and the infinite system. The solid lines clearly converge to the black dotted line with the smallest value, i.e. to the lowest damped one. Additionally, the values of the next larger damped BM (solid dotted lines) are shown, too. Over the entire frequency range all higher order modes are damped much stronger. In fact, the one with an imaginary part of $2.6\mu m^{-1}$ at 150 THz can couple only to y-polarized light and hence the next modes to which x-polarized light couples are damped even much higher. Only at 300 THz the imaginary part of a higher mode decrease significantly. Therefore, for frequencies up to 300 THz the effective propagation constant is very well described by the lowest damped BM, i.e. the phase advance in transmission is basically determined by that BM. Note, that the imaginary part of the refractive index is very low for frequencies larger than 240 THz.

Figure 4.5 (c) and (d) show the results for the value of ξ as retrieved from the finite system. For the case of TE-polarization ξ is given by $\xi = k_0/ZZ_0$, i.e. proportional to the inverse of the impedance Z. While the effective n is related to the phase advance

of the propagating mode in the bulk material, the impedance accounts for the coupling of the incident field to the structure. The impedance generally converges to the value as obtained from reflection at a semi-infinite half space of that material. I.e., when the value for the finite system is converging we know that either the single BM approximation is quite well satisfied or that simply the light which is back-reflected at the rear interface does not contribute to the overall reflection. Since the imaginary part of the effective index is quite large for frequencies smaller than 240 THz, the impedance is converging rapidly. For larger frequencies the imaginary part of n is quite small and back-reflected light may contribute significantly to the overall reflection. Since the effective impedance is converging worse in the present example, the single BM approximation is not quite well satisfied. Therefore, the bad convergence of the effective impedance limits the usefulness of these effective parameters to frequencies smaller than 250 THz.

The results of the effective permittivity ε and the effective permeability μ are shown in Fig. 4.5 (e)-(h). Since ε and μ are simply derived as products and ratios of n and ξ their convergence is limited by the convergence of n and ξ. Therefore, it is meaningful to discuss their dispersive behavior only up to 250 THz. As expected, the effective ε basically resembles the behavior of a metal, where the effective μ becomes resonant at the negative refractive index resonance. Note, that the artificial magnetic resonance is quite strong and the real part of μ achieves even negative values rendering the fishnet to be a double negative (DNG) medium.

Eventually, some general comments on the latter effective parameters ε and μ are necessary. Since x-polarized light is used to probe the fishnet, the effective parameters might be identified with the tensors elements ε_x and μ_y. However, such an identification implies that the fishnet is properly described by local effective material tensors. This assumption is not valid in general. There is only a single set of R and T for each frequency and illumination configuration and it is not known in general, if these effective parameters are valid for another angle of incidence, too. This is checked separately below. Therefore, we refrain here from calling them material parameters and simply understand them as a thickness independent representation of R and T. In that sense, they are best understood as wave parameters similar to n or k and ξ or Z, respectively.

Another remark concerns the antiresonances resulting in negative imaginary parts of either the effective permittivity or permeability (see e.g. Fig. 4.5). Such antiresonances are typically understood as artifacts of the applied retrieval methods, which are related to the periodicity of the MM [87, 170]. Since a negative imaginary part seems to violate the condition of passivity, these antiresonances are said to be unphysical. However, several considerations suggest that this is not valid in general. Sophisticated experiments are proposed to show, that materials exhibiting such a negative imaginary part act as a the source of energy. To

prove that, a thin layer of the particular material is placed in front of a perfect electric (magnetic) conductor (depending on the material parameter exhibiting the antiresonance) with a distance of $\lambda/2$. The electric (magnetic) field is supposed to have a zero crossing at this distance and hence only the magnetic (electric) field probes the material. Such calculations were performed for a cut-wire structure, showing that the conclusion to be drawn is not valid in general for simple reasons. For materials, that show the antiresonance, the thickness is too large to approximate the magnetic (electric) field as constant and the electric (magnetic) field as a linear function crossing zero. To allow for this approximation, the thickness has to be reduced significantly. Simultaneously, the antiresonances were shown to vanish. For all scenarios, that were considered (including random distance) the absorbed power is positive, rendering the argumentation to be invalid. Very recently, A. Alu published an article on the restoration of the meaning of effective material parameters [79]. Here, the physical origin of the antiresonances is related to effects of second order spatial dispersion. He transforms the constitutive relation containing 3 local effective parameters (ε, μ and κ accounting for second order spatial dispersion), which are free of antiresonance, to 2 so called equivalent effective parameters $\varepsilon_{\mathrm{eq}}$ and μ_{eq}, which show antiresonances. Since $\varepsilon_{\mathrm{eq}}$ and μ_{eq} are an equivalent description of the same medium, we simply have to conclude that for media exhibiting spatial dispersion the constraint of passivity, as identified from the imaginary part of the permittivity and permeability, has to be dropped. However, the issue of antiresonances is less important than any accidental angular dependency of the effective parameters (discussed below), that has to be investigated at first to probe for the locality of the effective parameters.

As shown above, the optical response of the fishnet is rapidly converging towards the bulk behavior for increasing number of functional layers and is very well described by the lowest damped BM. The case of oblique incidence remains to be checked. Since ε and μ are simply derived from k and ξ, the properties at oblique incidence are discussed by means of the latter two only. The results for different numbers of functional layers as well as for different angles of incidence ranging from 0 to 90 degrees are shown in Fig. 4.6. Similar to normal incidence the effective propagation constant of the equivalent slab is converging with an increasing number of functional layers (1,2,4 and 8 - solid colored lines) towards the propagation constant of the lowest damped BM (black dotted line) for all angles of incidence and all frequencies. The convergence, however, becomes slightly worse with an increasing angle of incidence as can be best seen from the results of the imaginary part of k in Fig. 4.6 (b). The abrupt change in the real as well as in the imaginary part for larger angles of incidence is attributed to the onset of the first diffraction order in reflection as well as transmission. In fact, for grazing incidence the kink occurs at 250 THz where $a = 600\,\mathrm{nm} = \lambda/2$. Although the influence of this higher diffraction order becomes negligible for thicker structures, describing the fishnet as an effective homogeneous medium becomes meaningless beyond these frequencies.

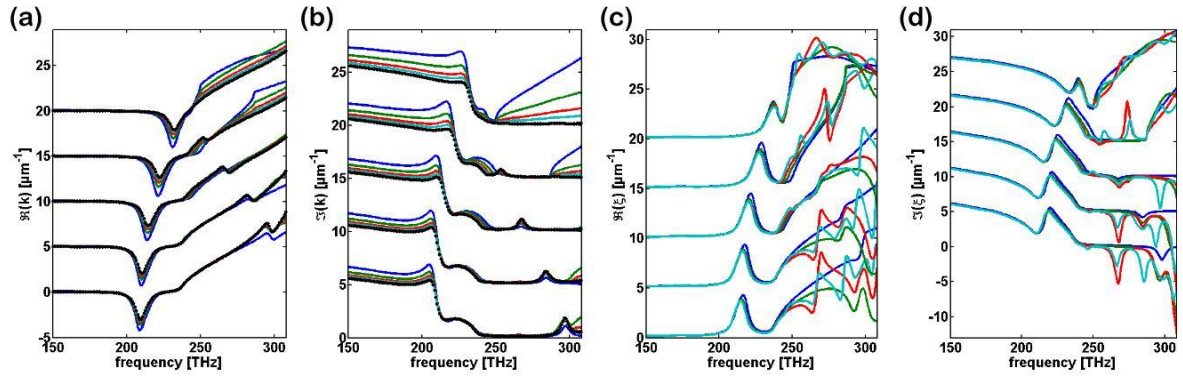

Figure 4.6: Effective parameters k and ξ of the fishnet over the frequency for discrete angles of incidence $k_t \in (0, 0.25, 0.5, 0.75, 1)k_0$. For increasing angle of incidence the values are shifted by $+5\mu m^{-1}$ with respect to the smaller angle to keep them clearly separated. The colored solid lines correspond to different numbers of functional layers of the fishnet (1-blue, 2-green, 4-red and 8-cyan). The solid dotted line in (a) and (b) correspond to the propagation constant of the lowest damped BM. Note the shift of the negative index resonance to larger frequencies with increasing angle of incidence and the good convergence of the effective parameters for frequencies up to 250 THz.

Figure 4.6 (c) and (d) shows the real and the imaginary part of ξ. Similar to normal incidence the values are converging reasonably only for frequencies up to 250 THz. Hence, considering the response to be effectively homogeneous is limited to frequencies up to 250 THz anyway. Very importantly, the resonance, where the real part of the propagation constant is negative, strongly shifts from 210 THz to 230 THz with an increasing angle of incidence. This may be understood by a very simple picture in terms of the phase advance between the metallic layers of a single functional layer. The artificial magnetic resonance and hence the negative propagation constant occurs at the antisymmetric resonance of the currents in subsequent metal layers. This resonance depends on the phase difference of the exciting field between the upper and the lower layer [64]. In a first approximation this resonance occurs independent of the frequency at a fixed phase difference $\Delta\Phi$. Keeping the distance fixed we have $\Delta\Phi \propto k_z \propto \sqrt{k_0^2 - k_x^2}$ in free space. For an increasing angle of incidence (k_x) the same phase difference is achieved for larger frequencies (k_0). This crude approximation predicts the shift of the resonance towards higher frequencies correctly. Note, that similar arguments hold, if the permittivity of the dielectric spacer is changed, whereas the situation becomes completely different, if the distance between the layers is changed due to the strong dependency of the coupling on the distance. With deceasing distance, the resonance shifts exponentially to smaller frequencies being in strong contrast to the simple picture introduced before.

The shift of the resonance as well as the similarity of the effective propagation constant compared with the fundamental BM becomes clearer in Fig. 4.7. Here, the real and the imaginary part of the propagation constant are plotted as retrieved from the single func-

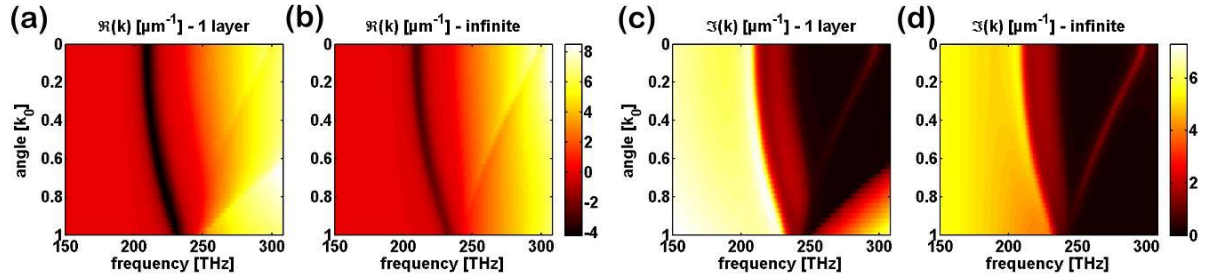

Figure 4.7: Comparison of the effective propagation constant of a single functional layer fishnet as obtained by the S-parameter retrieval with the propagation constant of the lowest damped BM of the infinite structure over the frequency and the angle of incidence. The real parts are shown in (a) and (b) for the finite and the infinite structure, respectively. The corresponding imaginary parts are shown in (c) and (d).

tional layer fishnet. Also, the propagation constant of the fundamental BM, i.e. for the infinite system, for varying angle of incidence as well as frequency is shown. Although slight variations with respect to the strength of the resonance are observed, the principal dispersive behavior is in very good agreement. The response of the single layer fishnet is very well understood in terms of the dispersive properties of the fundamental BM. Clearly the resonance shifts with increasing angle of incidence towards higher frequencies. This leads to the surprising phenomenon, that at frequencies above the negative index resonance, e.g. 220 THz, the negative index resonance occurs at higher angles of incidence but not at normal incidence. In Fig. 4.7 (c) the kink in k occurring at higher frequencies and larger angles of incidence due to appearance of the first diffraction order is again clearly visible.

In the preceding paragraphs it was shown at first, that the fishnet is well described by effective parameters k and ξ (Z), which are rapidly converging with an increasing number of functional layers towards their bulk values up to 250 THz and at second, that the response is well described by the fundamental BM. Already a single layer fishnet basically behaves like the infinite structure. The question remains, if such a fishnet might be properly described by local effective material tensors. In general, this is not possible, as will be shown in the following by evaluating the response at oblique incidence in greater detail. Subsequently, conditions on the applicability of local material tensors are discussed.

The fundamental requirement on local effective parameters with respect to the angular dependency of the wave parameters k and ξ is the invariance of the ratio k/ξ. If this ratio is constant for all angles of incidence, it can be identified with an element of the effective material tensors, i.e. for TE-polarization $k/\xi = 1/\alpha = \mu_y$. As a local effective parameter μ_y has to be independent of the angle of incidence. If the ratio is not constant, the assumption of locality has to be dropped. Then, the description of the optical response cannot be simplified and the characterisation is restricted to effective wave parameters k and ξ, that

have an intrinsic angular dependency. For the single layer fishnet that ratio is shown in Fig. 4.8 for varying frequency and angle of incidence in (a) and (b) and for the frequency where the real part of k is minimal in (c). Again, a shift is clearly observed for the artificial

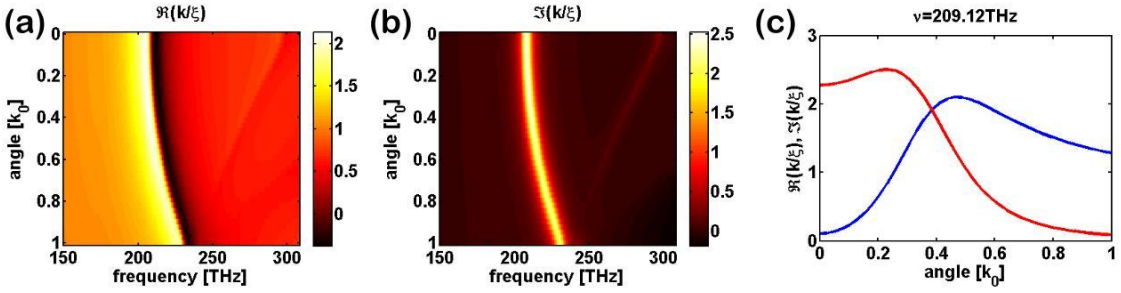

Figure 4.8: Real part (a) and imaginary part (b) of the ratio k/ξ over the frequency and the angle of incidence. In (c) k/ξ is shown for the frequency where $\Re(k)$ is minimal, i.e. most negative, at normal incidence (blue - $\Re(k/\xi)$, red - $\Im(k/\xi)$).

magnetic resonance towards higher frequencies with increasing angle of incidence. The cut in Fig. 4.8 (c), showing the ratio for a fixed frequency at resonance, impressively points out the strong angular dependence. The ratio is not constant with the angle and therefore the set of wave parameters cannot be further reduced to the smaller set of local material parameters, although weak spatial dispersion is taken into account. Hence, the fishnet, as used here, is obviously not operating in the regime of weak spatial dispersion. Naturally the question arises under which conditions the fishnet might be described by local effective material parameters, i.e. how small has the wavelength to be compared to the structure size so that the response is approximately local? To answer that question the fishnet is scaled down by a factor f, while keeping all other parameters constant. The scaling factor f ranges from 0.01 to 1, where 1 represents the fishnet as originally proposed (see Fig. 4.4). Note, that the underlying strong dispersion of the constituent materials inhibits an increase of the wavelength to cell size ratio by a simple decrease of the frequency.

At first, the effective parameters of the single functional layer fishnet are determined at normal incidence for varying frequency and the scaling factor f. The results for the most relevant quantities k, ε and μ are shown in Fig. 4.9. Simply speaking, with an increasing scaling factor the response, as obtained for $f = 1$, basically shifts towards larger frequencies. But even more important and eventually limiting the scaling behavior fundamentally, the strength of the resonance decreases considerably while decreasing the structure size and finally vanishes with $f \to 0$ [see e.g. the imaginary part of the effective permeability in Fig. 4.9 (f)]. Of course, the weaker the resonance gets, the less pronounced is the region of negative refraction (negative propagation constant k) as can be seen best from Fig. 4.9 (a). In the limit of $f \to 0$ the effective permeability becomes $\mu \to 1$ and the overall response is given by the metal-like behavior mediated entirely by the effective permittivity, as expected

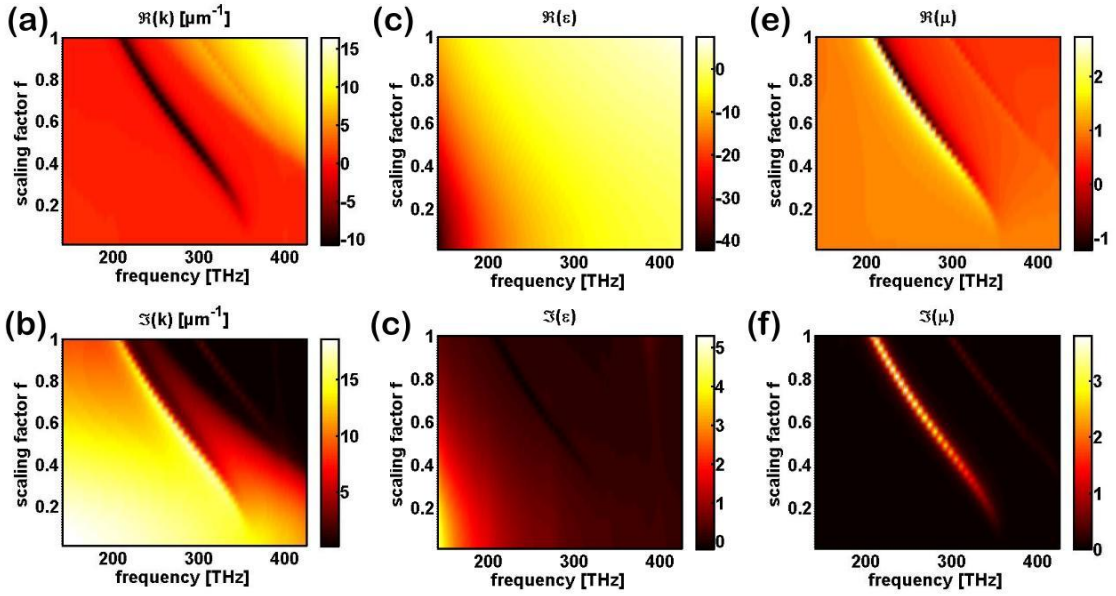

Figure 4.9: Real (upper row) and imaginary parts (lower row) of the effective parameters k, ε and μ for a single functional layer fishnet at normal incidence over the frequency and the scaling factor f as obtained by the S-parameter retrieval.

in the quasi-static limit.

Note, that the effective parameters of the fishnet are defined without the additional air layers, i.e. consisting only of the two metallic sheets and the dielectric spacer. As long as only single functional layers are considered, this is of no importance, since any additional air layer simply dilutes the response. For a single functional layer the thickness of the slab is arbitrary to a certain extent and can be defined meaningfully only for stacks by means of the distance between subsequent layers. Since the focus is here only on the characterisation of the single functional layer fishnet, this issue has no influence on the results in general.

In the second step the optical response (reflection and transmission) is determined for varying angles of incidence and again frequency and scaling factor f. For every single frequency the ratio $\alpha = \xi/k$ is probed on its angular behavior and the scaling factor is determined, for which the variation of the ratio with the angle of incidence does not exceed a certain value. The tangential wavevector component k_t is varied between 0 and $1.2\,k_0$ including a small part of the evanescent waves with respect to air. Of course, material parameters have to be valid for evanescent part of the angular spectrum, too. The following error estimate Δ is defined as

$$\Delta = \frac{\max(|\alpha(k_t) - \alpha(0)|)}{|\alpha(0)|} \tag{4.1}$$

with $k_t \in (0, 1.2\,k_0)$. Δ serves as a measure to characterize the variation of α and is displayed in Fig. 4.10 together with the real part of k at normal incidence. Several bounds for this deviation Δ are considered, ranging from 0.1% to 5%. Clearly, close to the resonance this

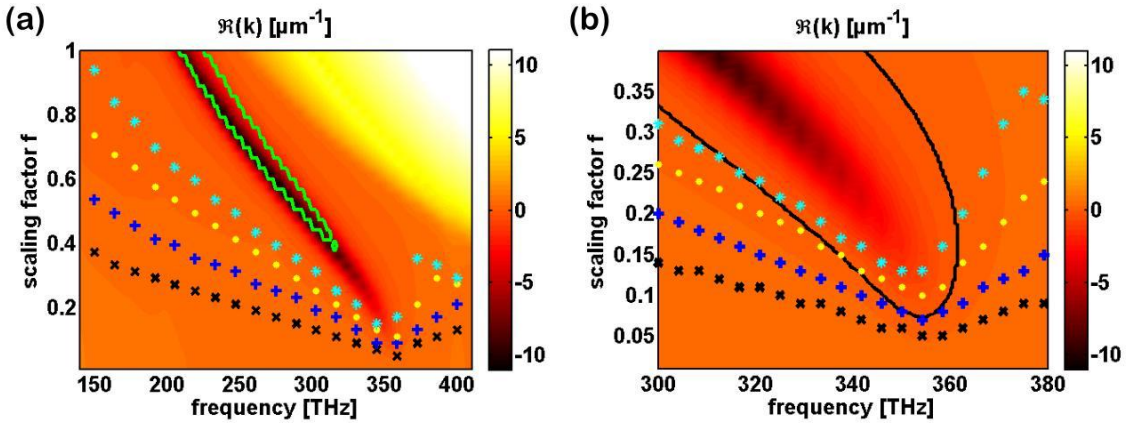

Figure 4.10: (a) Real part of the effective propagation constant of the single functional layer fishnet over the frequency and the scaling factor. (b) Magnified image of (a). The green solid line shown in (a) corresponds to the line of $\Re(\mu) = 0$, i.e. inside this domain the real part of the effective permeability is negative. For scaling factors smaller than $f = 0.4$ the permeability gets positive for all frequencies and hence the fishnet becomes a single negative medium. The black solid line shown in (b) corresponds to $\Re(k) = 0$, i.e. inside this domain the fishnet has a negative refractive index. For scaling factors smaller than $f = 0.08$ the region of the negative refractive index disappears. The dotted lines indicate the contours of constant deviation Δ. (cyan asterisks - 5%, yellow dots - 2%, blue plus - 0.5%, black crosses - 0.1%)

deviation is strongest for a fixed scaling factor. Since an effective description holds only for almost invariant α this deviation should be as small as possible, but values of 5% might be tolerable at most. This condition requires a scaling factor of about 0.15 in the resonance region; resulting in an wavelength to cell size ratio of $\lambda/P > 10$. Note, at frequencies close to the resonance the deviation does not vanish even for ratios of $\lambda/P \approx 100$, where the real part of k becomes positive everywhere [see the black solid line in Fig. 4.10 (b)]. Evidently, the resonance strength is very weak in this domain leading to a non-magnetic response of the material (see the green solid line in Fig. 4.10 (a) indicating $\Re(\mu) = 0$). This is consistent with the assumption that such small structures can be described in the quasi-static limit where no magnetic response is observed.

Hence, the result of this studies is quite discouraging, namely: a sufficiently strong magnetic response requires a certain minimum unit cell size/wavelength ratio (about 1:3), but this mesoscopic structure must not be described by conventional frequency-dependent effective permittivity and permeability tensors. We have proven this for a fishnet structure, but since all present optical MMs rely on similar resonances, we conclude that this will hold in general.

To sum up, based on the assumption of a weakly spatially dispersive conductivity in MM unit cells we have developed a method to verify/falsify an effective anisotropic medium description of MMs. We have shown that a prototypical magnetically active, and thus poten-

tially negative index, material, namely the fishnet, cannot be described as a homogeneous anisotropic medium in the relevant resonance region. By varying the ratio of wavelength to cell size we have elaborated the limitations of the weak spatial dispersion assumption. There is a trade off: If the spatial dispersion is weak and the material parameters have the usual meaning, the antisymmetric plasmonic resonance, which is responsible for magnetic activity, is also weak or disappears. Our work clearly indicates that for optical MMs the commonly assigned effective parameters do not have the physical meaning of conventional material parameters.

4.3 The Swiss cross - a polarization independent left-handed behavior

The development of structures, that are polarization independent, is an important step towards isotropic negative index MMs. In collaboration with the Institute of Applied Physics, Friedrich-Schiller-Universität Jena, we have designed and characterized both numerically and experimentally the polarization independent Swiss cross MM [162, 171]. All experimental work was done by C. Helgert (IAP) whereas the contribution of this author was to provide the numerical analysis and theoretical understanding.

The geometry of the Swiss cross MM is conceptually derived from the fishnet MM, where the formerly rectangular shaped holes now have a cross shape giving rise to the name (see Fig. 4.11). The focus of the present investigation is on the experimental realization and characterisation of the structure, whereas numerical simulations, which take into account all the details of the fabricated structure, are necessary to support the measurements.

Contrary to the millimeter and microwave domain, in the visible frequency domain only intensities can be measured with reasonable effort, whereas for the retrieval of effective parameters the complex scattering coefficients are required. However, it was recently shown that a measurement of the phase is feasible also in the visible domain [172]. To rely on the numerical simulations only, the simulations must describe the response of the sample properly, i.e. the measured intensities in reflection and transmission must coincide with the simulated ones. Therefore, the process of design and characterisation is usually threefold. At first, the structure is numerically investigated and optimized e.g. for a large negative refractive index at a certain wavelength. At that step the cross shaped holes where still assumed to have sharp edges with vertical sidewalls. At second the structure is fabricated in our case by lift-off lithography. Due to fabrication imperfections a third step is necessary, where the structure is again simulated with geometrical parameters as deduced from the SEM images from the fabricated sample. Having a closer look at Fig. 4.11 (a) is becomes

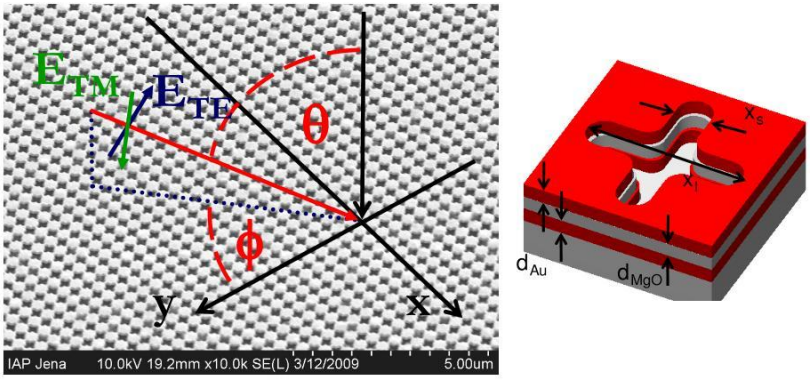

Figure 4.11: Left: SEM image of the fabricated sample together with the principal coordinate system and the definition of the angles of incidence and the polarization. We thank C. Helgert from the IAP Jena for providing this SEM image. Right: Artistic view of a single unit cell as used for the simulations. The red layers are made up of gold. The dielectric layer in between is made if MgO have almost the same permittivity as the substrate. The geometrical parameters are given in the main text.

obvious that the sidewalls of the holes are not perfectly vertical as initially proposed. They have a tilt angle of approximately 10 degrees. Also, the edges of the cross are rather round than sharp. Finally, the thicknesses of the metal and dielectric layers are known up to a precision of a few nanometers only. Therefore, simulations are done for varying geometrical parameters, where the range of parameters is given by the precision of the SEM image. The set of parameters, for which the deviation between measured and simulated intensities is minimal, describe the overall response best. Although this might sound questionable, it is on the one hand a widely accepted procedure and on the other hand yields very good results, as is shown in the remainder of this subsection. It was even suggested in a recent publication of Plum et al. [173] to be the method of choice at optical frequencies. In fact, the geometrical parameters, which reproduce the optical response at normal incidence best, will be shown to be capable of describing the actual response at any angle of incidence almost perfectly.

Both the numerically and experimentally obtained intensities of the reflected and transmitted field are shown in Fig. 4.12 (a). Clearly, the curves for the simulated and the measured intensities are almost in perfect agreement. The parameters used for the simulations [see also Fig. 4.11 (b)] are given by a period of $P = 410\text{nm}$, $d_{\text{Au}} = 30\text{nm}$, $d_{\text{MgO}} = 37.5\text{nm}$, $x_l = 310\text{nm}$ and $x_s = 80\text{nm}$. The values of x_l and x_s describe the width of the cross at the center of the dielectric layer, which has a permittivity of $\varepsilon_{\text{MgO}} = 2$. The width at the upper and lower gold layer are determined by an inclination angle of 10 deg. The substrate has a permittivity of $\varepsilon_{\text{sub}} = 2.07$. These parameters obviously describe the fabricated sample sufficiently good. Note, that we are mainly interested in the resonance at $1.4\,\mu\text{m}$. For wavelengths smaller than $0.9\,\mu\text{m}$ the deviation between both results is a little worse in reflection. But even there the characteristic dips are properly retained indicating a good representation.

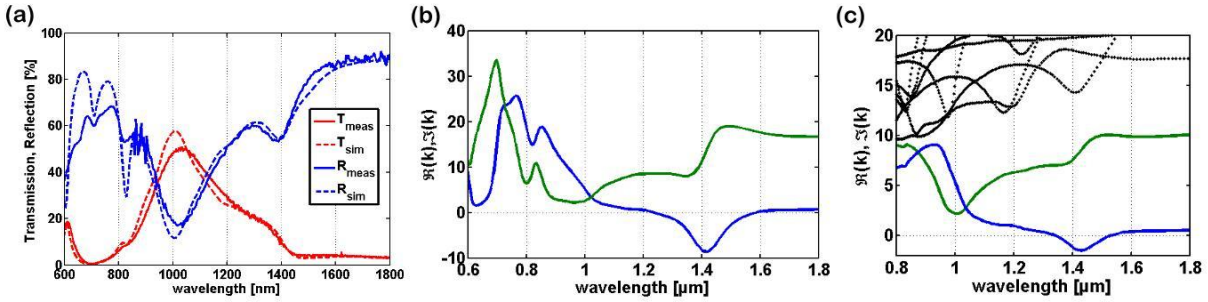

Figure 4.12: (a) Measured and numerically determined reflected and transmitted intensities. Both results are in almost perfect agreement rendering the geometrical parameters used for the simulations to be very well estimated. (b) Real (blue) and imaginary (green) part of the propagation constant as retrieved from the simulated complex scattering coefficients at a single layer SC MM. Note the pronounced negative index resonance at 1.4 μm. (c) Real (blue) and imaginary (green) part of the propagation constant fundamental BM of the infinitely extended SC MM. The dotted black curves give the imaginary parts of the higher order BMs, which are much stronger attenuated for all frequencies of interest. The values for k of the fundamental mode are slightly smaller than those in (b) because of the additional spacer between subsequent functional layers, which is missing for the single layer SC.

As shown above, the simulated data can be used to describe the structure. The effective propagation constant as retrieved from the simulated data is shown in Fig. 4.12 (b). The wavelength region of main interest is around 1.4 μm. Here, the real part of the propagation constant is negative. Due to quite large losses the FOM is smaller than 1. Values for the effective permeability and permittivity at normal incidence are shown in [162]. Due to the fourfold rotational symmetry of the structure, the optical response is polarization independent at normal incidence, which is also proven for the fabricated sample [162].

To prove, that the bulk Swiss cross MM behaves similar to the single layer SC, the dispersion relation of the BMs is calculated. Here each three-layer functional slab is placed on a 50nm substrate with 50nm dielectric spacer ($\varepsilon = 1$) above, to retain the surrounding and, hence, the resonances. The results are shown in Fig. 4.12 (c). The green and black lines correspond to the imaginary part of the least damped and higher order BMs, respectively. The blue curve is the real part of the least damped BM. The additional dielectric spacer is necessary to keep subsequent unit cells weakly coupled and hence retain the basic properties of the single slab. In the limit of a vanishing dielectric spacer the physics will change considerably. The spacer of course dilutes the medium and hence the negative index resonance is less pronounced compared to the single slab case Fig. 4.12 (b). However, the qualitative behavior is equivalent. This indicates, at first, that light propagation through the SC is dominated by the lowest damped BM. All higher order BMs (black curves) are much stronger damped in the entire frequency range. Note, that the domination of a single BM is a prerequisite for a MM to be considered as a homogeneous medium. And at second,

even if several SC slabs are stacked to form a thicker structure, the negative index resonance is retained.

In a next step the angular dependency of the optical response is investigated. Therefore, the transmission is measured for both polarizations (TE and TM) at two high symmetry planes of incidence, defined by $\varphi = 0$ and $\varphi = \pi/4$ and the surface normal, depending on the angle of incidence θ and the wavelength λ. The experimental (upper row) as well as the simulated results (lower row) for the zeroth diffraction order are shown in Fig. 4.13. The agreement between both is astonishing. At first glance they are almost identical. They

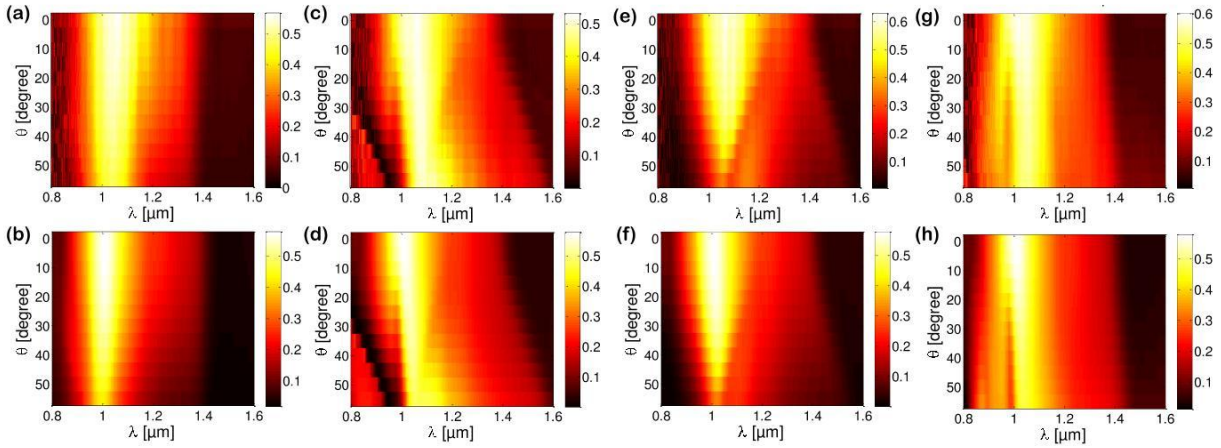

Figure 4.13: Transmission for various polarization states and planes of incidence over the wavelength and the angle of incidence. Upper row: measured data. Lower row: simulated data. [(a) and (b)] TE-polarization at $\varphi = 0°$. [(c) and (d)] TM-polarization at $\varphi = 0°$. [(e) and (f)] TE-polarization at $\varphi = 45°$. [(g) and (h)] TM-polarization at $\varphi = 45°$.

are distinguishable only by the small noise of the experimental data for small wavelengths. In particular, all experimental features of the spectra are fully revealed in the simulations. This again suggests that the geometrical parameters determined once for normal incidence describe the entire response of the sample correctly, i.e. for further considerations we can fully rely on the complex simulated data. That also implies, that the fabricated sample is almost perfectly periodic with negligible deviations of the unit cells across the sample.

Some words on the chosen planes of incidence are necessary. At first, at the chosen high symmetry planes the polarization, either TE or TM, will be maintained in transmission as well as in reflection due to the mirror-symmetry with respect to these planes. This holds for every structure having that kind of symmetry regardless of the wavelength to cell size ratio. Note that higher diffraction orders may become propagating in reflection as well as in transmission if the wavelength is too small. Then considering the zeroth diffraction order only becomes meaningless anyway. And at second, the conservation of the polarization is crucial for the application of the S-parameter retrieval as discussed in chapter [3]. For any other plane of incidence than the chosen ones the structure will not maintain the polarization

for TE and TM polarized waves in general [174].

A final comment concerns the abrupt variations in Fig. 4.13 (c) and (d) for smaller wavelengths/larger angles of incidence. They indicate the onset of a higher propagating diffraction order in the substrate. This higher diffraction order is significantly excited for TM polarization only. For TE polarization [Fig. 4.13 (a) and (b)] this first diffraction order is two orders of magnitude weaker, hence the transmission is almost continuous. For $\phi = 45°$ the first diffraction order appears for much smaller wavelengths or larger angles of incidence, respectively, since the effective period is increased by a factor of $\sqrt{2}$. Of course, the effective homogenization of MMs is restricted to wavelength domains, where only the zeroth diffraction order is propagating [165, 166].

The simulated data are used to retrieve the effective refractive index of the structure for the different planes of incidence and polarizations. Here, the effective refractive index is defined as

$$n_{\text{eff}}(k_x, k_y) = \frac{1}{k_0}\sqrt{k_x^2 + k_y^2 + k_z^2}, \tag{4.2}$$

where $k_0 = \frac{\omega}{c}$ is the wavenumber in free space, $k_x = k_0 \sin(\varphi)\sin(\theta)$ and $k_y = k_0 \cos(\varphi)\sin(\theta)$ are given by the angle of incidence (θ, φ) and k_z is determined by the S-parameter retrieval. So n_{eff} gives the length of $\mathbf{k}$ normalized to k_0 inside the structure. In that sense the effective refractive index is simply a different representation of the dispersion relation. The principal advantage of a refractive index lies in its potential to simplify the description of the dispersion relation. For example, for an isotropic medium n_{eff} is a constant with respect to the angle of incidence. Hence, the complex dispersion relation can be described by a single quantity only. For lossy anisotropic structures the general behavior is more subtle, but both the real and the imaginary part of n_{eff} are at least monotonous with varying angle of incidence. For structures like the SC MM with an axis of 4-fold rotational symmetry the response in the quasi-static limit is expected to be independent of φ for a given polarization, which is equivalent to polarization conservation for all φ. Since negative index MMs are often supposed to show a refractive index, which is polarization insensitive and independent of the angle of incidence, the use of n_{eff} is preferred. This means, in particular, that isotropy or quasi-isotropy is achieved, if this effective index remains (almost) constant with varying angle of incidence.

The actual results for the effective refractive indices are shown in Fig. 4.14 (a)-(d). Note, that the transmission is given only for angles accessible to the experimental setup between $\theta = 0..55°$, whereas the numerically obtained refractive index is given for angles up to $\theta = 80°$.

For normal incidence an asymmetric plasmonic eigenmode of the unit cell is excited at $\lambda = 1400\,\text{nm}$, where the angular dependence of optical response in this region is at the focus of the investigation. For TE polarization at $\phi = 0°$ the refractive index depends only slightly on the angle of incidence θ as given in Fig. 4.14 (a). In particular the wavelength

dependence of the left handed region does not change with θ [see Fig. 4.14 (e) and (f)] but its width decreases slightly. For TM polarization the situation is qualitatively different. The region of left handed behavior is shifted towards smaller frequencies by an increasing angle of incidence. For a fixed wavelength of $\lambda = 1400\,\text{nm}$ the refractive index becomes even positive with increasing θ, as shown in Fig. 4.14 (e). Even more peculiar, for $\lambda > 1400\,\text{nm}$ the strongest negative refractive index occurs for oblique incidence. This phenomenon was already discovered and discussed in [88, 175]. The asymmetric resonance is excited best for a nonvanishing tangential wavevector component. The discontinuous behavior of the refractive index for large θ at smaller wavelength is attributed to higher diffraction orders in the substrate as discussed for the transmission above. Note, that the optical response is very different for TE and TM polarization at $\phi = 0°$. For $\phi = 45°$ the situation is quite similar. For both polarizations the region of left handed behavior changes, if θ varies and

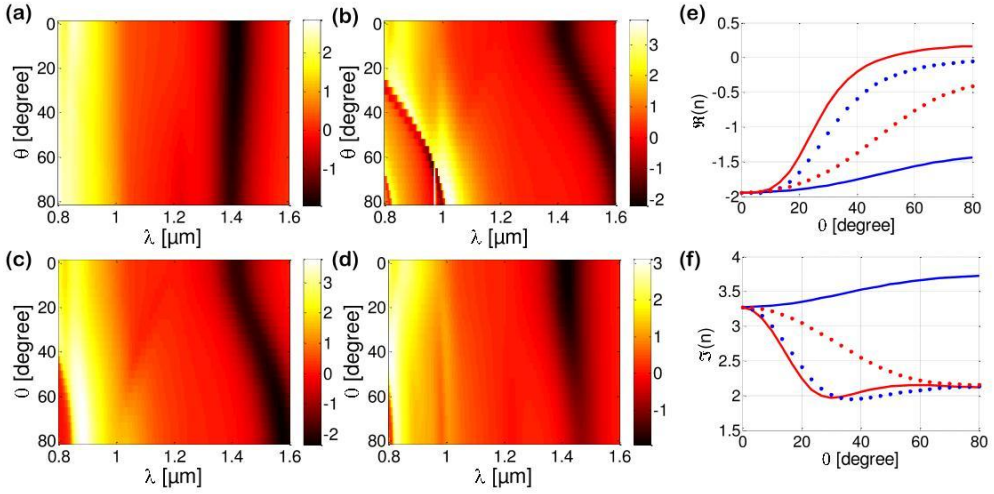

Figure 4.14: Real part of the effective index for selected combinations of polarization states and incidence planes as obtained from the numerical data. (a) TE, $\phi = 0°$, (b) TM, $\phi = 0°$, (c) TE, $\phi = 45°$, (d) TM, $\phi = 45°$) depending on the wavelength and the angle of incidence. (e) and (f) real and imaginary part of the effective refractive index at $\lambda = 1400\text{nm}$ for all four configurations of polarization states and planes of incidence. Solid lines: $\phi = 0°$, blue: TE, red: TM. Dotted lines: $\phi = 45°$, blue: TE, red: TM.

its width is typically decreasing with increasing θ. The refractive indices for $\phi = 0°$ and $\phi = 45°$ should be identical for an purely anisotropic medium with a C_4-symmetry and effective material tensors $\hat{\varepsilon}_{\text{eff}}(\omega)$ and $\hat{\mu}_{\text{eff}}(\omega)$. With Fig. 4.14 (e) and (f) it is clear that both the real and the imaginary part of the n are strongly depending on the polarization and the angle of incidence. Any attempt to use the SC as an imaging device will be limited by this variation [175].

Both, numerically and experimentally, the angular dependent optical response of a Swiss cross MM was investigated, which exhibits a polarization independent left handed behav-

ior/negative refractive index at normal incidence. Here, it turned out that the derived effective optical properties depend both on the polarization state and the angle of incidence reflecting the effect of spatial dispersion on the optical response. Hence, the angular resolved effective parameters cannot be understood as material parameters but may only serve to simplify the description of light propagation inside the MM. It was revealed, that only for a certain linear polarization and a specific plane of incidence a negative refractive index is observed to be almost independent on the angle of incidence. The experimental results are in almost perfect agreement with the numerical ones.

4.4 The split cube in carcass - a seemingly isotropic left-handed metamaterial

The majority of applications, in particular for negative index MMs, require the structures to act optically isotropic. A wide variety of publications is dedicated to their investigation either by group theoretical approaches aiming at identifying suitable geometries or by calculating the optical response of particular structures [176–183]. However, most of the proposals have severe shortcomings. On the one hand, the group theoretical approaches may provide geometries, that possesses identical optical properties along principal propagation directions due to e.g. the chosen cubic symmetry. But their overall response is optically isotropic only in the quasi-static limit. The investigations done on particular structures, on the other hand, are often performed only for certain high symmetry directions. They do not cover all possible directions and more importantly, they are mostly limited to lossless materials. Since resonant structures are typically made of metallic materials, this is an inadmissable assumption. In the following results are presented for a very promising candidate for an

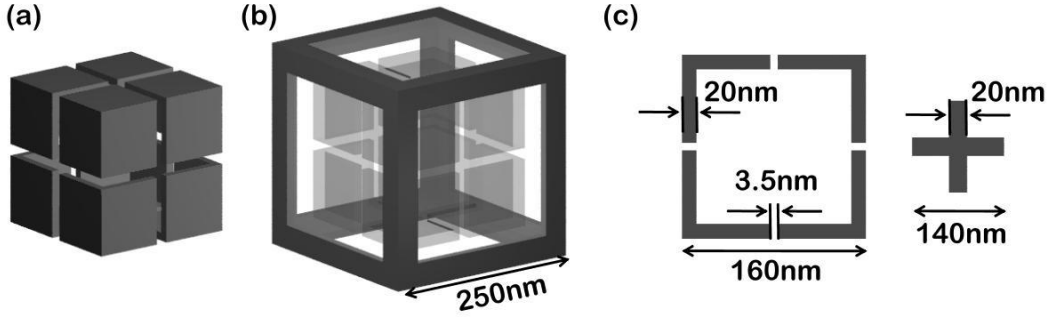

Figure 4.15: Artistic view of the split cube in carcass MM. All elements are supposed to be made of gold. The entire structure is embedded in a dielectric with $\varepsilon = 2.25$ to keep the structure technologically reasonable. (a) Image of the split cube. (b) Image of the Carcass building together with the semi-transparent split cube the unit cell of the SCiC MM. (c) Cross section of the Split cube and cross section of cross shaped wire defining the Carcass with geometrical parameters.

optically isotropic negative index MM, namely the Split Cube in Carcass (SCiC) MM [184]. It is shown to exhibit a frequency region of lefthandedness in the optical domain, where all requirements on a homogeneous medium are met. The dispersion relation of the BMs is calculated across the entire Brillouin zone, taking the dispersive and absorptive behavior of the materials correctly into account. However, based on these investigations it must be concluded, that the SCiC is far from being optically isotropic, in particular, in the resonant frequency region of lefthandedness.

The system under consideration is shown in Fig. 4.15. The metallic split cube is the three-dimensional analogue of a split ring resonator with cubic symmetry. It is designed to support resonant current eigenmodes resembling magnetic dipolar currents. These magnetic dipolar currents should result in the desired artificial magnetic response. By changing the width of the gaps the resonance frequency can be adjusted. The outer system of cross shaped wires resembles a three-dimensional wire medium. The wires where chosen to be cross shaped to assure a high density of the structure. The width and the thickness of the wires determines the amount of interconnected metal in the structure. The more metal is included the larger is the effective plasma frequency of the wire medium. Hence, for a fixed frequency the structure becomes more metal-like and the real part of the effective permittivity reaches larger negative values, with an increasing filling fraction. The geometrical parameters, as given in Fig. 4.15, where carefully adjusted by numerical optimization to obtain a pronounced region of lefthandedness at normal incidence. The unit cell has a cubic symmetry with a lattice constant $a = 250\,\mathrm{nm}$. The cubic symmetry of the overall system ensures that the optical response becomes isotropic in the quasi-static limit.

In a first step, the effective properties of the finite structure are investigated with an increasing number of functional layers. The application of the S-parameter retrieval allows for the calculation of the complex propagation constant k and the complex impedance Z. The results for the retrieved effective propagation constant as well as the effective refractive index $n = k/(\omega/c)$ are shown in Fig. 4.16. The solid lines correspond to the different values of functional layers used to build up the system, where blue indicates 1, green 2 and red 5 functional layers. Additionally the propagation constants of the first BMs are shown as black dotted lines, where the lowest damped BM coincides with the values retrieved for the finite structure. Importantly, across the entire frequency range the propagation constant of the lowest damped BM has a significant smaller imaginary part than all other modes. Hence, upon propagation through the structure that mode will dominate the behavior. The effective properties are converging very fast with an increasing thickness towards their bulk values. The deviation between the different lines is basically negligible. This has important consequences. At first the propagation inside the structure is dominated by the zeroth order BM. And at second an incident plane wave couples predominantly to that mode. Hence,

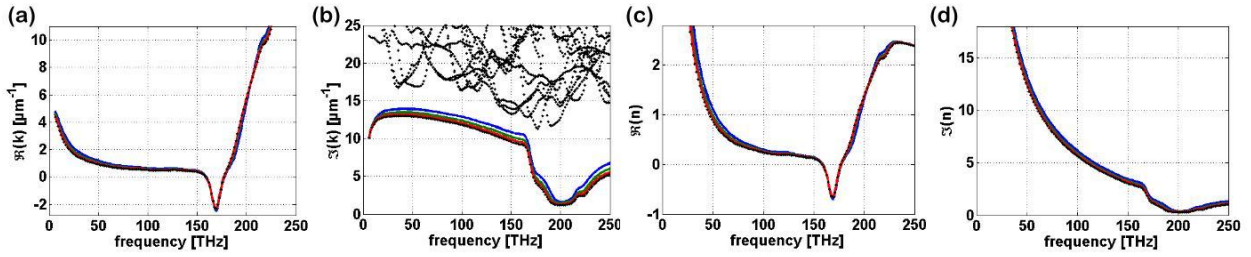

Figure 4.16: Effective propagation constant k and refractive index n of the SCiC over the frequency. The solid lines are the values as obtained for the finite structure for different numbers of functional layers: blue - 1 layer, green - 2 layers, red - 5 layers. The dotted lines are the values for the infinite structure, i.e. the propagation constants of the BMs. (a) Real part of k. (b) Imaginary part of k. (c) real part of n. (d) imaginary part of n.

the single BM approximation is quite well satisfied and the structure can be considered as homogeneous. That will allow us to characterize the structure later on by that zeroth order BM only.

Clearly the structure exhibits a region of $\Re(k) < 0$ around 170 THz. For frequencies smaller than 160 THz the SCiC is best described as a metallic slab with a small real part and a large imaginary part of k. For frequencies larger than 180 THz the SCiC behaves like a strongly absorbing dielectric. This may be anticipated also from Fig. 4.17, where the real

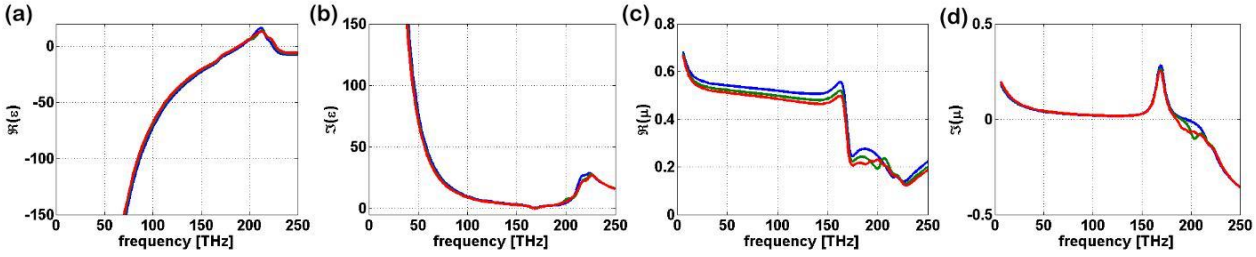

Figure 4.17: Spectral dependent effective permittivity ε and permeability μ of the SCiC. The lines are the values as obtained for the finite structure for different numbers of functional layers: blue - 1 layer, green - 2 layers, red - 5 layers. (a) Real part of ε. (b) Imaginary part of ε. (c) real part of μ. (d) imaginary part of μ.

and imaginary parts of the effective permittivity ε and the effective permeability μ are shown as retrieved from $k = \sqrt{\varepsilon\mu}$ and $Z = \sqrt{\mu/\varepsilon}$ at normal incidence. Although the results for Z are not shown here, the values of Z for different thicknesses obviously converge since those for ε and μ are converging. The real and imaginary part of the permittivity are indicating a purely metallic behavior below 160 THz. For frequencies larger than 180 THz the real part of ε becomes positive. For all frequencies below 200 THz, which actually is the highest frequency of interest, the effective permeability has small positive values. Hence, above 180 THz the response is similar to a strongly absorbing dielectric. The effective permeability has almost constant values both in real and imaginary part for frequencies below 160 THz.

At 170 THz the permeability shows considerable dispersion with a rather strong peak in the imaginary part. This is indeed the desired magnetic resonance induced by the split cube. The origin of the main features can be further clarified by investigating the comprising elements, namely the slit cube and the carcass, independently. This is presented here for the carcass only. The results for the real and the imaginary parts of the effective ε and the effective μ

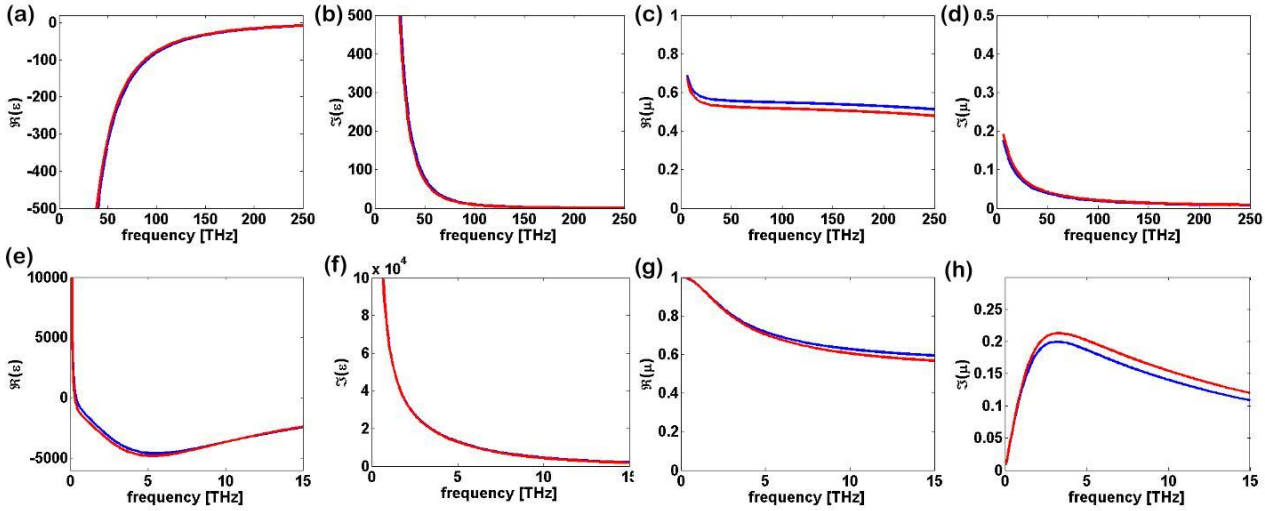

Figure 4.18: Effective permittivity ε and permeability μ of the Carcass over the frequency. The lines are the values as obtained for the finite structure for different numbers of functional layers: blue - 1 layer, red - 5 layers. (a) Real part of ε. (b) Imaginary part of ε. (c) real part of μ. (d) imaginary part of μ. The figure (e)-(h) provide a detailed view of the figures (a)-(d) for small frequencies.

are shown in Fig. 4.18 (a)-(d). The blue line indicates the use of a single layer, where the red lines corresponds to 5 layers. The difference between both is again negligible. Already a single layer acts bulk-like. By comparing these results with the results for the SCiC shown in Fig. 4.17 (a)-(d) it becomes obvious that the response of the SCiC is dominated by the metal-like behavior of the Carcass for frequencies smaller than 160 THz. Also we can conclude that the resonance at 170 THz is indeed due to the split cube. For larger frequencies the response of the SCiC is determined by a complex interplay of both. Interestingly, the carcass shows, additionally to the metal-like response, a diamagnetic behavior in the whole frequency range, where the real part of the effective permeability has an almost constant value of $\mu \approx 0.5$. This is rather unexpected at least for very small frequencies. Therefore, the response is recalculated with high frequency resolution between 0.1 and 15 THz. The results are shown in Fig. 4.18 (e)-(h). In fact, in the limit of $\omega \to 0$ the effective permeability reaches $\mu = 1$.

Let us shortly repeat the basic conclusions before we proceed in investigating the dispersion relation. The optical properties of the SCiC are shown to converge very fast towards their bulk values. Already a single layer of the SCiC MM can be described properly by bulk parameters. That essentially proves, that the single BM approximation is well satisfied and

the propagation characteristics are determined by the zeroth order Bloch only. Although the validity of the single BM approximation is shown for normal incidence only, it also holds for oblique incidence, which was proven for the main planes of incidence at TE-polarization. For the sake of brevity these redundant results are not shown here.

The cubic SCiC is, therefore, a promising candidate for an isotropic left-handed/negative refractive index MM. It remains to be investigated, whether the SCiC behaves optically isotropic, i.e. the refractive index is independent of the propagation direction, or not. Since the main focus is on the region of lefthandedness, the dispersion relation of the BMs is calculated for a fixed frequency of 170 THz, where the real part of the refractive index is most negative at normal incidence. Above, the lowest damped BM was shown to determine the optical response sufficiently well. Hence, only the properties of that mode have to be discussed here. The real as well as the imaginary part of the corresponding propagation constant are shown in Fig. 4.19 (a) and (b) in the first Brillouin zone. The first Brillouin

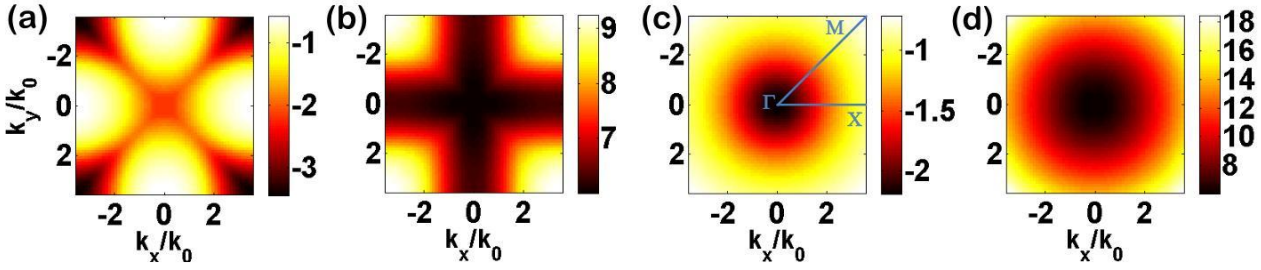

Figure 4.19: Real (a) and imaginary (b) part of the propagation constant of the lowest order BM in the first Brillouin zone. Real (c) and imaginary (d) part of the propagation constant of an isotropic medium with the same refractive index as the SCiC at normal incidence.

zone is determined by $k_{x,y} \in \{-\frac{\pi}{a}, \frac{\pi}{a}\}$ with $a = 250\,\text{nm}$ and $\mathbf{k}_\perp = (k_x, k_y)^T$. If the outer medium is vacuum, $|\mathbf{k}_\perp| = k_0$ means grazing incidence. For comparison we have also shown in Fig. 4.19 (c) and (d) the real and the imaginary part of the propagation constant for an ideal medium with an assumed isotropic refractive index identical to that of the real structure at normal incidence, i.e. $k_z = -\sqrt{k_0^2 n_0^2 - k_x^2 - k_y^2}$ with $n_0 = k_z(\mathbf{k}_\perp = 0)/k_0$.

At first we notice that both the real and the imaginary part of the propagation constant of the MM are not rotationally symmetric and monotonically changing with increasing absolute value of the tangential component $\mathbf{k}_\perp$ as for the isotropic medium. In particular, the dependency on the transverse wave vector is tremendously different when compared to the isotropic medium. While the real part is monotonically increasing with $|\mathbf{k}_\perp|$ in the ΓX-direction it is non-monotonously decreasing in the ΓM-direction. Also the imaginary part is strongly increasing in the ΓM-direction and only slowly varying in the ΓX-direction. Hence, any formally introduced effective refractive index would explicitly depend on the transverse wave vector $\mathbf{k}_\perp = (k_x, k_y)^T$. Therefore, the introduction of a global effective refractive in-

dex is pointless since no additional information is obtained. Nevertheless for paraxial wave propagation the introduction of a local effective refractive index is feasible. Near the Γ-point the isofrequency surface is approximately spherical where the validity of this approximation strongly depends on the frequency and the wavelength to cell size ratio.

It should be mentioned, that the choice of real valued k_x and k_y is arbitrary to a certain extent. In lossy media, the complex nature of the dispersion relation cannot be neglected. The dispersion relation could also be calculated for complex valued $\mathbf{k}_\perp$. On the other hand, it is pointless to provide these values as they are not accessible in any experiment. The tangential wave vector components are continuous at boundaries and only real valued plane wave solutions can exist in free space, therefore this choice reflects experimental constraints.

To evaluate the optical isotropy of the SCiC more quantitatively, the relative deviation between the numerically obtained propagation constant and the ideal spherical isofrequency surface is calculated. To quantify this deviation the effective refractive index at oblique incidence is compared to that at normal incidence. From symmetry considerations and the exemplary results in Fig. 4.19 it is clear, that an investigation of the dependency in the high symmetry ΓX and ΓM direction is sufficient, where it is assumed, that these points are extremes of the iso-frequency surface for a fixed value of $|\mathbf{k}_\perp|$. Fig. 4.20 (a) and (b) show the real part of the propagation constant for both high symmetry directions as a function of the frequency and of the tangential wave vector component $\mathbf{k}_\perp/k_0$, where k_0 is the free space propagation constant. The edge of the first Brillouin zone for the largest possible frequency (200THz) is at $|\mathbf{k}_\perp|/k_0 \approx 3$ since

$$\frac{|\mathbf{k}_\perp|}{k_0} = \frac{\pi}{ak_0} = \frac{\lambda(200\mathrm{THz})}{2a} = \frac{2\cdot 10^6}{200\cdot 10^{12}}\mathrm{c} \approx 3.$$

The most important frequency region is the black domain of lefthandedness, where the Split Cube provides an artificial magnetic response. Also, the iso-error lines for the relative error

$$\Delta = \left| \frac{|k_\mathrm{z}| - |k_\mathrm{z}|_\mathrm{ideal}}{|k_\mathrm{z}|_\mathrm{ideal}} \right| \tag{4.3}$$

with $|k_\mathrm{z}|_\mathrm{ideal} = |\sqrt{k_z^2(\mathbf{k}_\perp = 0) - |\mathbf{k}_\perp|^2}|$ are given as green lines for several values. The quantity Δ is a measure for the relative deviation of the modulus of the propagation constant for oblique incidence from that for normal incidence. The modulus is taken, because all quantities are complex-valued. The iso-error lines in the non-resonant regime ($\omega \lessapprox 150\,\mathrm{THz}$) scale approximately with $1/\omega \propto \lambda$. This results from the fact, that the homogeneous medium approximation improves with a decreasing unit cell size to wavelength ratio a/λ. For frequencies larger than 160 THz the structure becomes resonant and an abrupt change of the iso-error lines is clearly observable.

Obviously in the resonant regime the MM is approximately isotropic only, if the ratio a/λ is much less than in the non-resonant regime. In general, the situation is identical for both

planes of incidence (ΓX- and ΓM-direction). However, for larger frequencies the deviation of the calculated iso-frequency lines to the ideal ones is slightly smaller in ΓM- than in ΓX-direction but not significantly.

Note, that the introduction of the quantity Δ is only one option to quantify the deviation of the pertinent isofrequency surface from the ideal one. Other measures are also possible, where, for example, the deviation of the length of the actual wavevector compared to the length of the wavevector in an isotropic medium yields qualitatively the same results.

Before we proceed to discuss the results, some remarks concerning the investigated parameter space are in order. Here, the dispersion relation is not calculated up to the edge of the Brillouin zone, but for fixed, normalized tangential wave vectors, which translate for propagating waves into certain angles of incidence. This is more useful, since for very low

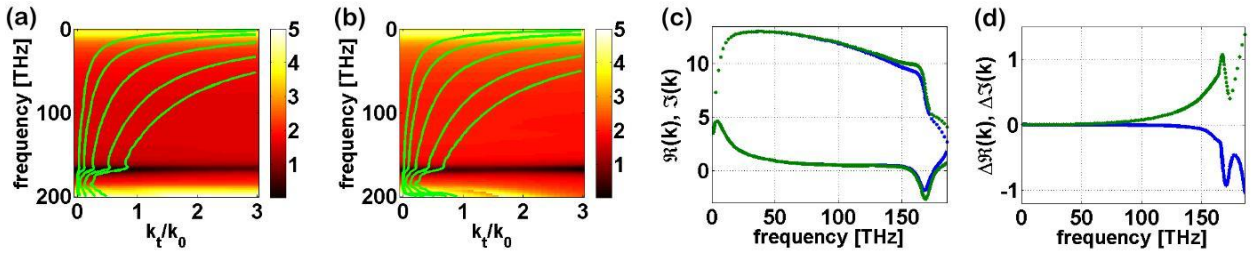

Figure 4.20: (a) Real part of the propagation constant as a function of the frequency and the angle of incidence where the plane of incidence is parallel to the coordinate axes. (b) The same as (a) with plane of incidence rotated by $\pi/4$, i.e. the ΓM direction. The green iso-error lines correspond to the relative deviations $\Delta \in [0.02, 0.1, 0.5, 2, 5]\%$ (from left to right). (c) Real part (solid line) and imaginary part (dotted line) of the propagation constant $k[\mu\mathrm{m}^{-1}]$ of the two lowest damped BMs at $|\mathbf{k}_\perp| = k_0$ that are degenerated at normal incidence. (d) difference between the real parts (blue line) and the imaginary parts (green line) of these two modes as function of the frequency. In the quasi-static limit, i.e. $\lambda \to \infty$ the difference is of course vanishing and both modes are degenerated.

frequencies it is not possible to provide incident plane waves with tangential wave vector components k_t that are in the order of π/a where a is the lattice constant. Furthermore, plane waves with wave vectors in the dimension of the lattice vector will always sense the details of the periodicity. In this case the issue of an optically isotropic structure is pointless. Of course, also for small frequencies the iso-surface are not rotationally invariant but these domains are in general not accessible to the experiment and are negligible. Assuming the outer medium to have a permittivity ε then the line given by $|\mathbf{k}_\perp|/k_0 = \sqrt{\varepsilon}$ corresponds to grazing incidence and to the angular domain accessible from free space.

Up to here only the properties of the fundamental BM with the smallest imaginary part are discussed, since this mode essentially dictates light propagation. While considering the coupling of an external field to this BM it is assumed that only this mode is excited, thus

restricting to a certain polarization state of the incident light.

Nevertheless, in the general case of arbitrarily polarized incident light one has to discuss both eigenstates of the polarization separately, as both may exhibit different propagation constants. Assuming an isotropic homogeneous medium the eigensolutions are always degenerated, i.e. the eigenmodes are orthogonally and linearly polarized plane waves with the same k_z. This is also the case for normally incident light on a C_4 symmetric structure. Here, the light encounters the same physical structure at normal incidence for any polarization, hence the eigensolutions are degenerated. For oblique incidence the situation changes dramatically because both linearly polarized eigenstates may encounter different structures. Both eigensolutions may have different eigenvalues for the propagation constant. One may compare the situation with an uniaxial crystal, where the optical axis is aligned with the z-axis. For normally incident light the structure can be considered as being isotropic, whereas at oblique incidence the eigenvalues for the two eigenpolarizations are different. Note that the eigenpolarizations are always orthogonally, linearly polarized for planes of incidence being identical with mirror planes of the MM.

Considering the SCiC as an effectively isotropic, homogeneous medium, both fundamental BMs are supposed to be degenerated. As soon as the eigenvalues for both BMs deviate from each other, the medium cannot be described as being effectively isotropic. This deviation can also serve as a measure for a meaningful MM homogenization. Figure 4.20 (c) shows the real and the imaginary part of the propagation constant for the two BMs with the smallest losses at a certain angle of incidence. Figure 4.20 (d) shows their difference as function of the frequency. Clearly, for low frequencies the propagation constants for both modes are identical. As soon as the frequency increases the propagation constants start to deviate from each other, hence the SCiC cannot be considered as optically isotropic anymore. The deviation is of course the stronger the larger the angle of incidence is. The conclusions to be drawn from these figures are of course in line with those from the angular dependency of the first BM only. The structure is isotropic only for small frequencies and a limited range of angles of incidence, where this angular range is larger for smaller the frequencies.

Finally, some remarks are necessary in order to elucidate the significance of the obtained results for other spectral domains. Although we have investigated a specific high-symmetry MM here , which is designed to operate in the optical domain, we firmly believe that the conclusions to be drawn will not change significantly by modifying the operational wavelength. First of all, the structure sizes when compared to the vacuum wavelength are already quite small. At the frequency of interest the wavelength to cell size ratio is approximately 7. Even in the GHz range this ratio does not exceed 10 considerably [176]. From Fig. 4.20 it can be anticipated, that even in the non-resonant regime for $\lambda/a \approx 15$ the deviation between the expected response and the achieved one exceeds 2% already at $k_t/_0 = 1$. The structure

cannot be made significantly electrically smaller, if resonant metallic particles are used to achieve the artificial magnetism. But since the unit cell design itself is already of cubic symmetry, the deviations of the expected isotropic optical response to the actual one is only due to the insufficiently large wavelength to cell size ratio. To overcome these obstacles, it is maybe necessary to go completely different ways [164].

Let us shortly summarize the foregoing results. We have investigated the optical response of a highly symmetric SCiC MM in the negative refractive index regime. The SCiC exhibits cubic symmetry, i.e. the highest possible symmetry for periodic MMs, and is therefore considered a very promising candidate for an isotropic negative refractive index material. By investigating at first a finite number of functional layers and the convergence of the corresponding effective parameters to the values obtained from the dispersion relation of the infinite structure, we can conclude that the SCiC fulfills all requirements of a homogenizable MM. Already a single functional layer can be described by its bulk properties as only a single BM determines light propagation inside the structure. Nevertheless, our investigation of the iso-frequency surface of the dispersion relation clearly shows that even this MM with the highest symmetry is far away from having an optically isotropic response in the region of lefthandedness. This non-isotropic response is rather due to the large electrical size of the resonant unit cells than due to an insufficient design and will unlikely be solved while shifting the spectral domain of operation to the microwave regime. Hence, the key result is that one must not conclude from high symmetry on an optically isotropic response. Hence, optical isotropy of a MM can be only deduced from a careful inspection of the dispersion relation by taking into account the material dispersion of metals, too. This is an important message to the designers of isotropic optical MMs.

4.5 Chapter summary and concluding remarks

In the preceding chapter the effective description of MMs, as developed in chapters 2 and 3, was applied to optical MMs of different symmetries. Besides the comprehensive investigation of finite structures either theoretically or both theoretically and experimentally for normal as well as oblique incidence, results were presented and discussed for infinite structures, too. It was shown, that an effective description of the optical response in terms of wave parameters might often be justified, whereas effective material parameters must not be assigned in particular near topological resonances. The ideas and methods to investigate the optical response were presented exemplarily for non-chiral structures only. Although not shown here, also chiral MMs were investigated based upon these methods and it was shown that very similar conclusions can be drawn [121, 166].

5 A Jones matrix approach to complex metaatoms

5.1 Introduction

Whereas in the beginning of research on metamaterials properties such as a dispersive permeability were at the focus of interest [49–51], the range of properties to be intentionally affected by suitably chosen MMs significantly increased over the last years. More and more complex [185–188] and most notably, chiral [20, 21, 27–31] or quasi-planar [121, 189, 190] chiral structures attracted a great deal of attention due to their polarization selective optical response and their potential to implement functional devices with unprecedented applications such as, e.g., broadband polarizers for circularly polarized light [19]. Moreover, from a scientific point of view, such complex MMs permit to observe unexpected and counterintuitive effects like asymmetric transmission for circular [22–25] or even for linearly polarized light [26].

In the chapters above we have shown that the assignment of effective material parameters is doubtful in many cases [89] and generally requires the assumption of complex constitutive relations [94, 191, 192]. Thus a more suitable target function to be tailored by an appropriate MM design is the optical response itself. This optical response comprises entirely the response functions, such as complex reflection and transmission coefficients, for a given input illumination. This paradigm shift reflects that for an actual application a certain value of some effective material parameter is of minor importance, as long as the sample exhibits the desired optical response.

The response, in particular in transmission, can be easily described by transmittances and polarization ellipses, averaged polarization rotation and polarization conversion [20, 21, 193]. These phenomenological quantities can be completely determined from the frequency dependent Jones matrix [194] that relates the complex amplitudes of the incident to the transmitted field. We will term this Jones matrix throughout the chapter the T-matrix since it fully describes how the light is transmitted through a metamaterial slab. This 2×2 matrix comprises, in general, four different complex and dispersive quantities, reflecting the

spectral properties of the MM. The associated Jones calculus can be applied to describe the transmission of an arbitrarily polarized incident plane wave through a MM slab if only the zeroth diffraction order emerges. This holds for MMs composed of periodically arranged subwavelength unit cells and we will assume this here. For the sake of simplicity we also assume that the structures are symmetrically embedded, i.e. the optical properties of substrate and cladding are identical. We assume that all materials are linear and reciprocal, i.e., excluding Faraday media. No further restrictions on the symmetry of the unit cells and the generally complex permittivity of the constituting materials are necessary.

With this work we intend to introduce a classification of periodic metamaterials based on their symmetry properties and to link them to their specific T-matrix. We will show that all metamaterials can be divided into only five distinct classes, each having an individual form of the T-matrix and specific eigenstates. Each of these five classes leads to a very specific transmission characteristics directly linked to the symmetry of the structure. Therefore, this investigation provides an useful tool to analyze the optical response of complex MMs and it may serve as a guide to identify designs for a desired polarization response. Although for fabricated MMs the geometry is usually known, the application of combinatorial approaches to explore new MM geometries in the near future requires such tool to classify the properties of MMs. The results reported in this chapter are basically published in [26, 195].

The chapter is structured as follows. In section 5.2 we present the necessary fundamentals to handle the generally complex valued T-matrices and derive general expressions for the eigenpolarizations. In section 5.3 we derive the form of the T-matrix for the most relevant symmetry classes. In section 5.4 we provide examples of metamaterials for these symmetry classes and discuss briefly their optical behavior. Finally, in section 5.5 conclusion and a comprehensive tabular overview is given to summarize the results. We finally present a simple scheme to classify MM samples without having a priori knowledge in terms of the presented formalism by measured transmittances only.

5.2 Basic theory

It is assumed that the MM slab is illuminated by a plane wave propagating in positive z-direction

$$\mathbf{E}_i(\mathbf{r},t) = \begin{pmatrix} I_x \\ I_y \end{pmatrix} e^{i(kz-\omega t)},$$

with ω being its frequency, $k = \omega/c\sqrt{\varepsilon(\omega)}$ the wavevector, and the complex amplitudes I_x and I_y describing the state of polarization. The transmitted field is then given by

$$\mathbf{E}_t(\mathbf{r},t) = \begin{pmatrix} T_x \\ T_y \end{pmatrix} e^{i(kz-\omega t)},$$

where we have assumed that the medium is sandwiched between a medium characterized by the permittivity $\varepsilon(\omega)$. A sketch of the geometry is depicted in Fig. 5.1. The unit cells are periodically arranged in x- and y-direction without restricting to a particular lattice. We assume coherent, monochromatic plane waves so to use a generalized Jones calculus instead of the Mueller calculus necessary for incoherent light [196, 197]. The Jones calculus is said to be generalized since we allow for arbitrary complex Jones matrices which we will call T-matrices (transmission matrices).

The T-matrix connects the generally complex amplitudes of the incident and the transmitted field:

$$\begin{pmatrix} T_x \\ T_y \end{pmatrix} = \begin{pmatrix} T_{xx} & T_{xy} \\ T_{yx} & T_{yy} \end{pmatrix} \begin{pmatrix} I_x \\ I_y \end{pmatrix} = \begin{pmatrix} A & B \\ C & D \end{pmatrix} \begin{pmatrix} I_x \\ I_y \end{pmatrix} = \hat{T}^{\mathrm{f}} \begin{pmatrix} I_x \\ I_y \end{pmatrix}, \tag{5.1}$$

where for convenience we have replaced the entries T_{ij} by A, B, C, D which form the actual T-matrix. In the following few subsections we will discuss some generic properties of this T-matrix.

5.2.1 Directional dependent properties

In the last term of Eq. (5.1) the T-matrix superscript f designates propagation in forward direction. Of course, the choice of forward (f) and backward (b) propagation is arbitrary. Thus $\hat{T}^{\mathrm{b}}$ describes the transmission matrix for light propagating through the structure rotated by 180° with respect to the x-axis, where the choice of x or y is arbitrary.

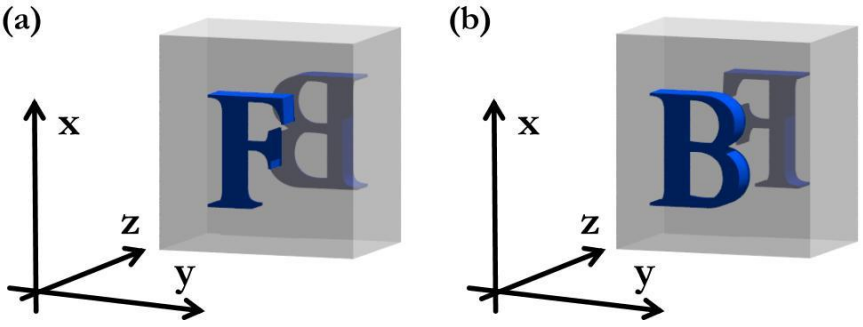

Figure 5.1: Schematic of the geometry. (a) and (b) show the sample from opposite sides with F and B indicating the front- and back-side, respectively.

Since only reciprocal media are considered we have:

$$\hat{T}^{b} = \begin{pmatrix} A & -C \\ -B & D \end{pmatrix}, \tag{5.2}$$

where the minus sign in the off-diagonal elements accounts for the rotation of the system looking from the backside [202]. Therefore, the complex matrix $\hat{T}^f$ already contains all information necessary to determine light transmission for arbitrarily polarized incident light from both main illumination directions. It is important to stress that this relation between $\hat{T}^{\mathrm{f}}$ and $\hat{T}^{\mathrm{b}}$ is in general only valid for this particular base where the coordinate axis from the backside are given by replacing those of the frontside by $x^{\mathrm{b}} = \pm x^{\mathrm{f}}$, $y^{\mathrm{b}} = \mp y^{\mathrm{f}}$. The actual sign depends on the definition of the rotation of the system.

5.2.2 Change of the base

For analytical as well as for experimental concerns it is useful to have at hand the transmission matrix in an arbitrary not necessarily orthogonal base. Let the vectors $\mathbf{i}$ and $\mathbf{t}$ denote the incident and the transmitted light in a certain base. Then the incident and the transmitted light in the Cartesian base is given by $\mathbf{I} = \hat{\Lambda}\mathbf{i}$ and $\mathbf{T} = \hat{\Lambda}\mathbf{t}$, respectively, with Λ being the change of basis matrix. Hence, the T-matrix for this new base is given by

$$\mathbf{T} = \hat{T}\mathbf{I} \;\rightarrow\; \mathbf{t} = \hat{\Lambda}^{-1}\hat{T}\hat{\Lambda}\mathbf{i} = \hat{T}_{\mathrm{new}}\mathbf{i} = \begin{pmatrix} T_{11} & T_{12} \\ T_{21} & T_{22} \end{pmatrix} \begin{pmatrix} i_1 \\ i_2 \end{pmatrix}. \tag{5.3}$$

All representations of the system are completely equivalent of course. A transformation of practical importance is the change from the Cartesian base to the circular base. Then the change of basis matrix reads as

$$\hat{\Lambda} = \frac{1}{\sqrt{2}} \begin{pmatrix} 1 & 1 \\ i & -i \end{pmatrix}, \tag{5.4}$$

where the columns of the $\hat{\Lambda}$ matrix are the new eigenstates. The T-matrix for circular states is then given by:

$$\hat{T}^{\mathrm{f}}_{\mathrm{circ}} = \begin{pmatrix} T_{++} & T_{+-} \\ T_{-+} & T_{--} \end{pmatrix} = \frac{1}{2} \begin{pmatrix} [A + D + i(B - C)] & [A - D - i(B + C)] \\ [A - D + i(B + C)] & [A + D - i(B - C)] \end{pmatrix}, \tag{5.5}$$

connecting the amplitudes of circularly polarized incident and transmitted light:

$$\begin{pmatrix} T_+ \\ T_- \end{pmatrix} = T^{\mathrm{f}}_{\mathrm{circ}} \begin{pmatrix} I_+ \\ I_- \end{pmatrix}, \tag{5.6}$$

By using Eqs. (5.2) and (5.5) it becomes obvious that the T-matrix for backward propagation is given by:

$$\hat{T}^{\mathrm{b}}_{\mathrm{circ}} = \begin{pmatrix} T_{++} & -T_{-+} \\ -T_{+-} & T_{--} \end{pmatrix}. \tag{5.7}$$

Note that the matrix $\hat{T}^{\mathrm{b}}$ in an arbitrary base is not simply given by Eq. (5.2), i.e. by interchanging the negative off-diagonal elements but by applying the corresponding change of basis matrix $\hat{\Lambda}$ to $\hat{T}^{\mathrm{f}}$ and $\hat{T}^{\mathrm{b}}$ in the linear base individually.

5.2.3 Asymmetric transmission

Although not having discussed any symmetry property at all, we want to discuss at this point the special effect of asymmetric transmission which attracted considerable interest due to its counter-intuitive occurrence and discuss peculiarities related to a change of the base. The difference of the T-matrices for opposite propagation directions is the key to that asymmetric transmission [22–26]. By asymmetric transmission Δ we understand the difference in the modulus of the total transmission between forward and backward propagation (see Fig. 5.1) for a certain base vector, e.g. $\mathbf{i} = i_1\mathbf{e}_1$:

$$\Delta = |T_{11}^{\mathrm{f}}|^2 + |T_{12}^{\mathrm{f}}|^2 - |T_{11}^{\mathrm{b}}|^2 - |T_{12}^{\mathrm{b}}|^2. \tag{5.8}$$

This quantity obviously depends on the chosen base, e.g., for a linear state coinciding with the coordinate axis we have ($\mathbf{i} = i_x\mathbf{e}_x$):

$$\Delta^{\mathrm{lin}} = |B|^2 - |C|^2, \tag{5.9}$$

whereas in the circular base we have ($\mathbf{i} = i_+\mathbf{e}_+$):

$$\Delta^{\mathrm{circ}} = |T_{-+}|^2 - |T_{+-}|^2 \neq \Delta^{\mathrm{lin}} \tag{5.10}$$

in general. This dependency on the base is exploited e.g. in [22, 23] where asymmetric transmission for circularly polarized light is observed without asymmetric transmission for linearly polarized light. Hence, the only proper choice is a linear base with base vectors parallel to the principal coordinate axes. Only in this base we can distinguish asymmetric transmission due to the structure from artificial asymmetric transmission due to the chosen base.

5.2.4 The eigenpolarizations

To characterize the different structures it is useful to determine the eigenstates of the polarization because they are uniquely related to the symmetry. Therefore, a simple eigenvalue problem has to be solved:

$$\begin{pmatrix} A & B \\ C & D \end{pmatrix} \begin{pmatrix} I_x \\ I_y \end{pmatrix} = \kappa \begin{pmatrix} I_x \\ I_y \end{pmatrix}, \tag{5.11}$$

with the eigenvalue κ. By solving these equations we obtain:

$$\kappa_{1,2} = \frac{1}{2}\left[(A+D) \pm \sqrt{(A-D)^2 + 4BC}\right], \tag{5.12}$$

where $\kappa_{1,2}$ gives the complex transmission for the eigenstates. The eigenpolarizations are then given by simply inserting $\kappa_{1,2}$ into Eq. (5.11) and solving for I_x and I_y. The eigenbasis

in matrix form can be written as

$$\hat{\Lambda} = \begin{pmatrix} 1 & 1 \\ \frac{\kappa_1 - A}{B} & \frac{\kappa_2 - A}{B} \end{pmatrix} \tag{5.13}$$

with

$$\mathbf{i}_1 = \begin{pmatrix} 1 \\ \frac{\kappa_1 - A}{B} \end{pmatrix} \text{ and } \mathbf{i}_2 = \begin{pmatrix} 1 \\ \frac{\kappa_2 - A}{B} \end{pmatrix}, \tag{5.14}$$

where the eigenvectors are not normalized yet. It is important to note that the eigenbasis depends in general on the frequency due to the dispersive behavior of the transmission. Only for highly symmetric structures the eigenbasis is frequency independent as will be shown later. With the use of the characteristic polynomial of Eq. (5.11) the matrix $\hat{\Lambda}$ can be rewritten as

$$\hat{\Lambda} = \begin{pmatrix} 1 & \frac{\kappa_2 - D}{C} \\ \frac{\kappa_1 - A}{B} & 1 \end{pmatrix} = \begin{pmatrix} 1 & -\frac{X}{2C} \\ \frac{X}{2B} & 1 \end{pmatrix}, \tag{5.15}$$

with $X = -(A-D) + \sqrt{(A-D)^2 + 4BC}$. Note that the matrices $\hat{\Lambda}$ in Eqs. (5.13) and (5.15) are different but both are denoted simply by $\hat{\Lambda}$ not to confuse the reader with additional indices. They are only a concatenation of eigenvectors that are determined up to an arbitrary complex factor. The matrix $\hat{\Lambda}$ becomes unique as soon as the eigenvectors are normalized. The fractions in Eq. (5.15) are complex numbers, hence we can express the eigenbasis as:

$$\hat{\Lambda} = \begin{pmatrix} 1 & 1 \\ R_1 e^{i\varphi_1} & \frac{1}{R_2} e^{-i\varphi_2} \end{pmatrix}, \tag{5.16}$$

with

$$R_1 e^{i\varphi_1} = \frac{X}{2B} \text{ and } R_2 e^{i\varphi_2} = -\frac{X}{2C}. \tag{5.17}$$

The eigenvectors are obviously orthogonal only if

$$R_1 = R_2 \text{ and } \varphi_1 + \varphi_2 = (2n+1)\pi \text{ with } n \in \mathbb{Z}.$$

This is only the case for linear, circular and a special class of elliptical polarization. In all other cases the eigenstates are non-orthogonal [198–200]. Note that systems with orthogonal eigenstates are sometimes termed homogeneous systems whereas systems with non-orthogonal states are termed inhomogeneous ones [201].

Once the eigenstates are derived, the transmission matrix can be determined within this eigenbase by applying the transformation (5.3). The corresponding T-matrix is then diagonal. Nevertheless, using the T-matrix in the eigenbase is only appropriate and convenient if the eigenstates are orthogonal and frequency independent.

The five different classes of periodic metamaterials that can be distinguished are closely related to their eigenstates. These five possible sets of eigenstates are linear, circular and

elliptic ones, whereas the elliptic ones can be separated into co-rotating, counter-rotating and general elliptic states with no fixed relation between ϕ_1 and ϕ_2. Later on we will show how the symmetry class determines the respective eigenstate.

5.3 Symmetry considerations

By symmetry considerations as performed in the next sections we will show how the symmetry properties of the structure affect the symmetry of the T-matrix. The emerging T-matrices can be reduced to five principal forms where in general a larger number of distinct matrices is possible by rotating the structure by an arbitrary angle with respect to the z-axis. On the other hand, such rotations can be used to remove redundant information. Rotation by an angle φ is accomplished by applying the following matrix operation:

$$D_\varphi = \begin{pmatrix} \cos(\varphi) & \sin(\varphi) \\ -\sin(\varphi) & \cos(\varphi) \end{pmatrix} \rightarrow \hat{T}_{\text{new}} = D_\varphi^{-1} \hat{T} D_\varphi \tag{5.18}$$

resulting in the new T-matrix $\hat{T}_{\text{new}}$ of the rotated sample. Note that the eigenvalues of the rotated system are invariant to this operation and are uniquely related to the principal symmetry. The actual form of the matrices and the derived, redundant matrices will be given later in section 5.4 to keep this part consistent.

In general all complex components of the T-matrix are different if the metamaterial does not exhibit any reflection or rotational symmetry. If such type of symmetry exists, the components of the T-matrix must reflect that. We will therefore briefly discuss a various symmetries and their corresponding impact on the T-matrices (see section 5.4 for figures of examples).

- If the metamaterial is mirror-symmetric with respect to the x-z-plane, the T-matrix for the structure reflected at that plane is identical to the original one. Therefore, we have:

$$M_x = \begin{pmatrix} 1 & 0 \\ 0 & -1 \end{pmatrix} : \quad M_x^{-1} \hat{T}^{\text{f}} M_x = \begin{pmatrix} A & -B \\ -C & D \end{pmatrix} = \hat{T}^{\text{f}} \rightarrow \hat{T}^{\text{f}} = \begin{pmatrix} A & 0 \\ 0 & D \end{pmatrix} \tag{5.19}$$

  with M_x being the reflection matrix with respect to the x-axis. So any structure that obeys that symmetry may be obviously described by a diagonal T-matrix.

- If the metamaterial is mirror-symmetric with respect to the y-z-plane, we have:

$$M_y = \begin{pmatrix} -1 & 0 \\ 0 & 1 \end{pmatrix} : \quad M_y^{-1} \hat{T}^{\text{f}} M_y = \begin{pmatrix} A & -B \\ -C & D \end{pmatrix} = \hat{T}^{\text{f}} \rightarrow \hat{T}^{\text{f}} = \begin{pmatrix} A & 0 \\ 0 & D \end{pmatrix}. \tag{5.20}$$

  Hence, if there exists any mirror plane parallel to the z-axis the T-matrix is diagonal provided that the mirror plane coincides with the x- or y-axes, respectively. In such a system the eigenstates of the polarization are obviously linear states.

- If the structure is C_2-symmetric with respect to the z-axis, we have:

$$D_\pi = \begin{pmatrix} -1 & 0 \\ 0 & -1 \end{pmatrix} : \quad D_\pi^{-1} \hat{T}^{\mathrm{f}} D_\pi = \begin{pmatrix} A & B \\ C & D \end{pmatrix} \equiv \hat{T}^{\mathrm{f}}. \tag{5.21}$$

  Hence, rotating any structure by 180° with respect to the z-axis does not change the response at all. Even if the structure does not have any further symmetry it fulfills that relation.

- If the structure is C_3-symmetric with respect to the z-axis, we have:

$$\rightarrow \hat{T}^{\mathrm{f}} = \begin{pmatrix} A & B \\ -B & A \end{pmatrix}. \tag{5.22}$$

  However that symmetry is almost never met without additional metamaterial mirror symmetries but given here for completeness.

- If the structure is C_4-symmetric with respect to the z-axis, we have:

$$D_{\frac{\pi}{2}} = \begin{pmatrix} -1 & 0 \\ 0 & -1 \end{pmatrix} : \quad D_{\frac{\pi}{2}}^{-1} \hat{T}^{\mathrm{f}} D_{\frac{\pi}{2}} = \begin{pmatrix} D & -C \\ -B & A \end{pmatrix} = \hat{T}^{\mathrm{f}} \rightarrow \hat{T}^{\mathrm{f}} = \begin{pmatrix} A & -B \\ -B & A \end{pmatrix}. \tag{5.23}$$

  Hence, the structure is insensitive to linearly polarized light of any state. If there is an additional mirror-symmetry with respect to a plane parallel or perpendicular to the z-axis, the off-diagonal elements will vanish; resulting in a completely polarization independent structure. Otherwise the eigenstates will be circularly polarized as will be shown later in detail.

- Further important conclusions can be drawn by investigating the possible mirror symmetries with respect to a plane perpendicular to the z-axis. If the structure possesses this type of symmetry, the reflected structure is the same as seen from the backside:

$$M_x^{-1} \hat{T}^{\mathrm{f}} M_x = \begin{pmatrix} A & -B \\ -C & D \end{pmatrix} = \begin{pmatrix} A & -C \\ -B & D \end{pmatrix} = \hat{T}^{\mathrm{b}} \rightarrow \hat{T}^{\mathrm{f}} = \begin{pmatrix} A & B \\ B & D \end{pmatrix}, \tag{5.24}$$

  i.e., the off-diagonal elements are identical. If the system possesses a center of inversion the matrix has also this form, because inversion is equivalent to applying a reflection and a subsequent rotation by π, where the latter does not change the response as shown in Eq. (5.21).

  By comparison with Eq. (5.23) it is obvious that the T-matrix will have the form $\hat{T}^{\mathrm{f}} = diag\{A, A\}$ if the structure is additionally C_4-symmetric with respect to the z-axis.

  That important relation in Eq. (5.24) is valid for all truly two-dimensional (planar) structures and all structures that possess any mirror plane perpendicular to a coordinate axis, i.e. achiral structures. In general, any substrate will break this symmetry [121, 189, 205], but usually the substrate effect is negligible compared to the effect of anisotropy [25].

- Most important for our investigations are structures that cannot be mapped onto their mirror image by proper rotations. Those structures are called chiral. In general, the components of the T-matrix for those structures are all different. In the context of the basic geometry analyzed here there exist only two exceptions. The first one is already discussed within the context of Eq. (5.23). The second one is an C_2-symmetry with respect to the x- or y-axis. For this type of symmetry the structure is identical from both sides, hence

$$\hat{T}^{\mathrm{f}} = \hat{T}^{\mathrm{b}} = \begin{pmatrix} A & B \\ -B & D \end{pmatrix}. \tag{5.25}$$

5.4 Examples and classification

To understand the usefulness of the approach presented, we will discuss the different symmetry classes for simple examples. The metaatoms exemplarily shown in the following are assumed to be periodically arranged in x- and y-direction. Importantly, the symmetry constraints applied to the unit cell have to be consistent with the symmetry of the lattice. That is crucial since e.g. even an achiral metaatom, can result in a chiral structure by a proper arrangement on a periodic lattice [203].

5.4.1 Simple anisotropic media

The most significant symmetry is that of reflection symmetry with respect to the x- or y-axis or both. As already explained within the context of Eqs. (5.19) and (5.20), the T-matrix is then diagonal. The eigenvalues are simply $\kappa_1 = A$ and $\kappa_2 = D$. The eigenstates are linear states parallel and orthogonal to the mirror plane, respectively. Only a dichroitic behavior will be obtained and no polarization rotation occurs for light being parallel or orthogonal to the mirror planes. If the coordinate system is not aligned parallel to the mirror plane, the T-matrix for that system will have off-diagonal elements, which disappear after a proper rotation. The most general form of the T-matrix for systems with linear eigenstates is

$$\hat{T}^{\mathrm{f}} = \begin{pmatrix} A & B \\ B & D \end{pmatrix}, \tag{5.26}$$

but in this case the components A, B and D are not independent but connected by trigonometric functions as is clear by explicitly evaluating Eq. (5.18) for a diagonal matrix.

An example for such a metamaterial is shown in Fig. 5.2 (a). Other examples are the fishnet [52] and its variations [157], cut wire pairs [158] and similar structures. In Fig. 5.2 (b) we have shown a special example of a structure with a symmetry plane which is 45° inclined

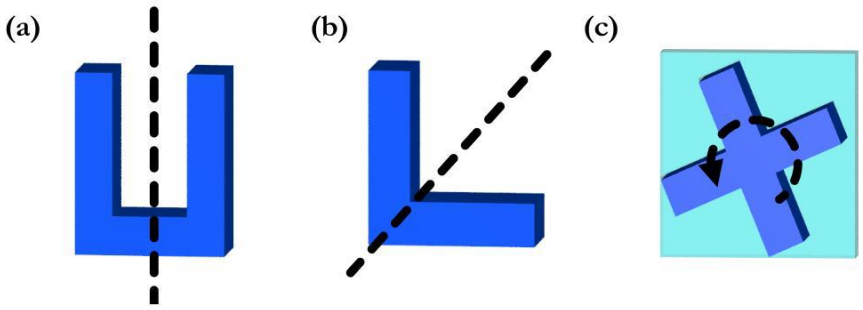

Figure 5.2: Examples for simple anisotropic (a,b) and simple chiral (c) metaatoms. The structures are located in the x-y plane with light impinging normally to the structure in z-direction. The black dashed lines indicate the mirror planes and the rotation axis ,respectively. (a) Split ring resonator with mirror plane parallel to the y-axis. (b) L-shaped particle with identical arms with mirror plane 45° inclined. (c) Cross on substrate with C_4 rotational symmetry with respect to the z-axis. The square shaped substrate indicates the arrangement on a square lattice, necessary for the C_4 of the entire system. Such an arrangement gives rise to so-called structural chirality although the particle itself is achiral.

with respect to both the x- and y-axis. In this case the T-matrix has the form:

$$\hat{T}^{\mathrm{f}} = \begin{pmatrix} A & B \\ B & A \end{pmatrix}. \tag{5.27}$$

The eigenstates are linearly orthogonal polarized, hence a rotation by an angle $\varphi = 45°$ leads to a diagonal form:

$$\hat{T}^{\mathrm{f}}_{\mathrm{new}} = D^{-1}_{\frac{\pi}{4}} \hat{T}^{\mathrm{f}} D_{\frac{\pi}{4}} = \begin{pmatrix} A' & 0 \\ 0 & D' \end{pmatrix} = \begin{pmatrix} A+B & 0 \\ 0 & A-B \end{pmatrix}. \tag{5.28}$$

A similar structure obeying the same relations is the one published in [187]. There, the unit cell consisting of four split-ring resonators has no rotational symmetry. But reflecting the structure at a plane diagonal to the given unit cell leads to a structure that is shifted by half a period in x- or y-direction. Due to the invariance of the optical response for periodic systems to any translation, this mirror plane leads, in fact, to linearly polarized eigenstates. Therefore, rotating the structure by 45° results in a diagonal T-matrix.

5.4.2 Simple chiral media

The second important group are those structures exhibiting C_4-symmetry but without any additional reflection symmetry. The T-matrix is then given by Eq. (5.23). Since these matrices are invariant to an arbitrary rotation D_φ, Eq. (5.23) is already the most general form of the T-matrix in a linear orthogonal base for such systems. The T-matrix in the

circular base is then diagonal:

$$T^{\mathrm{f}}_{\mathrm{circ}} = \begin{pmatrix} T_{++} & 0 \\ 0 & T_{--} \end{pmatrix} = \begin{pmatrix} A+iB & 0 \\ 0 & A-iB \end{pmatrix}. \tag{5.29}$$

Obviously the eigenpolarizations are circular states, since the T-matrix is diagonal and the eigenvalues are simply $\kappa_1 = A + iB$ and $\kappa_2 = A - iB$. The y-components of the eigenvectors [Eq. (5.14)] are $I_{y,1,2} = \pm i$, i.e. frequency independent. At such systems all effects related to circular dichroism are observable whereas emphasis is put on the fact that circular dichroism is in general accompanied by a difference in the phase advance for right- (rcp) and left-circular polarized (lcp) light due to causality, i.e., the real and imaginary part of the wavenumber for rcp and lcp differ in general [207].

The difference $T_{++} - T_{--} = 2iB$ is given by the off-diagonal elements in the linear polarization representation and specifies the optical rotation power. Systems adhering to such symmetry are prototypical optically active materials. Examples are gammadions, swastikas [see Fig. 5.2 (c)] or C_4-spirals. Note that the influence of the substrate is important for planar structures [121, 205]. The rotational power of such structures is independent of the structure height since it is a result of the substrate only.

5.4.3 Generalized anisotropic media

The third group consists of those systems that have a mirror symmetry perpendicular to the z-axis or a center of inversion and at most a C_2-symmetry with respect to the z-axis. From the latter one we know, that it has no influence on the transmission matrix [Eq. (5.21)]. Examples are given in Fig. 5.3. The only necessary symmetry is the reflection symmetry perpendicular to the z-axis without any further restrictions. Hence, there is no preferable alignment in the x-y-plane and the basic form of the T-matrix is unaffected by any rotation with respect to the z-axis.

For those systems the T-matrices in the linear and circular representation are given by:

$$T^{\mathrm{f}} = \begin{pmatrix} A & B \\ B & D \end{pmatrix}, \; T^{\mathrm{f}}_{\mathrm{circ}} = \frac{1}{2} \begin{pmatrix} A+D & A-D+2iB \\ A-D-2iB & A+D \end{pmatrix}, \tag{5.30}$$

hence the eigenstates are neither linearly nor circularly states polarized.

Since we have $T_{++} = T_{--}$ there is no polarization rotation due to chirality. In fact, it can be shown that the averaged polarization rotation accounting for chirality vanishes in such systems [91]. The off-diagonal elements in the circular basis are different, hence the polarization conversion from left- to right-hand polarized light and vice versa is different. The difference in conversion is again given by the off-diagonal elements in the linear basis $T_{+-} - T_{-+} = 2iB$. This difference is also the source of the asymmetric transmission for

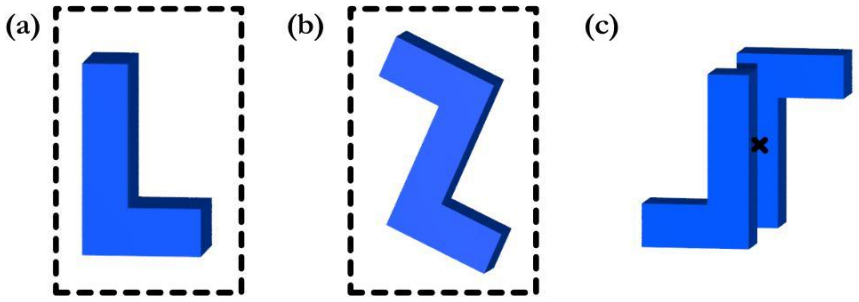

Figure 5.3: Examples for generalized anisotropic metaatoms. The metaatoms are located in the x-y plane with light impinging normally to the structure in z-direction. The black dashed lines indicate the mirror planes (a,b) and the black cross (c) a center of inversion symmetry, respectively. (a) A planar L-shaped metaatom with different arms. (b) A planar S-shaped metaatom with a C_2-symmetry with respect to the z-axis. (c) Three-dimensional metaatom made of L-shaped particles with a center of inversion.

circularly polarized light. Assuming (+)-polarized incident light the total transmission τ in forward direction is $\tau^{\mathrm{f}} = |T_{++}|^2 + |T_{-+}|^2$, whereas for the backward direction we have $\tau^{\mathrm{b}} = |T_{++}|^2 + |T_{+-}|^2$ due to Eq. (5.24). Therefore, the difference in the total transmission is determined by B. For (-)-polarized incident light, the results are identical. Note that there is no asymmetric transmission for linearly polarized light, as $\hat{T}^{\mathrm{f}}$ is symmetric.

It is important to note that the moduli of the off-diagonal elements are in general in the order of those of the diagonal elements (10^{-1}). Hence, the asymmetric transmission can become quite large. As already indicated before, any substrate will break the mirror symmetry in z-direction resulting in $B \neq C$, $|B - C| \ll |B|$, $B \approx C$. As this difference due to the small effect of the substrate is very weak (typically 10^{-3}), it is often neglected and hardly measurable compared to the asymmetric transmission effect.

The eigenstates for such a system are elliptical, co-rotating states, as discussed e.g. in [204]. The effects of light propagating through such structures can be understood in terms of the concept of elliptical dichroism [206]. By using Eqs. (5.16), (5.17) and $B = C$ they can be expressed in normalized form as

$$\mathbf{i}_1 = \frac{1}{\sqrt{1+R^2}} \begin{pmatrix} 1 \\ Re^{i\varphi} \end{pmatrix}, \; \mathbf{i}_2 = \frac{R}{\sqrt{1+R^2}} \begin{pmatrix} 1 \\ -\frac{1}{R}e^{-i\varphi} \end{pmatrix}. \tag{5.31}$$

They are only orthogonal for $\varphi = n\pi$ with $n \in \mathbb{N}$ leading to linear eigenstates.

Note that planar structures with that symmetry can be described by an effective permittivity tensor independent of the wavevector, i.e. without magnetoelectric coupling [65]. That is why we call this group generalized anisotropic structures.

The most general form is again obtained by applying a rotation by an arbitrary angle φ

leading to

$$\hat{T}^{\mathrm{f}}_{\mathrm{new}} = D_{\varphi}^{-1}\hat{T}^{\mathrm{f}}D_{\varphi} = \begin{pmatrix} A' & B' \\ B' & D' \end{pmatrix}, \tag{5.32}$$

hence the general form is invariant since no preferred alignment exists.

5.4.4 Generalized chiral media

The forth group are chiral structures that have an additional C_2-symmetry with respect to the x- or y-axis. The T-matrix obeys the form:

$$T^{\mathrm{f}} = \begin{pmatrix} A & B \\ -B & D \end{pmatrix}, T^{\mathrm{f}}_{\mathrm{circ}} = \frac{1}{2}\begin{pmatrix} A+D+2iB & A-D \\ A-D & A+D-2iB \end{pmatrix}, \tag{5.33}$$

hence there is no difference in the polarization conversion and hence no asymmetric transmission neither for linear nor for circular polarized light. Furthermore there is obviously no asymmetric transmission in any base, since the structure is identical from both sides when the axis of rotation coincides with the x- or y-axis.

But there is a difference in the quantity $T_{++} - T_{--} = 2iB$ determining the optical rotation

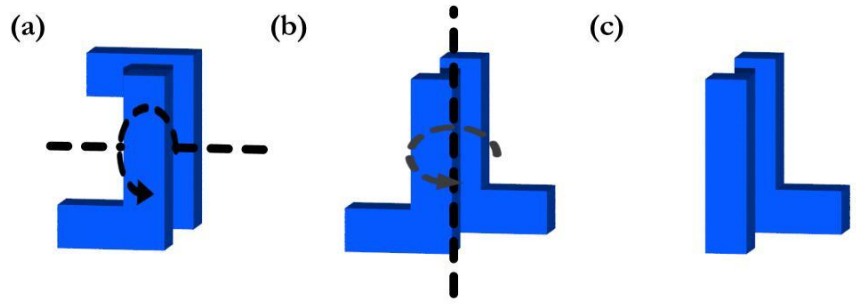

Figure 5.4: Examples for generalized chiral metaatoms (a,b) and a no-symmetry metaatom (c). The structures are located in the x-y plane with light impinging normally to the structure in z-direction. The black dashed lines indicate the axes of rotational symmetry (a,b). (a,b) Three-dimensional structures made of two L-shaped particles with C_2-symmetry with respect to the x- or y-axis, respectively. They are identical for forward and backward propagation. (c) A three-dimensional structure made of an L-shaped particle and an I-shaped particle with no symmetry at all.

power typical for chiral structures. In contrast to the second group we have an additional anisotropy ($A \neq D$) hence the eigenstates are not circular but elliptical counter-rotating. Again, by using Eqs. (5.16), (5.17) and $C = -B$ they can be expressed in normalized form as

$$\mathbf{i}_1 = \frac{1}{\sqrt{1+R^2}}\begin{pmatrix} 1 \\ Re^{i\varphi} \end{pmatrix}, \mathbf{i}_2 = \frac{R}{\sqrt{1+R^2}}\begin{pmatrix} 1 \\ \frac{1}{R}e^{-i\varphi} \end{pmatrix}. \tag{5.34}$$

They are only orthogonal if $\varphi = \frac{\pi}{2} + n\pi$ with $n \in \mathbb{N}$ leading to circular counter-propagating eigenstates typical for chiral structures. That is why we term this group generalized chiral structures.

Typical examples are shown in Fig. 5.4 (a) and (b). Another important example are three-dimensional spirals [208–212] with $\frac{N}{2}$ whorls aligned along the z-axis. Spirals with integer whorls are clearly identical for both propagation directions, whereas spirals with half-integer whorls are identical after rotation by π around the z-axis keeping the response unaffected [see Eq. (5.21)].

Note that for an arbitrary rotation D_φ all matrix elements are different, hence the symmetry axis must be aligned with a principal coordinate axis to achieve the form of Eq. (5.33). In particular if the system is rotated by 45° the T-matrix has the form:

$$T^f = \begin{pmatrix} A' & B' \\ C' & A' \end{pmatrix}. \tag{5.35}$$

Nevertheless, if the eigenvectors of the arbitrarily oriented system are elliptical counter-rotating the convenient form of Eq. (5.33) can be achieved by a proper alignment of the system.

5.4.5 Arbitrary complex media

The fifth and last group are chiral structures without any symmetry. A simple example is shown in Fig. 5.4 (c). For this group all elements of the T-matrices in the linear as well as in the circular base are different:

$$T^{\mathrm{f}} = \begin{pmatrix} A & B \\ C & D \end{pmatrix}. \tag{5.36}$$

It is impossible to achieve $|B| = |C|$ by a proper rotation. Therefore, independent of the chosen base, asymmetric transmission occurs always and in particular also for linearly polarized light. All effects of generalized anisotropy as well as generalized chirality can be observed. The normalized eigenvectors can be expressed as:

$$\mathbf{i}_1 = \frac{1}{\sqrt{1+R_1^2}} \begin{pmatrix} 1 \\ R_1 e^{i\varphi_1} \end{pmatrix}, \mathbf{i}_2 = \frac{R_2}{\sqrt{1+R_2^2}} \begin{pmatrix} 1 \\ \frac{1}{R_2} e^{-i\varphi_2} \end{pmatrix}.$$

whereas $R_1(\omega) \neq R_2(\omega)$ and $\varphi_1(\omega) \neq \varphi_2(\omega)$. The eigenstates are strongly depending on the actual value of the components of $\hat{T}$ and are simply elliptical, whereas no principal rotation direction can be assigned. Linear as well as elliptical counter- and co-rotating states and combinations of them with no fixed phase relation can be found in general. An example of such an structure is investigated in detail both numerically and experimentally in [26] and discussed below.

For the first time it is shown that this structure supports asymmetric transmission for linearly polarized light. We emphasize that also in this case the reciprocity theorem is not violated since only reciprocal materials are involved. Since our approach is solely based on symmetry considerations, it is valid for lossless systems, too. Prior to any further consider-

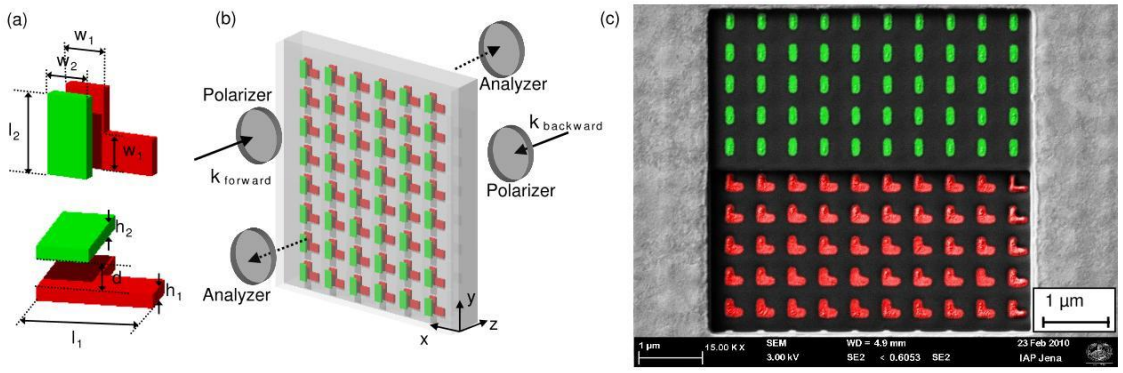

Figure 5.5: (a) Two sketches of the MM unit cell from different perspectives with the definition of the geometrical parameters: l_1=l_2=290 nm, w_1=w_2=130 nm, h_1=h_2=40 nm, d=80 nm. (b) Schematic of the experimental setup: Normally incident light was linearly polarized before propagating through the MM and subsequently analyzed by means of a second linear polarizer. (c) Normal view electron micrograph with false colors of the fabricated MM. The meta-atoms were completely embedded in an index-matched dielectric. Focused ion beam slicing reveals the two layers composing the MM. Green and red colors represent the nanowires and the L-structures in the top and bottom layer, respectively. The periods in both the x- and y-directions are 500 nm.

ations we concisely discuss the effect of a potential MM substrate that is, after all, in most cases required to fabricate planar MMs. Generally speaking, just this supporting substrate breaks the mirror symmetry for any planar structure perpendicular to the propagation direction [134, 205]. However, the effect of this break in symmetry is almost negligible when compared to the impact of a strong structural anisotropy that leads e.g. to asymmetric transmission of circularly polarized light [22, 24]. On the other hand, if no structural anisotropy is present, like e.g., for gammadions, the chirality of the planar metaatom-substrate system yields a measurable polarization rotation [121]. So, although asymmetric transmission for linearly polarized light may have been observed already, its magnitude was too weak and it was merely attributed to an insufficient measurement accuracy rather than to a true physical mechanism. To unambiguously enhance the effect towards a measurable extent, it is necessary to deliberately break the symmetry in the third dimension of the metaatom itself and not just relying on the rather perturbative effect of a supporting substrate. Exactly this goal is pursued with the structure proposed here.

From the analysis above we know, that for MMs featuring $A \neq B \neq C \neq D$ asymmetric transmission will be observable in any base and in particular for linearly polarized light, too. To prove this statement we designed a metaatom that is essentially three-dimensional, non-

symmetric, and consists of strongly coupled plasmonic elements. To rule out asymmetric effects due to the presence of a substrate [134], the metaatoms are completely embedded in an index-matched dielectric host. The geometry of the structure is shown in Fig. 5.5 (a). It consists of two closely spaced layers. The first layer comprises an L-shaped metallic particle and the second one a single nanowire. The L-shaped structure on its own causes an anisotropic response if both arms are dissimilar, giving rise to asymmetric transmission for circularly polarized light. Adding the nanowire breaks the remaining symmetry in the principal propagation direction and leads to a genuine three-dimensional chiral metaatom. Note that the particles themselves, in general, sustain three first-order plasmonic resonances; one may be associated with the nanowire and the two others with the L-shaped particle. The coupling of these particles results in a complex response featuring various resonances. The specific hybrid plasmonic eigenmodes are of minor importance for our purpose and beyond the scope of this work; though they can be easily accessed within the framework of an oscillator model [64]. The metaatoms are periodically arranged on a square lattice in the x-y-plane with periods smaller than the wavelength so that only the zeroth diffraction order propagates. A schematic of the experiment is shown in Fig. 5.5 (b), where the transmitted intensities through a single MM layer at normal incidence for both forward and backward propagation direction; corresponding to positive and negative z-direction. Note that resonant, lossy metaatoms enhance considerably the effect of asymmetric transmission but are not required to observe the very effect. However, the effect can be hardly measured in lossless media.

The MM was fabricated as follows: Both layers were defined in gold using standard electron-beam lithography (Vistec SB350OS) and a lift-off technique. Each single layer was planarized with spin-on glass resist (Dow Corning XR-1541) matching the refractive index of the fused silica substrate. Atomic force microscopy confirmed that the resulting surfaces were ideally planar within a measurement accuracy of 1 nm. For the writing of the top layer multiple alignment marks were used to ensure an alignment accuracy of better than 20 nm to the bottom layer [Fig. 5.5 (c)]. The squared moduli $t_{ij} = |T_{ij}|^2$ of the T-matrix of the MM were determined experimentally [Fig. 5.6 (a) and (b)]. Clearly t_{xy} and t_{yx} interchange for opposite propagation directions proving that all elements in the linear base are different in general. Additional deviations between the forward and backward propagation are negligible and can be attributed to a non-ideal alignment of the polarizers. For comparison, the complex transmission coefficients T_{ij} are computed by using the Fourier Modal Method [139] and shown in Fig. 5.6 (c) and (d). The spectral dispersion of gold was properly accounted for [144] using the bulk permittivity. Hence, possible quantum effects resulting in a size dependent permittivity of the metal are neglected because of the relatively large dimensions of the gold particles. The experimental and numerically computed intensities are in almost perfect agreement. Minor deviations are attributed to an approximative modeling of the

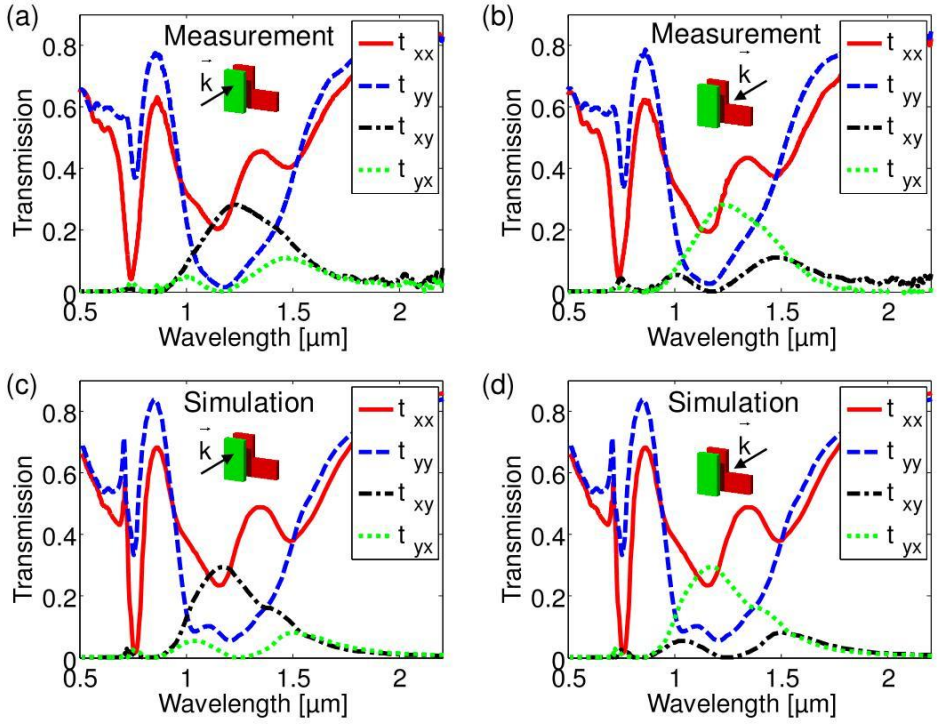

Figure 5.6: Squared moduli of the four T-Matrix components of the MM. (a), (b) Measurements and (c), (d) simulations. (a), (c) The k-vector of the plane waves illuminating the MM was directed in (a), (c) positive and (b), (d) negative z-direction. Note that t_{xy} and t_{yx} interchange when k is reversed.

structure with geometrical parameters as deduced from electron microscopy images. As expected from the design of the metaatoms the spectra reveal a complex multi-resonant behavior. The values for the asymmetric transmission Δ as determined from numerical data are calculated according to Eq. (5.9) and Eq. (5.10) in the linear as well as in the circular base [Fig. 5.7 (a) and (b)]. Clearly, they are different for different bases and achieve values up to 25% in the linear base. The asymmetry for a certain state is of course identical to the asymmetry for the complementary state with negative sign since the total transmission for unpolarized light from both sides has to be the same in a reciprocal medium. Figure 5.7 represents the main result, that is an experimental prove of asymmetric transmission for linearly polarized light in a truly three-dimensional chiral metaatom.

Any system made of complex metaatoms is characterized by its eigenstates, i.e. those polarization states that do not change upon transmission. For these eigenstates, being in general not orthogonal, the T-matrix is diagonal when transformed into that eigenbase. For planar quasi-chiral structures with additional rotational symmetries like gammadions, the eigenstates are circular counter-rotating, whereas for anisotropic, 2D chiral structures the eigenstates are elliptical co-rotating with fixed phase relations [204]. For three-dimensional chiral systems without any additional symmetry like those considered here, the eigenstates

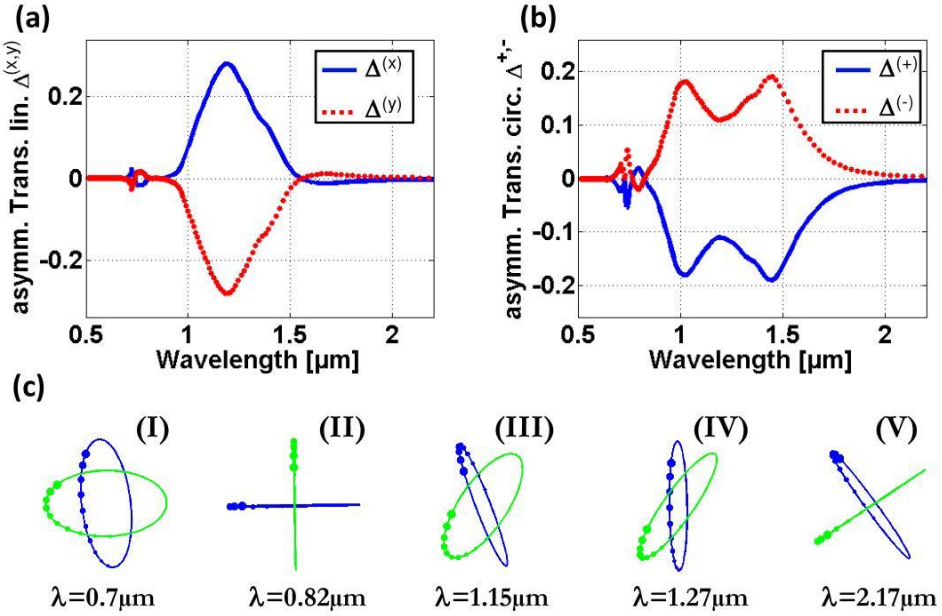

Figure 5.7: Values for the asymmetric transmission Δ for linear (a) and circular (b) states as determined by the numerical data. The color of the lines indicates the particular input state. (c) Eigenstates of the polarization at different wavelengths. The rotation direction is indicated by increasing spot sizes.

can be arbitrarily complex. Both elliptical co- and counter-rotating as well as linear and circular states and combinations of them are expected. In Fig. 5.7 (c) we exemplarily show the eigenstates of the present MM for different wavelengths. Most notably, elliptical co-rotating states (I and IV) as well as elliptical counter-rotating states (III), almost linear states (II) and combined ones (V) may be observed. Even the angle between the polarization ellipses obeys no fixed relation. For structures lacking any symmetry, the eigenstates of the polarization have obviously no preferred orientation and rotation direction. Note that the principle form of eigenstates of the T-matrix is invariant to any proper rotation with respect to the z-axis. Hence, their complex behavior is a clear indication that it is not possible to symmetrize the T-matrix by a proper rotation since there is no preferable orientation of the metaatoms. We suggest that our findings can be exploited for the design of a purely MM-based optical isolator basing on the rich variety of possible combinations of complex T-matrices in low-symmetry and three-dimensional chiral metaatoms.

5.5 Chapter summary and concluding remarks

A summarizing overview of possible structures and the corresponding basic forms of the T-matrices are shown in Table 5.1. Once the general form of the T-matrix is known all effects regarding the observable polarization phenomena can be fully deduced. Based on

our investigations it is easy to provide an algorithm to determine the general form of the T-matrix for an unknown sample by measuring transmitted intensities with the help of linear polarizers only. A possible approach can be as follows:

symmetry	**examples**	**T-matrix**	**eigenstates**
M_{xz} (M_{yz})	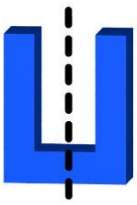	$T = \begin{pmatrix} A & 0 \\ 0 & D \end{pmatrix}$	linear
$C_{4,z}$ ($C_{3,z}$)		$T = \begin{pmatrix} A & B \\ -B & A \end{pmatrix}$	circular
M_{xy} ($C_{2,z}$, inversion symmetry)	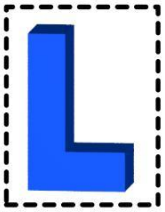	$T = \begin{pmatrix} A & B \\ B & D \end{pmatrix}$	elliptic, co-rotating
$C_{2,y}$ ($C_{2,x}$)	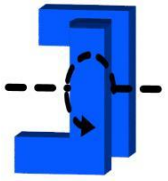	$T = \begin{pmatrix} A & B \\ -B & D \end{pmatrix}$	elliptic, counter-rotating
no symmetry ($C_{2,z}$)		$T = \begin{pmatrix} A & B \\ B & D \end{pmatrix}$	elliptic

Table 5.1: Overview of possible symmetries, typical metaatoms, the corresponding T-matrices and their eigenstates of the polarization. For every symmetry group only a single example is shown. Other possible symmetries resulting in the same type of T-matrices are given in brackets. Here M_{ij} designates mirror symmetry with respect to the ij-plane and C_n, i means n-fold rotational symmetry with respect to the i-axis.

1. Use linearly polarized light and measure the orthogonally polarized output while rotating the sample. If the output vanishes for every rotation angle, the medium is polarization independent, i.e., a simple isotropic medium. If the output vanishes for some rotation angles and this angle is independent of the wavelength, the structure is simple anisotropic. If no

such rotation angle can be found, there is obviously no mirror plane parallel to the z-axis. 2. If the transmitted intensity is independent of the rotation of the sample for both co- and cross-polarized light, the eigenstates are circular polarized and the structure is simple chiral. 3. If both aforementioned procedures do not provide a positive results, the structure is more complex and the measurements become more difficult, too. To distinguish between the remaining possible forms it is necessary to measure the off-diagonal entries of the T-matrix simultaneously. If these off-diagonal elements are identical for a fixed wavelength and a fixed rotation angle independent of their particular choice, the structure is generalized anisotropic. If the off-diagonal elements are identical only for a fixed rotation angle, but for every wavelengths the structure is generalized chiral. In all other cases we have $A \neq B \neq C \neq D$. By using circular polarized light a similar scheme can be obtained however it would require circular analyzers as well.

Taking advantage of symmetry considerations the potential of various MMs to affect the polarization state of light upon transmission was analyzed. By focusing the attention on any optical response that is directly accessible in an experiment, the properties of MMs may become so involved that the establishment of valid constitutive relation may be beyond what is possible for structures with an ever increasing complexity. It was explicitly shown that all MMs belong to one of five different classes; each being characterized by certain relations that connect the entries of the T-matrix and each class is able to support specific polarization phenomena. The sub-wavelength nature of MMs is the only requirement for these considerations. Moreover, the symmetry operations applied to the metaatoms have to be consistent with the symmetry of the lattice and it is required that the MM is sandwiched between identical media. Nonetheless, all relevant structures where a violation of this assumption causes deviations have been explicitly listed. To foster practical application of this classification a protocol was finally provided that is useful to reveal the underlying symmetry of an unknown MM and its T-matrix from far-field measurements of the transmitted intensities only. Once it is identified, all the achievable optical properties that affect the state of polarization are fully disclosed.

Finally, the first experimental observation and theoretical analysis of asymmetric transmission for linearly polarized light in a 3D low-symmetry MM was reported. Contrary to previous works focusing exclusively on circularly polarized light, the key for asymmetric transmission in any polarization base is the complete symmetry breaking of the metaatom. The composition of three-dimensional chiral metaatoms considerably enriches the variety of transmission functionalities and offers yet a new freedom of design for photonic MMs. In particular, optical isolation based on MMs seems to be in reach.

6 Summary and perspective

In this thesis we have developed methods to describe the interaction of light with metamaterials in a simplified form by means of effective wave or material parameters. Most importantly, we established an understanding of these effective parameters and accessed their meaning. It was shown that a reduction of the complex optical response of nowadays metamaterials, in particular at frequencies close to resonances, to only a few frequency dependent effective material parameters is seldom possible. However, light propagation can often be described by effective wave parameters. They simplify the description and characterisation considerably. A clear relation between both sets of effective parameters is established by means of constitutive relations - strategies to probe for the limits for the applicability of material parameters have been obtained. That is one of the major contributions of this thesis to recent metamaterials research. The impossibility to reduce the optical response to effective material parameters reflects the requirement of a paradigm shift in the understanding of metamaterials. For practical applications it is rather necessary to tailor the desired optical functionality instead of tailoring the material properties. For this purpose an easy to handle formalism is introduced by means of Jones matrices, which allows for a classification of metamaterials in terms their symmetry. With a certain optical functionality in mind, this formalism allows to identify structures that may provide the desired functionality in particular with respect to complex polarization manipulation. Sequences of metamaterial slabs may also be treated and optimized by this method.

At the end of this thesis it has to be said, that the initial concept to tailor the metamaterials and thereby extending the possibilities offered by natural materials to affect the light propagation in an arbitrary manner is unlikely; if not impossible. Achieving an isotropic artificial magnetism at optical frequencies, which can be properly described by an isotropic effective permeability, is shown to be inaccessible by recent metamaterial proposals. Therefore, applications like the perfect lens or the cloaking device, which require a great flexibility in optical material parameters, in particular without losses, are out of reach. However, the investigations made with respect to metamaterials raised fundamental questions on material parameters - and has been providing answers. For example, it was shown that one has to distinguish between effective material and wave parameters - a very fundamental issue that will certainly enter future textbooks on optics. The issue of defining material parameters and

constitutive relations gained an enormous interest on fundamental questions with respect to Maxwell's equations. The question of passivity and causality in the context of Kramers-Kronig relations as well as the definition of the Poynting vector or the energy density were reconsidered. Also the issue of homogenization of metamaterials and the description of light propagation with averaged equations was recapitulated. In the context of estimating effective parameters either from finite or infinite systems, concepts for the impedance were reconsidered with great advance also for other disciplines like waveguide theory. Furthermore, the need for small resonant structures supporting circulating current distributions, which are necessary for an artificial magnetism, generated a huge impetus for research on plasmonic particles and waveguides. Technical means had to be developed for their fabrication, characterisation and also to design them.

On a more conceptual level research on metamaterials revealed a variety of functionalities that will enter even commercial applications in any case. For example, in the context of realizing the cloaking device, a new field of research called transformation optics was established. Whereas at the beginning of the investigations sophisticated anisotropic and inhomogeneous materials with defined permeability and permittivity tensors were necessary to realize the desired functionality, new implementations were put forward recently, which require an inhomogeneous permittivity only. This tremendously simplifies the realization of devices based on transformation optics. Also, instead of tailoring the materials response, new concepts based on optimization routines were put forward to tailor the dispersion relation of waves directly, e.g., to achieve subwavelength focussing of light. Concentrating light by plasmonic particles on small scales with respect to the wavelength allows for a variety of sensing applications which promise to detect target substances at extremely low concentration; potentially at the single molecule level. For example, the perfect absorber as a concept directly born out of metamaterials research might be used for such kind of sensing devices as well as structures supporting the electromagnetic induced transparency. Due to the resonant nature of the optical metamaterial's response highly dispersive phase as well as polarization manipulation and even nonlinear conversion is possible on the μm scale, which allows for on-chip integration of complex optical functionality.

In that sense, research on metamaterials was shown to exhibit great impact on fundamentals as well as applications no one had in mind initially, and will considerably help to improve the world of optics.

Bibliography

[1] A. Sihvola, S. Tretyakov, and A. de Baas, Metamaterials with Extreme Material Parameters, Journal of Communications Technology and Electronics **52**, 986 (2007).

[2] V. Veselago, The electrodynamics of substances with simultaneously negative values of ε and μ, Sov. Phys. Usp. **10**, 509 (1968).

[3] J. B. Pendry, Negative Refraction Makes a Perfect Lens, Phys. Rev. Lett. **85**, 3966 (2000).

[4] J. B. Pendry, A. J. Holden, D. J. Robbins, and W. J. Stewart, Magnetism from Conductors and Enhanced Nonlinear Phenomena, IEEE Transactions on microwave theory and techniques **47**, 2075 (1999).

[5] D. R. Smith, Willie J. Padilla, D. C. Vier, S. C. Nemat-Nasser, and S. Schultz, Composite Medium with Simultaneously Negative Permeability and Permittivity, Phys. Rev. Lett. **84**, 4184 (2000).

[6] Zubin Jacob, Leonid V. Alekseyev and Evgenii Narimanov, Optical Hyperlens: Far-field imaging beyond the diffraction limit, Optics Express **14**, 8247 (2006).

[7] Zhaowei Liu, Hyesog Lee, Yi Xiong, Cheng Sun, Xiang Zhang, Far-Field Optical Hyperlens Magnifying Sub-Diffraction-Limited Objects, Science **315**, 1686 (2007).

[8] Kosmas L. Tsakmakidis, Allan D. Boardman, and Ortwin Hess, 'Trapped rainbow' storage of light in metamaterials, Nature **450**, 397 (2007).

[9] N. I. Landy, S. Sajuyigbe, J. J. Mock, D. R. Smith, and W. J. Padilla, Perfect Metamaterial Absorber, Phys. Rev. Lett. **100**, 207402 (2008).

[10] Ulf Leonhardt, Optical Conformal Mapping, Science **312**, 1777 (2006).

[11] J. B. Pendry, D. Schurig, D. R. Smith, Controlling Electromagnetic Fields, Science **312**, 1780 (2006).

[12] Wenshan Cai, Uday K. Chettiar, Alexander V. Kildishev, and Vladimir M. Shalaev, Optical cloaking with metamaterials, Nat. Phot. **1**, 224 (2007).

[13] Jason Valentine, Jensen Li, Thomas Zentgraf, Guy Bartal and Xiang Zhang, An optical cloak made of dielectrics, Nat. Mat. **8**, 568 (2009).

[14] Tolga Ergin, Nicolas Stenger, Patrice Brenner, John B. Pendry, Martin Wegener,

Three-Dimensional Invisibility Cloak at Optical Wavelengths, Science **328**, 337 (2010).

[15] Huanyang Chen, C. T. Chan, and Ping Sheng, Transformation optics and metamaterials, Nat. Mat. **9**, 387 (2010).

[16] Martin Schmiele, Vineeth S. Varma, Carsten Rockstuhl, and Falk Lederer, Designing optical elements from isotropic materials by using transformation optics, Phys. Rev. A **81**, 033837 (2010).

[17] Nader Engheta, Circuits with Light at Nanoscales: Optical Nanocircuits Inspired by Metamaterials, Science **317**, 1698 (2007).

[18] Gunnar Dolling, Christian Enkrich, Martin Wegener, Costas M. Soukoulis, and Stefan Linden, Simultaneous Negative Phase and Group Velocity of Light in a Metamaterial, Science **312**, 892 (2006).

[19] J. K. Gansel, M. Thiel, M. S. Rill, M. Decker, K. Bade, V. Saile, G. v. Freymann, S. Linden, and M. Wegener, Gold helix photonic metamaterial as broadband circular polarizer, Science **325**, 1513 (2009).

[20] A. V. Rogacheva, V. A. Fedotov, A. S. Schwanecke, and N. I. Zheludev, Giant gyrotropy due to electromagnetic-field coupling in a bilayered chiral structure, Phys. Rev. Lett. **97**, 177401 (2006).

[21] C. Rockstuhl, C. Menzel, T. Paul, and F. Lederer, Optical activity in chiral media composed of three-dimensional metallic meta-atoms, Phys. Rev. B **79**, 035321 (2009).

[22] V. A. Fedotov, P. L. Mladyonov, S. L. Prosvirnin, A.V. Rogacheva, Y. Chen, and N. I. Zheludev, Asymmetric Propagation of Electromagnetic Waves through a Planar Chiral Structure, Phys. Rev. Lett. **97**, 167401 (2006).

[23] V. A. Fedotov, A. S. Schwanecke, N. I. Zheludev, V. V. Khardikov, and S. L. Prosvirnin, Asymmetric Transmission of Light and Enantiomerically Sensitive Plasmon Resonance in Planar Chiral Nanostructures, Nano Lett. **7**, 1996 (2007).

[24] A. S. Schwanecke, V. A. Fedotov, V. V. Khardikov, S. L. Prosvirnin, Y. Chen, and N. I. Zheludev, Nanostructured Metal Film with Asymmetric Optical Transmission, Nano Lett. **8**, 2940 (2008).

[25] R. Singh, E. Plum, C. Menzel, C. Rockstuhl, A. K. Azad, R. A. Cheville, F. Lederer, W. Zhang, and N. I. Zheludev, Terahertz metamaterial with asymmetric transmission, Phys. Rev. B **80**, 153104 (2009).

[26] C. Menzel, C. Helgert, C. Rockstuhl, E.-B. Kley, A. Tünnermann, T. Pertsch, and F. Lederer, Asymmetric Transmission of Linearly Polarized Light at Optical Metamaterials, Phys. Rev. Lett. **104**, 253902 (2010).

[27] S. Zhang, Y. S. Park, J. Li, X. Lu, W. Zhang, and X. Zhang, Negative refractive index

in chiral metamaterials, Phys. Rev. Lett. **102**, 023901 (2009).

[28] E. Plum, J. Zhou, J. Dong, V. A. Fedotov, T. Koschny, C. M. Soukoulis, and N. I. Zheludev, Metamaterial with negative index due to chirality, Phys. Rev. B **79**, 035407 (2009).

[29] J. Zhou, J. Dong, B. Wang, T. Koschny, M. Kafesaki, and C. M. Soukoulis, Negative refractive index due to chirality, Phys. Rev. B **79**, 121104(R) (2009).

[30] B. Wang, J. Zhou, T. Koschny, M. Kafesaki, and C. M. Soukoulis, Chiral metamaterials: simulations and experiments, J. Opt. A **11**, 114003 (2009).

[31] Yuqian Ye and Sailing He, 90° polarization rotator using a bilayered chiral metamaterial with giant optical activity, Appl. Phys. Lett. **96**, 203501 (2010).

[32] J. B. Pendy, A Chiral Route to Negative Refraction, Science **306**, 1353 (2004).

[33] Alexander A. Zharov, Ilya V. Shadrivov, and Yuri S. Kivshar, Nonlinear Properties of Left-Handed Metamaterials, Phys. Rev. Lett. **91**, 037401 (2003).

[34] Ilya V. Shadrivov, Alexander A. Zharov, and Yuri S. Kivshar, Second-harmonic generation in nonlinear left-handed metamaterials, J. Opt. Soc. Am. B **23**, 529 (2006).

[35] A. K. Popov, and V. M. Shalaev, Negative-index metamaterials: second-harmonic generation, Manley-Rowe relations and parametric amplification, Appl. Phys. B **84**, 131 (2006).

[36] Matthias W. Klein, Christian Enkrich, Martin Wegener, and Stefan Linden, Second-Harmonic Generation from Magnetic Metamaterials, Science **313**, 502 (2006).

[37] Yong Zeng, Walter Hoyer, Jinjie Liu, Stephan W. Koch, and Jerome V. Moloney, Classical theory for second-harmonic generation from metallic nanoparticles, Phys. Rev. B **79**, 235109 (2009).

[38] J. Petschulat, A. Chipouline, A. Tünnermann, T. Pertsch, C. Menzel, C. Rockstuhl, and F. Lederer, Multipole nonlinearity of metamaterials, Phys. Rev. A **80**, 063828 (2009).

[39] Christoph Menzel, Optik in Medien mit stark dispersiver Permittivität und Permeabilität - Diplomarbeit, Friedrich-Schiller-Universität Jena (2006).

[40] Ilya V. Shadrivov, Andrey A. Sukhorukov, and Yuri S. Kivshar, Guided modes in negative-refractive-index waveguides, Phys. Rev. E **67**, 057602 (2003).

[41] Ilya V. Shadrivov, Andrey A. Sukhorukov, and Yuri S. Kivshar, Nonlinear surface waves in left-handed materials, Phys. Rev. E **69**, 016617 (2004).

[42] Martin W. McCall, Akhlesh Lakhtakia, and Werner S. Weiglhofer, The negative index of refraction demystified, Eur. J. Phys. **23**, 353 (2002).

[43] Johannes Skaar, On resolving the refractive index and the wave vector, Opt. Lett. **31**,

3372 (2006).

[44] P. Kinsler and M. W. McCall, Criteria for negative refraction in active and passive media, Microwave and Opt. Techn. Lett. **50**, 1804 (2008).

[45] Martin W. McCall, What is negative refraction?, Journal of Modern Optics **56**, 1727 (2009).

[46] W. N. Hardy, L. A. Whitehead, Split-ring resonator for use in magnetic resonance from 200-2000 MHz, Review of Scient. Instr. **52**, 213 (1981).

[47] P. Gay-Balmaz, and O. J. F. Martin, Electromagnetic resonances in individual and coupled split-ring resonators, J. Appl. Phys. **92**, 2929 (2002).

[48] J. Zhou, Th. Koschny, M. Kafesaki, E. N. Economou, J. B. Pendry, and C. M. Soukoulis, Saturation of the Magnetic Response of Split-Ring Resonators at Optical Frequencies, Phys. Rev. Lett. **95**, 223902 (2005).

[49] S. Linden, C. Enkrich, M. Wegener, J. Zhou, T. Koschny, C. M. Soukoulis, Magnetic response of metamaterials at 100 terahertz, Science **306**, 1351 (2004).

[50] C. Enkrich, M. Wegener, S. Linden, S. Burger, L. Zschiedrich, F. Schmidt, J. F. Zhou, Th. Koschny, and C. M. Soukoulis, Magnetic Metamaterials at Telecommunication and Visible Frequencies, Phys. Rev. Lett. **95**, 203901 (2005).

[51] C. M. Soukoulis, S. Linden, and M. Wegener, Low-loss negative-index metamaterial at telecommunication wavelengths, Science **315**, 47 (2007).

[52] S. Zhang, W. Fan, K. J. Malloy, S.R. Brueck, N. C. Panoiu, and R. M. Osgood, Experimental Demonstration of Near-Infrared Negative-Index Metamaterials, Opt. Exp. **13**, 4922 (2005).

[53] Mark S. Wheeler, J. Stewart Aitchison, and Mohammad Mojahedi, Three-dimensional array of dielectric spheres with an isotropic negative permeability at infrared frequencies, Phys. Rev. B **72**, 193103 (2005).

[54] I. Vendik, O. Vendik, I. Kolmakov und M. Odit, Modelling of isotropic double negative media for microwave applications, Opto-Electronics Review **14**, 179 (2006).

[55] Jon A. Schuller, Rashid Zia, Thomas Taubner, and Mark L. Brongersma, Dielectric Metamaterials Based on Electric and Magnetic Resonances of Silicon Carbide Particles, Phys. Rev. Lett. **99**, 107401 (2007).

[56] Mark S. Wheeler, J. Stewart Aitchison, Jennifer I. L. Chen, Geoffrey A. Ozin, and Mohammad Mojahedi, Infrared magnetic response in a random silicon carbide micropowder, Phys. Rev. B **79**, 073103 (2009).

[57] A. Sihvola, Metamaterials in electromagnetics, Metamaterials **1**, 2 (2007).

[58] V. M. Agranovich and V. L. Ginzburg, Crystal Optics with Spatial Dispersion and

Excitons, 2nd ed., Springer (1984).

[59] L. D. Landau and E. M. Lifschitz, Lehrbuch der theoretischen Physik - Elektrodynamik der Kontiunua, Akademie Verlag Berlin (1985).

[60] A. Sihvola, Electromagnetic Mixing Formulas and Applications, IEEE Electromagnetic Waves Series 47 (1999).

[61] R. Ruppin, Validity Range of the Maxwell-Garnett Theory, Phys. Stat. Sol. b, **87**, 619 (1978).

[62] R. Ruppin, Evaluation of extended Maxwell-Garnett theories, Optics Communications **182**, 273 (2000).

[63] S. Mühlig, C. Menzel, C. Rockstuhl and F. Lederer, Multipole Analysis of Meta-Atoms, Metamaterials **5**, 64 (2011).

[64] J. Petschulat, C. Menzel, A. Chipouline, C. Rockstuhl, A. Tünnermann, F. Lederer and T. Pertsch, Multipole approach to metamaterials, Phys. Rev. A **78**, 043811 (2008).

[65] J. Petschulat, A. Chipouline, A. Tünnermann, T. Pertsch, C. Menzel, C. Rockstuhl, T. Paul and F. Lederer, Simple and versatile analytical approach for planar metamaterials, Phys. Rev. B **82**, 075102 (2010).

[66] David J. Cho, Feng Wang, Xiang Zhang, and Y. Ron Shen, Contribution of the electric quadrupole resonance in optical metamaterials, Phys. Rev. B **78**, 121101(R) (2008).

[67] Yong Zeng, Colm Dineen, and Jerome V. Moloney, Magnetic dipole moments in single and coupled split-ring resonators, Phys. Rev. B **81**, 075116 (2010).

[68] J. Petschulat, J. Yang, C. Menzel, C. Rockstuhl, A. Chipouline, P. Lalanne, A. Tünnermann, F. Lederer, and T. Pertsch, Understanding the electric and magnetic response of isolated metaatoms by means of a multipolar field decomposition, Optics Expr. **18**, 14454 (2010).

[69] C. Rockstuhl, C. Menzel, S. Mühlig, J. Petschulat, C. Helgert, C. Etrich, A. Chipouline, T. Pertsch, and F. Lederer, Scattering properties of metaatoms, Phys. Rev. B **83**, 245119 (2011).

[70] P. Belov, and C. R. Simovski, Homogenization of electromagnetic crystals formed by uniaxial resonant scatterers, Phys. Rev. E **72**, 026615 (2005).

[71] C. R. Simovski, and S. A. Tretyakov, Local constitutive parameters of metamaterials from an effective-medium perspective, Phys. Rev. B **75**, 195111 (2007).

[72] C. R. Simovski, Analytical modelling of double-negative composites, Metamaterials **2**, 169 (2008).

[73] M. G. Silveirinha, Nonlocal homogenization model for a periodic array of epsilon-negative rods, Phys. Rev. E **73**, 046612 (2006).

[74] David R. Smith, and John B. Pendry, Homogenization of metamaterials by field averaging (invited paper), J. Opt. Soc. Am. B **23**, 391 (2006).

[75] M. G. Silveirinha, Metamaterial homogenization approach with application to the characterisation of microstructured composites with negative parameters, Phys. Rev. B **75**, 115104 (2007).

[76] M. G. Silveirinha, Generalized Lorentz-Lorenz formulas for microstructured materials, Phys. Rev. B **76**, 245117 (2007).

[77] M. G. Silveirinha, Poynting vector, heating rate, and stored energy in structured materials A first-principles derivation, Phys. Rev. B **80**, 235120 (2009).

[78] M. G. Silveirinha, Time domain homogenization of metamaterials, Phys. Rev. B **83**, 165104 (2011).

[79] Andrea Alu, Restoring the physical meaning of metamaterial constitutive parameters, Phys. Rev. B **83**, 081102(R) (2001).

[80] A. M. Nicolson, Measurement of the Intrinsic Properties of Materials by Time-Domain Techniques, G. F. Ross, IEEE Trans. Instr. Measur. **IM-19**, 377 (1970).

[81] W. B. Weir, Automatic Measurement of Complex Dielectric Constant and Permeability at Microwave Frequencie, Proc. IEEE **62**, 33 (1974).

[82] D. R. Smith, S. Schultz, P. Markos, and C. M. Soukoulis, Determination of effective permittivity and permeability of metamaterials from reflection and transmission coefficients, Phys. Rev. B **65**, 195104 (2002).

[83] C. R. Simovski, Bloch material parameters of magneto-dielectric metamaterials and the concept of Bloch lattices, Metamaterials **1**, 62 (2007).

[84] C. R. Simovski, Material Parameters of Metamaterials (a Review), Optics and Spectroscopy **107**, 726 (2009).

[85] C. R. Simovski, and S. A. Tretyakov, On effective electromagnetic parameters of artificial nanostructured magnetic materials, Photonics and Nanostruct. - Fund. and Appl. **8**, 254 (2010).

[86] P. A. Belov, E. A. Yankovskaya, I. V. Melchakova, and C. R. Simovski, Studying the Possibility of Extracting Material Parameters from Reflection and Transmission Coefficients of Plane Wave for Multilayer Metamaterials Based on Metal Nanogrids, Optics and Spectroscopy **109**, 85 (2010).

[87] C. R. Simovski, On electromagnetic characterisation and homogenization of nanostructured metamaterials, J. Opt. **13**, 013001 (2011).

[88] C. Menzel, C. Rockstuhl, T. Paul, T. Pertsch and F. Lederer, Retrieving effective parameters for metamaterials at oblique incidence, Phys. Rev. B **77**, 195328 (2008).

[89] C. Menzel, T. Paul, C. Rockstuhl, T. Pertsch, S. Tretyakov, and F. Lederer, Validity of effective material parameters for optical fishnet metamaterials, Phys. Rev. B **81**, 035320 (2010).

[90] D. R. Smith, D. C. Vier, Th. Koschny, and C. M. Soukoulis, Electromagnetic parameter retrieval from inhomogeneous metamaterials, Phys. Rev. E **71**, 036617 (2005).

[91] Eric Plum, Chirality and Metamaterials - PhD-thesis, Southhapmton (2010).

[92] Christian Helgert, Symmetry related effects of optical metamaterials - Dissertation, FSU Jena (2011).

[93] J. D. Jackson, Klassische Elektrodynamik, 3. überarb. Auflage, Berlin, New York: de Gruyter (2002).

[94] A. N. Serdyukov, I. V. Semchenko, S. A. Tretyakov, A. Sihvola, Electromagnetics of bi-anisotropic materials: Theory and applications, Amsterdam: Gordon and Breach Science Publishers (2001).

[95] R. E. Raab and O. L. de Lange, Multipole Theory in Electromagnetism - Classical, quantum, and symmetry aspects, with applications, Oxford University Press (2004).

[96] G. Russakoff, A Derivation of the Macroscopic Maxwell Equations, Am. Journal of Physics **38**, 1188 (1970).

[97] D. B. Melrose, and R. C. McPhedran, Electromagnetic processes in dispersive media, Cambridge University Press (1991).

[98] F. Forstmann, and R. R. Gerhardts, Metal Optics Near the Plasma Frequency, Springer Tracts in Modern Physics, Vol. 109 (1986).

[99] Y. Zeng, W. Hoyer, J. Liu, S. W. Koch, and J. V. Moloney, Classical theory for second-harmonic generation from metallic nanoparticles, Phys. Rev. B **79**, 235109 (2009).

[100] Th. Koschny, L. Zhang, and C. M. Soukoulis, Isotropic three-dimensional left-handed metamaterials, Phys. Rev. B **71**, 121103(R) (2005).

[101] Na Liu, Hongcang Gue, Liwei Fu, Stefan Kaiser, Heinz Schweizer, and Harald Giessen, Three-dimensional photonic metamaterials at optical frequencies, Nat. Mat. **7**, 31 (2008).

[102] Michael S. Rill, Christine Plet, Michael Thiel, Isabelle Staude, Georg v. Freymann, Stefan Linden, and Marting Wegener, Photonic metamaterials by direct laser writing and silver chemical vapour deposition, Nat. Mat. **7**, 543 (2008).

[103] Fumiaki Miyamaru, Shiro Kuboda, Kazuo Taima, Keisuke Takano, Masanori Hangyo, and Mitsuo Wada Takeda, Three-dimensional bulk metamaterials operating in the terahertz range, Appl. Phys. Lett. **96**, 081105 (2010).

[104] Jason Valentine, Shuang Zhang, Thomas Zentgraf, Erick Ulin-Avila, Dentcho A.

Genov, Guy Bartal, Xiang Zhang, Three-dimensional optical metamaterial with a negative refractive index, Nature **455**, 376 (2008).

[105] P. Mazur and B. R. A. Nijboer, On the statistical mechanics of matter in an electromagnetic field, Physica **19**, 971 (1953).

[106] J. Petschulat, The Multipole Description of Complex Plasmonic Nanostructures - Dissertation, FSU Jena (2011).

[107] J. Petschulat, C. Rockstuhl, C. Menzel, A. Chipouline, A. Tünnermann, F. Lederer, and T. Pertsch, Multipole Metamaterials, (contributed bookchapter, submitted), appearing in Plasmonics and Plasmonic Metamaterials: Analysis and Applications.

[108] T. P. Meyrath, T. Zentgraf, C. Rockstuhl, and H. Giessen, Electromagnetic induction in metamaterials, Appl. Phys. B **93**, 107 (2008).

[109] Sergei Tretyakov, Analytical Modeling in Applied Electromagnetics, Norwood, MA: Artech House (2003).

[110] C. R. Simovski, S. A. Tretyakov, A. H. Sihvola, and M. M. Popov, On the surface effect in thin molecular or composite layers, European Physical Journal - Applied Physics **9**, 195 (2000).

[111] C. R. Simovski, M. Popov, and Sailing He, Dielectric properties of a thin film consisting of a few layers of molecules or particles, Phys. Rev. B **62**, 13718 (2000).

[112] P. Drude, The Theory of Optics, 3d ed. Dover, London, (1959).

[113] Ling Li Hou, Jessie Yao Chin, Xin Mi Yang, Xian Qi Lin, Ruopeng Liu, Fu Yong Xu, and Tie Jun Cui, Advanced parameter retrievals for metamaterial slabs using an inhomogeneous model, J. Appl. Phys. **103**, 064904 (2008).

[114] K. Henneberger, Additional Boundary Conditions: An Historical Mistake, Phys. Rev. Lett. **80**, 2889 (1998).

[115] D. F. Nelson, and B. Chen, Comment on Additional Boundary Conditions: An Historical Mistake, Phys. Rev. Lett. **83**, 1263 (1999).

[116] R. Zeyher, Comment on Additional Boundary Conditions: An Historical Mistake, Phys. Rev. Lett. **83**, 1264 (1999).

[117] K. Henneberger, Henneberger Replies:, Phys. Rev. Lett. **83**, 1265 (1999).

[118] A. P. Vinogradov and A. V. Aivazyan, Scaling theory for homogenization of the Maxwell equations, Phys. Rev. E **60**, 987 (1999).

[119] Carsten Rockstuhl, Falk Lederer, Christoph Etrich, Thomas Zentgraf, Jürgen Kuhl, and Harald Giessen, On the reinterpretation of resonances in split-ring-resonators at normal incidence, Opt. Express **14**, 8827 (2006).

[120] S. I. Maslovski, C. R. Simovski, S. A. Tretyakov, Constitutive equations for media with

second-order spatial dispersion, Bianisotropics '98; Proceedings of the 7th International Conference on Complex Media, Technische Univ. Braunschweig, Germany (1998)

[121] Christoph Menzel, Carsten Rockstuhl, Thomas Paul, and Falk Lederer, Retrieving effective parameters for quasiplanar chiral metamaterials, Appl. Phys. Lett. **93**, 233106 (2008).

[122] Do-Hoon Kwon, Douglas H. Werner, Alexander V. Kildishev, and Vladimir M. Shalaev, Material parameter retrieval procedure for general bi-isotropic metamaterials and its application to optical chiral negative-index metamaterial design, Opt. Express **16**, 11822 (2008).

[123] Xudong Chen, Bae-Ian Wu, Jin Au Kong, and Tomasz M. Grzegorczyk, Retrieval of the effective constitutive parameters of bianisotropic metamaterials, Phys. Rev. E **71**, 046610 (2005).

[124] Christine Eliane Kriegler, Michael Stefan Rill, Stefan Linden, and Martin Wegener, Bianisotropic Photonic Metamaterials, IEEE Journal of Selected Topics in Quant. Electr. **16**, 367 (2010).

[125] J. Yang, C. Sauvan, T. Paul, C. Rockstuhl, F. Lederer, and P. Lalanne, Retrieving the effective parameters of metamaterials from the single interface scattering problem, Appl. Phys. Lett. **97**, 061102 (2010).

[126] Andrei Andryieuski, Radu Malureanu, and Andrei V. Lavrinenko, Wave propagation retrieval method for metamaterials: Unambiguous restoration of effective parameters, Phys. Rev. B **80**, 193101 (2009)

[127] Andrei Andryieuski, Radu Malureanu, and Andrei V. Lavrinenko, Wave propagation retrieval method for chiral metamaterials, Opt. Express **18**, 15498 (2010).

[128] Pochi Yeh, Optical waves in layered media, John Wiley and Sons, Inc., Hoboken, New Jersey (2005).

[129] D. W. Berreman, Optics in Stratified and Anisotropic Media: 4x4-Matrix Formulation, J. Opt. Soc. Am **62**, 502 (1972).

[130] I.V. Lindell, A.H. Sihvola, S.A. Tretyakov, A.J. Viitanen, Electromagnetic waves in chiral and bi-isotropic media, Norwood, MA: Artech House (1994).

[131] V. Lucarini, J.J. Saarinen, K.-E. Peiponen, E.M. Vartiainen, Kramers-Kronig Relations in Optical Materials Research, Springer-Verlag Berlin Heidelberg (2005).

[132] K. Sakoda, Optical properties of photonic crystals, Springer Series in Optical Sciences (2005).

[133] T. Paul, C. Menzel, C. Rockstuhl, F. Lederer, W. Smigaj and P. Lalanne, Reflection and transmission of light at periodic layered metamaterial films, Phys. Rev. B. **84**,

115142 (2011).

[134] David A. Powell, and Yuri S. Kivshar, Substrate-induced bianisotropy in metamaterials, Appl. Phys. Lett. **97**, 091106 (2010).

[135] Zhongyan Sheng, and Vasundara V. Varadan, Tuning the effective properties of metamaterials by changing the substrate properties, J. Appl. Phys. **101**, 014909 (2007).

[136] R. A. Shelby, D. R. Smith, S. Schultz, Experimental Verification of a Negative Index of Refraction, Science **292**, 77 (2001).

[137] M. G. Moharam, and T. K. Gaylord, Rigorous coupled-wave analysis of planar-grating diffraction, J. Opt. Soc. Am. A **71**, 811-818 (1981).

[138] L. Li, Use of Fourier series in the analysis of discontinuous periodic structures, J. Opt. Soc. Am. A **13**, 1870-1876 (1996).

[139] L. Li, New formulation of the Fourier modal method for crossed surface-relief gratings, J. Opt. Soc. Am. A **14**, 2758-2766 (1997).

[140] E. Noponen, and J. Turunen, Eigenmode method for electromagnetic synthesis of diffractive elements with three-dimensional profiles, J. Opt. Soc. Am. A **11**, 2494-2502 (1994).

[141] L. C. Botten, N. A. Nicorovici, R. C. McPhedran, C. Martijn de Sterke, and A. A. Asatryan, Photonic band structure calculations using scattering matrices, Phys. Rev. E **64**, 046603 (2001).

[142] B. Gralak, S. Enoch, and G. Tayeb, From scattering or impedance matrices to Bloch modes of photonic crystals, J. Opt. Soc. Am. A **19**, 1547-1554 (2002).

[143] Z.-Y. Li, and K.-M. Ho, Application of structural symmetries in the plane-wave-based transfer-matrix method for three-dimensional photonic crystal waveguides, Phys. Rev. B **68**, 245117 (2003).

[144] P. B. Johnson, and R. W. Christy, Optical constants of the noble metals, Phys. Rev. B **6**, 4370 (1972)

[145] J. Garcia-Garcia, F. Martin, J. D. Baena, R. Marqués, and L. Jelinek, On the resonances and polarizabilities of split ring resonators, J. Appl. Phys. **98**, 033103 (2005).

[146] Frank Hesmer, Eugen Tatartschuk, Oleksandr Zhuromskyy, Anna A. Radkovskaya, Mikahil Shamonin, Tong Hao, Chris J. Stevens, Grahame Faulkner, David J. Edwards, Ekaterina Shamonina, Coupling mechanisms for split ring resonators: Theory and experiment, Phys. Stat. Sol. B **244**, 1170 (2007).

[147] Koray Aydin, Irfan Bulu, Kaan Guven, Maria Kafesaki, Costas M. Soukoulis, and Ekmel Ozbay, Investigation of magnetic resonances for different split-ring resonator parameters and designs, New J. Phys. **7**, 168 (2005).

[148] C. Rockstuhl, T. Zentgraf, H. Guo, N. Liu, C. Etrich, I. Loa, K. Syassen, J. Kuhl, F. lederer, and H. Giessen, Resonances of split-ring resonator metamaterials in the near infrared, Appl. Phys. B **84**, 219 (2006).

[149] Carsten Rockstuhl, Thomas Zentgraf, Ekaterina Pshenay-Severin, Jörg Petschulat, Arkadi Chipouline, Jürgen Kuhl, Thomas Pertsch, Harald Giessen, and Falk Lederer, The origin of magnetic polarizability in metamaterials at optical frequencies - an electrodynamic approach, Opt. Express **15**, 8871 (2007).

[150] Ricardo Marqués, Francisco Medina, and Rachid Rafii-El-Idrissi, Role of bianisotropy in negative permeability and left-handed metamaterials, Phys. Rev. B **65**, 144440 (2002).

[151] David R. Smith, Jonah Gollub, Jack J. Mock, Willie J. Padilla, David Schurig, Calculation and measurement of bianisotropy in a split ring resonator metamaterial, J. Appl. Phys. **100**, 024507 (2006).

[152] E. Prodan, C. Radloff, N. J. Halas, P. Nordlander, A Hybridization Model for the Plasmon Response of Complex Nanostructures, Science **302**, 419 (2003).

[153] Y. Svirko, N. Zheludev, and M. Osipov, Layered chiral metallic microstructures with inductive coupling, Appl. Phys. Lett. **78**, 498 (2001).

[154] G. Dolling, C. Enkrich, M. Wegener, J. F. Zhou, C. M. Soukoulis, and S. Linden, Cut-wire pairs and plate pairs as magnetic atoms for optical metamaterials, Opt. Lett. **30**, 3198 (2005).

[155] V. M. Shalaev, W. Cai, U. K. Chettiar, H.-K. Yuan, A. K. Sarychev, V. P. Drachev, and A. V. Kildishev, Negative index of refraction in optical metamaterials, Opt. Lett. **30**, 3356 (2005).

[156] Gunnar Dolling, Christian Enkrich, Martin Wegener, Costas M. Soukoulis, and Stefan Linden, Low-loss negative-index metamaterial at telecommunication wavelengths, Opt. Lett. **31**, 1800 (2006).

[157] M. Kafesaki, I. Tsiapa, N. Katsarakis, Th. Koschny, C. M. Soukoulis, and E. N. Economou, Left-handed metamaterials: The fishnet structure and its variations, Phys. Rev. B **75**, 235114 (2007).

[158] V. M. Shalaev, Optical negative-index metamaterials, Nat. Phot. **1**, 41 (2007).

[159] Kamil Boratay Alici, Ekmel Ozbay, A planar metamaterial: Polarization independent fishnet structure, Phot. and Nanostruc. - Fund. and Appl. **6**, 102 (2008).

[160] C. García-Meca, R. Ortuno, F. J. Rodriguez-Fortuno, J. Marti, and A. Martinez, Double-negative polarization-independent fishnet metamaterial in the visible spectrum, Opt. Lett. **34**, 1603 (2009).

[161] G. Dolling, M. Wegener, C. M. Soukoulis, S. Linden, Negative-index metamaterial at 780 nm wavelength, Opt. Lett. **32**, 53 (2007).

[162] C. Helgert, C. Menzel, C. Rockstuhl, E. Pshenay-Severin, E.-B. Kley, A. Chipouline, A. Tünnermann, F. Lederer and T. Pertsch, Polarization-independent negative-index metamaterial in the near infrared, Opt. Lett. **34**, 704 (2009).

[163] C. Rockstuhl, C. Menzel, T. Paul, T. Pertsch and F. Lederer, Light propagation in a fishnet metamaterial, Phys. Rev. B **78**, 155102 (2008).

[164] Thomas Paul, Christoph Menzel, Carsten Rockstuhl, and Falk Lederer, Advanced Optical Metamaterials, Adv. Mat. **22**, 1 (2010).

[165] Carsten Rockstuhl, Thomas Paul, and Falk Lederer, Thomas Pertsch, Thomas Zentgraf, Todd P. Meyrath, and Harald Giessen, Transition from thin-film to bulk properties of metamaterials, Phys. Rev. B **77**, 035126 (2008).

[166] Andrei Andryieuski, Christoph Menzel, Carsten Rockstuhl, Radu Malureanu, Falk Lederer, and Andrei Lavrinenko, Homogenization of resonant chiral metamaterials, Phys. Rev. B **82**, 235107 (2010).

[167] Jiangfeng Zhou, Thomas Koschny, Maria Kafesaki, Costas M. Soukoulis, Size dependence and convergence of the retrieval parameters of metamaterials, Phot. and Nanostruc. - Fund. and Appl. **6**, 96 (2008).

[168] Jiangfeng Zhou, Thomas Koschny, Maria Kafesaki, and Costas M. Soukoulis, Negative refractive index response of weakly and strongly coupled optical metamaterials, Phys. Rev. B **80**, 035109 (2009).

[169] Alexander Minovich, Dragomir N. Neshev, David A. Powell, Ilya V. Shadrivov, Mikhail Lapine, Ian McKerracher, Haroldo T. Hattori, Hark Hoe Tan, Chennupati Jagadish, and Yuri S. Kivshar, Tilted response of fishnet metamaterials at near-infrared optical wavelengths, Phys. Rev. B **81**, 115109 (2010).

[170] T. Koschny, P. Markos, D. R. Smith, and C. M. Soukoulis, Resonant and antiresonant frequency dependence of the effective parameters of metamaterials, Phys. Rev. E **68**, 065602(R) (2003).

[171] C. Menzel, C. Helgert, J. Üpping, C. Rockstuhl, E.-B. Kley, R.-B. Wehrspohn, T. Pertsch and F. Lederer, Angular resolved effective optical properties of a Swiss cross metamaterial, Appl. Phys. Lett. **95**, 131104 (2009).

[172] E. Pshenay-Severin, F. Setzpfandt, C. Helgert C, U. Hübner, C. Menzel, A. Chipouline, C. Rockstuhl, A. Tünnermann, F. Lederer and T. Pertsch, Experimental determination of the dispersion relation of light in metamaterials by white-light interferometry, J. Opt. Soc. Am. B **27**, 660 (2010).

[173] E. Plum, K. Tanaka, W. T. Chen, V. A. Fedotov, D. P. Tsai, and N. I. Zheludev, A combinatorial approach to metamaterials discovery, J. Opt. **13**, 055102 (2011).

[174] Bruno Gompf, Julia Braun, Thomas Weiss, Harald Giessen, Martin Dressel, and Uwe Hübner, Periodic Nanostructures: Spatial Dispersion Mimics Chirality, Phys. Rev. Lett. **106**, 185501 (2011).

[175] Thomas Paul, Carsten Rockstuhl, Christoph Menzel, and Falk Lederer, Anomalous refraction, diffraction, and imaging in metamaterials, Phys. Rev. B **79**, 115430 (2009).

[176] P. Gay-Balmaz and O. J. F. Martin, Efficient isotropic magnetic resonators, Appl. Phys. Lett. **81**, 939 (2002).

[177] A. Kussow, A. Akyurtlu, and N. Angkawisittpan, Optically isotropic negative index of refraction metamaterial, Phys. Stat. Sol. B. **245**, 992-997 (2008).

[178] I. Vendik, O. Vendik and M. Odit, Isotropic artificial media with simultaneously negative permittivity and permeability, Microwave and Optical Techn. Lett. **48**, 2553 (2006).

[179] L. Jelinek, J. Machac, and J. Zehentner, A magnetic metamaterial composed of randomly oriented SRRs, PIERS Online **2**, 624 (2006).

[180] J. D. Baena, L. Jelinek, R. Marqués and J. Zehentner, Electrically small isotropic three-dimensional magnetic resonators for metamaterial design, Appl. Phys. Lett. **88**, 134108 (2006)

[181] C. R. Simovski, S. He, Frequency range and explicit expressions for negative permittivity and permeability for an isotropic medium formed by a lattice of perfectly conducting Ω particles, Phys. Lett. A **311**, 254 (2003).

[182] E. Verney, B. Sauviac, and C. R. Simovski, Isotropic metamaterial electromagnetic lens, Phys. Lett. A **331**, 244 (2004).

[183] J. D. Baena, L. Jelinek, and R. Marqués, Towards a systematic design of isotropic bulk magnetic metamaterials using the cubic point groups of symmetry, Phys. Rev. B. **76**, 245115 (2007).

[184] A. Andryieuski, C. Menzel, C. Rockstuhl, R. Malureanu, F. Lederer and A. Lavrinenko, Homogenization of resonant chiral metamaterials, Phys. Rev. B **82**, 235107 (2010)

[185] W. J. Padilla, M. T. Aronsson, C. Highstrete, Mark Lee, A. J. Taylor, and R. D. Averitt, Electrically resonant terahertz metamaterials: Theoretical and experimental investigations, Phys. Rev. B **75**, 041102(R) (2007).

[186] C. M. Bingham, H. Tao, X. Liu, R. D. Averitt, X. Zhang, and W. J. Padilla, Planar wallpaper group metamaterials for novel terahertz applications, Opt Exp. **16**, 18565 (2008).

[187] M. Decker, S. Linden, and M. Wegener, Coupling effects in low-symmetry planar split-ring resonator arrays, Opt. Lett. **34**, 1579 (2009).

[188] N. Liu, H. Liu, S. Zhu and H. Giessen, Stereometamaterials, Nat. Phot. **3**, 157 (2009).

[189] B. Bai, Y. Svirko, J. Turunen, and T. Vallius, Optical activity in planar chiral metamaterials: Theoretical study, Phys. Rev. A **76**, 023811 (2007).

[190] K. Jefimovs, N. Saito, Y. Ino, T. Vallius, P. Vahimaa, J. Turunen, R. Shimano, M. Kauranen, Y. Svirko, M. Kuwata-Gonokami, Optical activity in chiral gold nanogratings, Microelec. Eng. **78**, 448 (2005).

[191] Willie J. Padilla, Group theoretical description of artificial electromagnetic metamaterials, Opt. Exp. **15**, 1639 (2007).

[192] L. R. Arnaut, Chirality in multi-dimensional space with application to electromagnetic characterisation of multi-dimensional chiral and semi-chiral media, J. Electromagn. Waves Appl. **11**, 1459 (1997).

[193] E. Plum, V. A. Fedotov, A. S. Schwanecke, Giant optical gyrotropy due to electromagnetic coupling , N. I. Zheludev, and Y. Chen, Appl. Phys. Lett. **90**, 223113 (2007).

[194] R. C. Jones, A New Calculus for the Treatment of Optical Systems, J. Opt. Soc. Am. **31**, 488 (1941).

[195] C. Menzel, C. Rockstuhl and F. Lederer, Advanced Jones calculus for the classification of periodic metamaterials, Phys. Rev. A **82**, 053811 (2010).

[196] A. Drezet, C. Genet, J.-Y. Laluet, and T. W. Ebbesen, Optical chirality without optical activity: How surface plasmons give a twist to light, Opt. Exp. **16**, 12559 (2008).

[197] Shih-Yau Lu and Russell A. Chipman, Interpretation of Mueller matrices based on polar decomposition, J. Opt. Soc. Am. A **13**, 1106 (1996).

[198] Sudha and A. V. Gopala Rao, Polarization elements: a group-theoretical study, J. Opt. Soc. Am. A **18**, 3130 (2001).

[199] S. N. Savenkov, O. I. Sydoruk, and R. S. Muttiah, Eigenanalysis of dichroic, birefringent, and degenerate polarization elements: a Jones-calculus study, Appl. Opt. **46**, 6700 (2007).

[200] O. Sydoruk, and S. N. Savenkov, White polarization sandwiches: optical elements with non-orthogonal eigenpolarizations, J. Opt. **12**, 035702 (2010).

[201] Shih-Yau Lu and Russell A. Chipman, Homogeneous and inhomogeneous Jones matrices, J. Opt. Soc. Am. A **11**, 766 (1994).

[202] R. J. Potton, Reciprocity in optics, Rep. Prog. Phys. **67**, 717 (2004).

[203] S. N. Volkov, K. Dolgaleva, R. W. Boyd, K. Jefimovs, J. Turunen, Y. Svirko, B. K. Canfield, and M. Kauranen, Optical activity in diffraction from a planar array of achiral

nanoparticles, Phys. Rev. A **79**, 043819 (2009).

[204] E. Plum, V. A. Fedotov, and N. I. Zheludev, Planar metamaterial with transmission and reflection that depend on the direction of incidence, Appl. Phys. Lett. **94**, 131901 (2009).

[205] S. I. Maslovski, D. K. Morits and S. A. Tretyakov, Symmetry and reciprocity constraints on diffraction by gratings of quasi-planar particles, J. Opt. A **11**, 074004 (2009).

[206] S. V. Zhukovsky, A. V. Novitsky, and V. M. Galynsky, Elliptical dichroism: operating principle of planar chiral metamaterials, Opt. Lett. **34**, 1988 (2009).

[207] M. Decker, M. W. Klein, M. Wegener, and S. Linden, Circular dichroism of planar chiral magnetic metamaterials, Opt. Lett. **32**, 856 (2007).

[208] J. C. W. Lee, and C. T. Chan, Polarization gaps in spiral photonic crystals, Opt. Expr. **13**, 8083 (2005).

[209] J. K. Gansel, M. Wegener, S. Burger, and S. Linden, Gold helix photonic metamaterials: A numerical parameter study, Opt. Expr. **18**, 1059 (2010).

[210] M. G. Silveirinha, Design of Linear-to-Circular Polarization Transformers Made of Long Densely Packed Metallic Helices, IEEE Trans. Anten. and Prop. **56**, 390 (2008).

[211] I. Hodgkinson, Q. H. Wu, B. Knight, A. Lakhtakia, and K. Robbie, Vacuum Deposition of Chiral Sculptured Thin Films with High Optical Activity, Appl. Opt. **39**, 642 (2000).

[212] A. Lakhtakia, V. C. Venugopal, M. W. McCall, Spectral holes in Bragg reflection from chiral sculptured thin films: circular polarization filters, Opt. Comm. **177**, 57 (2000).

Zusammenfassung

Die vorliegende Arbeit beschäftigt sich mit der Charakterisierung von Metamaterialien. Für eine umfassendere Einführung in die Thematik sei auf Kapitel 1 verwiesen. Als künstliche Medien mit Perioden kleiner als die relevante Wellenlänge werden diese zumeist als effektiv homogene Materialien beschrieben. Diese Art der Beschreibung und deren kritische Untersuchung und Bewertung stehen im Mittelpunkt der Kapitel 2-4. Im Kapitel 2 werden die Grundlagen für die Beschreibung künstlicher Strukturen mittels homogenener Maxwell Gleichungen und insbesondere der entsprechenden Materialgleichungen gelegt. In diesem Kapitel wird vor allem die Beschreibung künstlich magnetischer Materialien auf der Basis einer komplexen, räumlichen dispersiven Materialantwort abgeleitet. Die erzielten Materialgleichungen für Medien mit schwacher räumlicher Dispersion werden dann in Kapitel 3 zur Bestimmung der effektiven Eigenschaften zugrundegelegt. Die Bestimmung erfolgt durch den sogenannten S-parameter retrieval, d.h. der Inversion der Fresnelgleichung für Reflexion und Transmission an einer optischen Schicht. Diese Methode wird ausführlich auch vom Standpunkt allgemein periodischer Medien her betrachtet, wodurch sich grundsätzliche Zusammenhänge und insbesondere Limitierungen der Methodik ableiten lassen. Diese Methode erweist sich auch dann noch als sinnvoll zur effektiven Beschreibung der Lichtausbreitung, wenn eine Reduktion der optischen Anwort auf Materialparameter nicht mehr möglich ist. In Kapitel 4 werden die zuvor bereitgestellten Methoden der Charakterisierung auf Metamaterialien mit zunehmender Symmetrie angewandt, die als prototypisch verstanden werden im optischen Spektralbereich zu einem links-händigen Medium zu führen; zu einem Medium in dem der Energiefluss antiparallel zur Phasengeschwindigkeit ist. Es wird gezeigt, dass eine Reduktion der optischen Antwort auf einzelne effektive Materialparameter insbesondere in der Nähe von Resonanzen nicht möglich ist. In Konsequenz der vorherigen Resultate und mit Hinblick auf ein Design optischer Funktionalität anstatt des Designs etwaiger Materialien wird in Kapitel 5 eine Beschreibung der optischen Antwort auf Basis von Jones-Matrizen vorgeschlagen. Hierbei wird insbesondere ein Zusammenhang zwischen Symmetrie und allgemeiner Form der Jones-Matrix hergeleitet, wobei sich periodische Metamaterialien in 5 grundsätzlich verschiedene Gruppen bzgl. ihrer Symmetrie unterteilen lassen. Dieser Ansatz erlaubt sowohl die Beschreibung als auch das Design der polarisationsabhängigen Response von Metamaterialien.

Publications

Peer-reviewed Journals

1. C. Menzel, C. Rockstuhl, T. Paul, S. Fahr and F. Lederer, *Imbert-Fedorov shift at metamaterial interfaces*, Phys. Rev. A **77**, 013810 (2008).
2. **C. Menzel, C. Rockstuhl, T. Paul, T. Pertsch and F. Lederer, *Retrieving effective parameters for metamaterials at oblique incidence*, Phys. Rev. B 77, 195328 (2008).**[1]
3. T. Paul, C. Rockstuhl, C. Menzel and F. Lederer, *Resonant Goos-Haenchen and Imbert-Fedorov shifts at photonic crystal slabs*, Phys. Rev. A **77**, 053802 (2008).
4. J. Petschulat, C. Menzel, A. Chipouline, C. Rockstuhl, A. Tünnermann, F. Lederer and T. Pertsch, *Multipole approach to metamaterials*, Phys. Rev. A **78**, 043811 (2008).
5. C. Rockstuhl, C. Menzel, T. Paul, T. Pertsch and F. Lederer, *Light propagation in a fishnet metamaterial*, Phys. Rev. B **78**, 155102 (2008).
6. **C. Menzel, C. Rockstuhl, T. Paul and F. Lederer, *Retrieving effective parameters for quasiplanar chiral metamaterials*, Appl. Phys. Lett. 93, 233106 (2008).**
7. C. Rockstuhl, C. Menzel, T. Paul and F. Lederer, *Optical activity in chiral media composed of three-dimensional metallic meta-atoms*, Phys. Rev. B**79**, 035321 (2009).
8. **C. Helgert, C. Menzel, C. Rockstuhl, E. Pshenay-Severin, E.-B. Kley, A. Chipouline, A. Tünnermann, F. Lederer and T. Pertsch, *Polarization-independent negative-index metamaterial in the near infrared*, Opt. Lett. 34, 704 (2009).**
9. T. Paul, C. Rockstuhl, C. Menzel and F. Lederer, *Anomalous refraction, diffraction, and imaging in metamaterials*, Phys. Rev. B **79**, 115430 (2009).
10. R. Singh, C. Rockstuhl, C. Menzel, T. P. Meyrath, M. He, H. Giessen, F. Lederer and W. L. Zhang, *Spiral-type terahertz antennas and the manifestation of the Mushiake principle*, Opt. Expr. **17**, 9971 (2009).

[1] Publications directly relevant to this thesis are typed in bold.

11. E. Pshenay-Severin, U. Hübner, C. Menzel, C. Helgert, A. Chipouline, C. Rockstuhl, A. Tünnermann, F. Lederer and T. Pertsch, *Double-element metamaterial with negative index at near-infrared wavelengths*, Opt. Lett. **34**, 1678 (2009).
12. C. Helgert, C. Rockstuhl, C. Etrich, C. Menzel, E.-B. Kley, A. Tünnermann, F. Lederer and T. Pertsch, *Effective properties of amorphous metamaterials*, Phys. Rev. B **79**, 233107 (2009).
13. **C. Menzel, C. Helgert, J. Üpping, C. Rockstuhl, E.-B. Kley, R.-B. Wehrspohn, T. Pertsch and F. Lederer, *Angular resolved effective optical properties of a Swiss cross metamaterial*, Appl. Phys. Lett. 95, 131104 (2009).**
14. A. Andryieuski, C. Menzel, C. Rockstuhl, R. Malureanu and A. V. Lavrinenko, *The split cube in a cage: bulk negative-index material for infrared applications*, J. Opt. A **11**, 114010 (2009).
15. R. Singh, E. Plum, C. Menzel, C. Rockstuhl, A. K. Azad, R. A. Cheville, F. Lederer, W. Zhang and N. I. Zheludev, *Terahertz metamaterial with asymmetric transmission*, Phys. Rev. B **80**, 153104 (2009).
16. C. Menzel, R. Singh, C. Rockstuhl, W. L. Zhang and F. Lederer, *Effective properties of terahertz double split-ring resonators at oblique incidence*, J. Opt. Soc. Am. B **26**, B143 (2009).
17. J. Petschulat, A. Chipouline, A. Tünnermann, T. Pertsch, C. Menzel, C. Rockstuhl and F. Lederer, *Multipole nonlinearity of metamaterials*, Phys. Rev. A **80**, 063828 (2009).
18. **C. Menzel, T. Paul, C. Rockstuhl, T. Pertsch, S. Tretyakov and F. Lederer, *Validity of effective material parameters for optical fishnet metamaterials*, Phys. Rev. B 81, 035320 (2010).**
19. E. Pshenay-Severin, F. Setzpfandt, C. Helgert C, U. Hübner, C. Menzel, A. Chipouline, C. Rockstuhl, A. Tünnermann, F. Lederer and T. Pertsch, *Experimental determination of the dispersion relation of light in metamaterials by white-light interferometry*, J. Opt. Soc. Am. B **27**, 660 (2010).
20. **C. Menzel, C. Rockstuhl, R. Iliew, F. Lederer, A. Andryieuski, R. Malureanu and A. Lavrinenko, *High symmetry versus optical isotropy of a negative-index metamaterial*, Phys. Rev. B 81, 195123 (2010).**
21. T. Paul, C. Menzel, C. Rockstuhl and F. Lederer, *Advanced Optical Metamaterials*, Adv. Mat. **22**, 2354 (2010).
22. **C. Menzel, C. Helgert, C. Rockstuhl, E.-B. Kley, A. Tünnermann, T. Pertsch and F. Lederer, *Asymmetric Transmission of Linearly Polarized Light at Optical Metamaterials*, Phys. Rev. Lett. 104, 253902 (2010).**

23. J. Petschulat, J. Yang, C. Menzel, C. Rockstuhl, A. Chipouline, P. Lalanne, A. Tünnermann, F. Lederer and T. Pertsch, *Understanding the electric and magnetic response of isolated metaatoms by means of a multipolar field decomposition*, Opt. Expr. **18**, 14454 (2010).

24. J. Petschulat, A. Chipouline, A. Tünnermann, T. Pertsch, C. Menzel, C. Rockstuhl, T. Paul and F. Lederer, *Simple and versatile analytical approach for planar metamaterials*, Phys. Rev. B **82**, 075102 (2010).

25. **C. Menzel, C. Rockstuhl and F. Lederer, *Advanced Jones calculus for the classification of periodic metamaterials*, Phys. Rev. A 82, 053811 (2010).**

26. **A. Andryieuski, C. Menzel, C. Rockstuhl, R. Malureanu, F. Lederer and A. Lavrinenko, *Homogenization of resonant chiral metamaterials*, Phys. Rev. B 82, 235107 (2010).**

27. A. Chipouline, J. Petschulat, A. Tuennermann, T. Pertsch, C. Menzel, C. Rockstuhl und F. Lederer, *Multipole approach in electrodynamics of metamaterials*, Appl. Phys. A published online, DOI: 10.1007/s00339-011-6339-7.

28. S. Mühlig, C. Menzel, C. Rockstuhl and F. Lederer, *Multipole Analysis of Meta-Atoms*, Metamaterials **5**, 64 (2011).

29. C. Rockstuhl, C. Menzel, S. Mühlig, J. Petschulat, C. Helgert, C. Etrich, A. Chipouline, T. Pertsch, and F. Lederer, *Scattering properties of metaatoms*, Phys. Rev. B **83**, 245119 (2011).

30. T. Paul, C. Menzel, C. Rockstuhl, F. Lederer, W. Smigaj and P. Lalanne, *Reflection and transmission of light at periodic layered metamaterial films*, Phys. Rev. B **84**, 115142 (2011).

31. C. Helgert, E. Pshenay-Severin, M. Falkner, C. Menzel, E.-B. Kley, C. Rockstuhl, A. Tünnermann, F. Lederer and T. Pertsch, *Chiral Metamaterial Composed of Three-Dimensional Plasmonic Nanostructures*, Nano Lett. **11**, 4400 (2011).

Conference proceedings

1. C. Rockstuhl, C. Etrich, C. Helgert, C. Menzel, T. Paul, S. Fahr, T. Pertsch, J. Dorfmüller, R. Esteban, W. Khunsin, R. Vogelgesang, K. Kern, A. Dmitriev, K. Bittkau, T. Beckers, R. Carius and F. Lederer, *Large scale simulations in the realm of nanooptics*, SPIE, Vol. 7604, 7604D, (2010)

2. J. Petschulat, A. Chipouline, E. Pshenay-Severin, A. Tünnermann, T. Pertsch, C. Menzel, C. Rockstuhl, T. Paul, and F. Lederer, *Analytical Modelling of linear and nonlinear properties of metamaterials based on multipole expansion*, SPIE, Vol. 7353,

7353D, (2009)

3. J. Petschulat, A. Chipouline, T. Pertsch, C. Menzel, C. Rockstuhl, A. Tünnermann, and F. Lederer, *On the dispersion relation in metamaterials: an analytic approach*, SPIE, Vol. 6987, 69871T, (2008)
4. C. Rockstuhl, C. Menzel, T. Paul, C. Helgert, E. Pshenay-Severin, J. Petschulat, A. Chipouline, T. Pertsch, and F. Lederer, *Bulk properties of metamaterials*, SPIE, Vol. 6987, 69871O, (2008)

Invited talks

1. F. Lederer, C. Rockstuhl, C. Menzel, and T. Paul, and T. Pertsch, *On the dispersion relation and refractive index of optical metamaterials - from thin film to bulk*, International Conference on Computational and Experimental Engineering and Sciences 2008, Honolulu, Hawaii, USA
2. C. Rockstuhl, C. Menzel, T. Paul F. Lederer, E. Pshenay-Severin, M. Falkner, C. Helgert, A. Chipouline, W. Smigaj, J. Yang, and P. Lalanne, *Effective properties of metamaterials*, SPIE Optics + Photonics 2011, San Diego, USA
3. T. Pertsch, E. Pshenay-Severin, C. Helgert, A. Chipouline, E.-B. Kley, C. Menzel, C. Rockstuhl, and F. Lederer, *Characterization of the complex transfer matrix of metamaterials*, Nanometa 2011, Seefeld, Austria
4. C. Rockstuhl, C. Menzel, T. Paul, A. Andryieuski, R. Malureanu, A. Lavrinenko and F. Lederer, *Isotropic optical metamaterials*, Metamaterials' 2010, Karlsruhe, Germany
5. C. Rockstuhl, C. Menzel, T. Paul, A. Andryieuski, R. Malureanu, A. Lavrinenko and F. Lederer, *Isotropic optical metamaterials*, MediNano 2010, Belgrade, Serbia
6. F. Lederer, T. Paul, C. Rockstuhl, and C. Menzel, *Light Propagation in Optical Metamaterials*, CIMTEC 2010, Montecatini Terme, Italy
7. A. Chipouline, J. Petschulat, C. Menzel, C. Rockstuhl, A. Tünnermann, F. Lederer, and T. Pertsch, *Multipole approach in electrodynamics of metamaterials*, META 10 2010, Cairo, Egypt
8. C. Rockstuhl, C. Menzel, T. Paul, S. Fahr, F. Lederer, C. Etrich, C. Helgert and T. Pertsch, *Large scale simulations in the realm of nanooptics*, SPIE Photonics West 2010, San Francisco, USA
9. T. Pertsch, C. Helgert, C. Rockstuhl, E. Pshenay-Severin, C. Menzel, E.-B. Kley, A. Chipouline, C. Etrich, U. Hübner, J. Üpping, A. Tünnermann, and F. Lederer, *Tailoring the Properties of Optical Metamaterials*, OSA-COS Topical Meeting on Ap-

plications of Optical Metamaterials 2009, Nankai, China

10. F. Lederer, C. Rockstuhl, C. Menzel, and T. Pertsch, *Can optical metamaterials be described by effective material parameters?*, Metamaterials' 2009, London, UK
11. F. Lederer, C. Rockstuhl, C. Menzel, and T. Paul, *The dispersion relation in metamaterials - from thin film to bulk*, Metamaterials' 2008, Pamplona, Spain
12. C. Rockstuhl, C. Menzel, T. Paul, J. Petschulat, E. Pshenay-Severin, C. Helgert, A. Chipouline, T. Pertsch, and F. Lederer, *Properties of bulk metamaterials*, SPIE Photonics Europe 2008, Strasbourg, France
13. T. Pertsch, F. Garwe, C. Rockstuhl, U. Hübner, C. Etrich, C. Menzel, E. Pshenay-Severin, A. Chipouline, A. Tünnermann and F. Lederer, *Impact of Plasmonic Resonances for Negative Index Materials*, PIERS 2007, Beijing, China

International conference contributions

1. A. Andryieuski, C. Menzel, C. Rockstuhl, R. Malureanu, F. Lederer, and A. Lavrinenko, *Is It Possible To Homogenize Resonant Chiral Metamaterials?*, TaCoNa-Photonics 2010 Bad Honnef, Germany
2. C. Helgert, C. Menzel, C. Rockstuhl, E.-B. Kley, A. Tünnermann, F. Lederer, and T. Pertsch, *3D chiral metamaterials enabling asymmetric transmission of linearly polarized light*, Metamaterials' 2010, Karlsruhe, Germany
3. J. Petschulat, A. Chipouline, C. Menzel, T. Paul, C. Rockstuhl, A. Tünnermann, F. Lederer, and T. Pertsch, *Assembling metamaterials - A building block approach for conductively or near-field coupled plasmonic entities*, Metamaterials' 2010, Karlsruhe, Germany
4. C. Menzel, J. Petschulat, J. Yang, S. Mühlig, A. Chipouline, C. Rockstuhl, P. Lalanne, T. Pertsch, and F. Lederer, *Scattering properties of 3D metaatoms*, Metamaterials' 2010, Karlsruhe, Germany
5. C. Menzel, T. Paul, C. Rockstuhl, R. Iliew, A. Andryieuski, R. Malureanu, A. V. Lavrinenko, and F. Lederer, *Optical Isotropic Negative Index Metamaterials*, META 2010 Tucson, Arizona, USA
6. C. Menzel, C. Rockstuhl, T. Paul, C. Helgert, J. Petschulat, E.-B. Kley, F. Eilenberger, T. Pertsch, and F. Lederer, *Asymmetric Transmission of Linearly Polarized Light through Low Symmetry Metamaterials*, CLEO/QELS 2010 San Jose, California, USA
7. J. Petschulat, C. Menzel, A. Chipouline, C. Rockstuhl, A. Tünnermann, F. Lederer,

and T. Pertsch, *Understanding Optical Activity and EIT-Analogous in Optical Metamaterials with an Analytical Multipole Analysis*, CLEO/QELS 2010 San Jose, California, USA

8. C. Helgert, E. Pshenay-Severin, C. Menzel, J. Petschulat, C. Rockstuhl, E.-B. Kley, F. Lederer, and T. Pertsch, *Experimental demonstration of nanostructured metamaterials in the optical regime*, PhoNa International Workshop 2010, Jena, Germany
9. J. Petschulat, A. Chipouline, C. Menzel, C. Rockstuhl, A. Tünnermann, F. Lederer, and T. Pertsch, *Multipole nonlinearity - an additional bulk effect for particular metamaterials*, PhoNa International Workshop 2010, Jena, Germany
10. C. Menzel, C. Rockstuhl, S. Mühlig, T. Paul, and F. Lederer, *Chirality as a bulk property retrieved from the dispersion relation*, PhoNa International Workshop 2010, Jena, Germany
11. T. Paul, C. Menzel, S. Fahr, S. Mühlig, C. Rockstuhl, and F. Lederer, *Anomalous diffraction and refraction in negative-index metamaterials*, PhoNa International Workshop 2010, Jena, Germany
12. E. Pshenay-Severin, M. Falkner, F. Setzpfandt, C. Helgert, U. Hübner, C. Menzel, A. Chipouline, C. Rockstuhl, E.-B. Kley, A. Tünnermann, F. Lederer, and T. Pertsch, *Direct experimental optical characterisation of metamaterials*, PhoNa International Workshop 2010, Jena, Germany
13. T. Paul, C. Menzel, C. Rockstuhl, S. Bin Hasan, and F. Lederer, *Enhancing higher harmonics generation using plasmonic nanostructures*, 74. Annual Meeting of the Deutsche Physikalische Gesellschaft 2010, Regensburg, Germany
14. C. Rockstuhl, C. Menzel, T. Paul, T. Pertsch, S. Tretyakov, and F. Lederer, *How feasible are effective material parameters for metamaterials?*, META 10 2010, Cairo, Egypt
15. E. Pshenay-Severin, F. Setzpfandt, C. Helgert, Uwe Hübner, C. Menzel, C. Rockstuhl, A. Tünnerman, F. Lederer, and T. Pertsch, *Direct experimental optical characterisation of metamaterials*, META 10 2010, Cairo, Egypt
16. J. Petschulat, A. Chipouline, A. Tünnermann, T. Pertsch, C. Menzel, C. Rockstuhl, T. Paul, and F. Lederer, *Multipole Metamaterials: A Mesoscopic Investigation towards Effective Linear and Nonlinear Optical Material Interaction*, Frontiers in Optics 2009, San Jose, California
17. C. Menzel, C. Helgert, C. Rockstuhl, E. Pshenay-Severin, J. Üpping, E.-B. Kley, F. Lederer, R. Wehrspohn, and T. Pertsch, *Effective optical properties of a Swiss cross metamaterial beyond normal incidence*, Metamaterials' 2009, London, UK
18. T. Paul, C. Menzel, C. Rockstuhl, and F. Lederer, *Isotropic optical metamaterials*,

Metamaterials' 2009, London, UK

19. C. Helgert, C. Etrich, C. Menzel, C. Rockstuhl, E.-B. Kley, T. Pertsch, E. Tünnerman, and F. Lederer, *Effective properties of periodic, partially disordered, and amorphous metamaterials*, Metamaterials' 2009, London, UK
20. J. Petschulat, A. Chipouline, C. Menzel, C. Rockstuhl, A. Tünnermann, F. Lederer, and T. Pertsch, *Multipole induced Nonlinearity of Metamaterials*, Metamaterials' 2009, London, UK
21. J. Petschulat, A. Chipouline, C. Menzel, C. Rockstuhl, A. Tünnermann, F. Lederer, and T. Pertsch, *Multipole Metamaterials*, CLEO Europe 2009 Munich, Germany
22. C. Rockstuhl, C. Menzel, T. Paul, and F. Lederer, *Chirality as a bulk property retrieved from the dispersion relation*, CLEO Europe 2009 Munich, Germany
23. C. Helgert, C. Menzel, C. Rockstuhl, E. Pshenay-Severin, J. Üpping, E.-B. Kley, F. Lederer, and T. Pertsch, *Measuring Angular Dependent Effective Properties Of Metamaterials*, CLEO/QELS 2009 Baltimore, Maryland, USA
24. C. Menzel, C. Rockstuhl, T. Paul, T. Pertsch, and F. Lederer, *Effective Parameters For Anisotropic Metamaterials*, CLEO/QELS 2009 Baltimore, Maryland, USA
25. C. Rockstuhl, S. Fahr, T. Paul, C. Menzel, F. Lederer, K. Bittkau, T. Beckers, and R. Carius, *Photon Management in Thin Film Solar Cells*, CLEO/QELS 2009 Baltimore, Maryland, USA
26. S. Fahr, C. Menzel, T. Paul, C. Rockstuhl, and F. Lederer, *Periodic arrays of metallic nanoparticles as efficient intermediate reflectors in aSi:H-μcSi solar cells*, OWTNM 2009, Jena, Germany
27. T. Paul, C. Menzel, S. Fahr, C. Rockstuhl, and F. Lederer, *Adapted Fourier modal method for the analysis of higher harmonic generation in arbitrary bi-periodic multilayer structures*, OWTNM 2009, Jena, Germany
28. C. Menzel, T. Paul, C. Rockstuhl and F. Lederer, *Retrieving Effective Parameters of Anisotropic Metamaterials*, OWTNM 2009, Jena, Germany
29. A. Chipouline, J. Petschulat, E. Pshenay-Severin, A. Tünnermann, T. Pertsch, C. Menzel, C. Rockstuhl, T. Paul, and F. Lederer, *Analytical modelling of linear and nonlinear properties of metamaterials based on multipole expansion*, SPIE Photonics Europe 2009, Prague, Czech Republic
30. F. Lederer, C. Rockstuhl, R. Singh, C. Menzel, T. Paul, and W. Zhang, *Resonances in THz Metamaterials and Nanoantennas*, PECS VIII 2009, Sydney, Australia
31. C. Rockstuhl, C. Menzel, T. Paul, F. Lederer, R. Singh and W. Zhang, *Resonances of Coupled Split-Ring-Resonators with Broken Symmetry*, Nanometa 2009, Seefeld, Aus-

tria

32. C. Rockstuhl, C. Menzel, T. Paul, F. Lederer, J. Petschulat, C. Helgert, E. Pshenay-Severin, A. Chipouline, and T. Pertsch, *Three Dimensional Chiral Meta-Atoms*, Nanometa 2009, Seefeld, Austria
33. J. Petschulat, A. Chipouline, E. Pshenay-Severin, A. Tünnermann, T. Pertsch, C. Menzel, C. Rockstuhl, T. Paul, and F. Lederer, *Linear and Nonlinear Properties of Metamaterials: Analytical Modelling Based on Multipole Expansion*, Nanometa 2009, Seefeld, Austria
34. C. Menzel, C. Rockstuhl, T. Paul, and F. Lederer, *On the reliability of effective parameters for anisotropic metamaterials*, Nanometa 2009, Seefeld, Austria
35. T. Paul, C. Rockstuhl, C. Menzel, and F. Lederer, *Anomalous diffraction and refraction in negative-index metamaterials*, Nanometa 2009, Seefeld, Austria
36. C. Helgert, E. Pshenay-Severin, E.-B. Kley, A. Chipouline, A. Tünnermann, T. Pertsch, C. Menzel, C. Rockstuhl, and F. Lederer, *Demonstration of a polarization-independent optical negative-index metamaterial*, Nanometa 2009, Seefeld, Austria
37. J. Petschulat, C. Menzel, C. Rockstuhl, A. Chipouline, T. Pertsch, and F. Lederer, *The dispersion relation for metamaterials: An analytical approach*, Near-Field Optics 10 2008, Buenos Aires, Argentina
38. A. Chipouline, J. Petschulat, T. Pertsch, A. Tünnermann, C. Rockstuhl, C. Menzel, F. Lederer, *Plane wave propagation in metamaterials in framework of macroscopic Maxwell's equations: analytical approach*, SPIE Optics + Photonics 2008, San Diego, USA
39. T. Paul, C. Rockstuhl, C. Menzel, and F. Lederer, *Anomalous Diffraction and Imaging Properties of Metamaterials*, OSA topical meeting 2008: Photonic Metamaterials: From Random to Periodic, Rochester, USA
40. C. Menzel, C. Rockstuhl, T. Paul and F. Lederer, Q*uantifying Chirality of Metamaterials*, Metamaterials' 2008, Pamplona, Spain
41. J. Petschulat, C. Menzel, C. Rockstuhl, A. Chipouline, T. Pertsch, and F. Lederer, *The dispersion relation for metamaterials: An analytical approach*, NATO Advanced Research Workshop Metamaterials for Secure Information and Communication Technologies 2008, Marrakesh, Morocco
42. C. Menzel, T. Paul, C. Rockstuhl, T. Pertsch, and F. Lederer, *Angle-Dependent Effective Properties of Metamaterials - Material vs. Wave Parameters*, CLEO/QELS 2008 San Jose, California, USA
43. T. Paul, C. Rockstuhl, C. Menzel, and F. Lederer, *The Imbert-Fedorov and Goos-*

Hänchen shift at metamaterial interfaces, CLEO/QELS 2008 San Jose, California, USA

44. J. Petschulat, C. Menzel, A. Chipouline, C. Rockstuhl, T. Pertsch, F. Lederer, *Light Propagation and Effective Parameters of Nanowire Based Metamaterials: An Analytical Approach*, CLEO/QELS 2008 San Jose, California, USA
45. C. Rockstuhl, T. Paul, C. Menzel, T. Pertsch, and F. Lederer, *Dispersion Relation of Light in Metamaterials*, CLEO/QELS 2008 San Jose, California, USA
46. C. Rockstuhl, C. Menzel, T. Paul, T. Pertsch, and F. Lederer, *On the dispersion relation of light in metamaterials*, 72. Annual Meeting of the Deutsche Physikalische Gesellschaft 2008, Berlin, Germany
47. T. Paul, C. Menzel, C. Rockstuhl, and F. Lederer, *The Goos-Hänchen and Imbert-Fedorov shift at metamaterial interfaces*, 72. Annual Meeting of the Deutsche Physikalische Gesellschaft 2008, Berlin, Germany
48. C. Menzel, T. Paul, C. Rockstuhl, T. Pertsch, and F. Lederer, *Retrieving angle dependent effective parameters of metamaterials*, 72. Annual Meeting of the Deutsche Physikalische Gesellschaft 2008, Berlin, Germany
49. J. Petschulat, A. Chipouline, T. Pertsch, C. Rockstuhl, C. Menzel, F. Lederer, and A. Tünnermann, *The Dispersion Relation of Split Ring Resonators and Double Wire Structures: An Analytic Investigation*, SPIE Photonics Europe 2008, Strasbourg, France

Acknowledgements

This work would never exist, if there wouldn't be several people and organizations that supported me. Most of all I would like to thank Prof. Dr. Falk Lederer and Prof. Dr. Carsten Rockstuhl for kindly housing me as a PhD student at the Institute of Condensed Matter Theory and Solid State Optics at the Friedrich-Schiller-Universität Jena.

Especially, I would like to thank Prof. Dr. Carsten Rockstuhl for the time he spent to supervise me during the last years. I know, it sometimes was a hard job fighting my "Beratungsresistenz". Thank you for introducing me to the real world of scientific research and teaching me scientific soft skills. Special thanks for your persistence with respect to my manuscripts. I would like to thank Thomas Paul for fruitful discussions, collaborations and proofreading of so many manuscripts. I enjoyed our business trips very much. I would like to thank Stephan Fahr for his continuous criticism and persistence with respect to technical issues of any kind. I also thank Stefan Mühlig for introducing me to the topic of spheres. Thanks for proofreading my thesis. Thanks for all the delicious cake. You guys considerably helped me surviving my PhD time successfully.
Furthermore, I would like to thank all members of the photonics group for their support.

I appreciate the collaborations with Prof. Dr. Thomas Pertsch and his group. Especially I would like to thank Ekaterina Pshenay-Severin, Christian Helgert and Jörg Petschulat for enriching my research portfolio considerably. Special thanks for the nice conference trips.

Many thanks also to A. Andryieuski from the group of Prof. A. Lavrinenko (DTU, Denmark), to R. Singh from the group of Prof. W. Zhang (OSU, USA) and to E. Plum from the group of Prof. N. Zheludev (Southampton, UK).

I gratefully acknowledge the careful reading and evaluation of this thesis by all referees.

Last but not least, I thank all my family and my friends that supported me during the last years of failure and success.

Short Curriculum Vitae

Personal data

Name	Christoph Menzel
Date of birth	10/03/1981
Place of birth	Halle/Saale, Germany

Academic career

06/2011	Submittance of doctoral thesis entitled "Characterisation of Optical Metmaterials- Effective Parameters and Beyond"
02/2007 - current	Scientific employee and PhD student at the IFTO at the Friedrich-Schiller-Universität Jena, Germany

Lecture activity

summer term 2007	Electrodynamics, seminar (2 SWS)
summer term 2008	Fundamentals of Optics, seminar (2 SWS)
winter term 2009	Electrodynamics, seminar (2 SWS)
summer term 2010	Supervisor "Oberseminar"
summer term 2011	Supervisor "Oberseminar"

Education

11/2006	Diploma degree in Physics from the Friedrich-Schiller-Universität Jena, Germany
10/2006	Diploma thesis entitled "Optik in Medien mit stark dispersiver Permittivität und Permeabilität"
10/2003 - 12/2006	Study of Physics at the Friedrich-Schiller-Univ. Jena, Germany
10/2001 - 09/2003	Study of Physics at the Martin-Luther-Univ. Halle, Germany
11/2000 - 08/2001	Military service in Koblenz and Hohenmölsen, Germany
08/1992 - 07/2000	Landesgymnasium Latina AHF Halle, Germany

Ehrenwörtliche Erklärung

Hiermit erkläre ich ehrenwörtlich, dass ich die vorliegende Arbeit selbständig, ohne unzulässige Hilfe Dritter und ohne Benutzung anderer als der angegebenen Hilfsmittel und Literatur angefertigt habe. Die aus anderen Quellen direkt oder indirekt übernommenen Daten und Konzepte sind unter Angabe der Quelle gekennzeichnet.

Weitere Personen waren an der inhaltlich-materiellen Erstellung der vorliegenden Arbeit nicht beteiligt. Insbesondere habe ich hierfür nicht die entgeltliche Hilfe von Vermittlungs bzw. Beratungsdiensten (Promotionsberater oder andere Personen) in Anspruch genommen. Niemand hat von mir unmittelbar oder mittelbar geldwerte Leistungen für Arbeiten erhalten, die im Zusammenhang mit dem Inhalt der vorgelegten Dissertation stehen.

Die Arbeit wurde bisher weder im In- noch im Ausland in gleicher oder ähnlicher Form einer anderen Prüfungsbehörde vorgelegt.

Die geltende Promotionsordnung der Physikalisch-Astronomischen Fakultät ist mir bekannt.

Ich versichere ehrenwörtlich, dass ich nach bestem Wissen die reine Wahrheit gesagt und nichts verschwiegen habe.

Jena, Unterschrift